Studies on the device structure of electrochemically prepared copper oxide photovoltaic devices

（電気化学的に形成した酸化銅太陽電池のデバイス構造に関する研究）

January, 2016

DOCTOR OF ENGINEERING

Mohd Zamzuri Bin Mohammad Zain

TOYOHASHI UNIVERSITY OF TECHNOLOGY

平成 28 年　1　月　8　日

Department 機械工学専攻	Student ID Number 学籍番号	第 139106 号
Applicant's name 氏名	Mohd Zamzuri Bin Mohammad Zain	

Supervisors 指導教員	Masanobu Izaki Seiji Yokoyama

Abstract

Title of Thesis 博士学位論文名	Studies on the device structure of electrochemically prepared copper oxide photovoltaic devices.（電気化学的に形成した酸化銅太陽電池のデバイス構造に関する研究）

(Approx. 800 words)
(要旨　1,200 字程度)

Recently, the need for sustainable power generation has encouraged research into a variety of photovoltaic (PV) systems, which have the potential to cope with the global energy crisis in the future. Oxide thin film photovoltaic devices are promising for renewable energy applications due to their low material usage and inexpensive manufacturing potential. Cuprous oxide (Cu_2O) is a p-type semiconductor with the band-gap energy of 2.1 eV has received broad attention as a light-absorbing layer in a photovoltaic device, because of its non-toxicity, abundance, and theoretical conversion efficiency of 18%. The conversion efficiency of 6.1% has been reported for the AZO/Al-doped Ga_2O_3/Na-doped Cu_2O PV device prepared by the thermal oxidation of metallic Cu sheet in air followed by a pulse-laser deposition of Ga_2O_3 and AZO layers. In contrast, the electrodeposition process in aqueous solutions is a well-known technique due to several advantages such as low-fabrication cost, low temperature, ambient pressure processing, controllable film thickness, and possible large scale deposition. The conversion efficiency of 3.9% with Voc of 1.2 V has been reported for the AZO/Ga_2O_3/Cu_2O PV device prepared by electrodeposition of Cu_2O layer followed by an atomic layer deposition of AZO and Ga_2O_3 layers. The conversion efficiency, however, was limited at 1.28% for the randomly oriented super-straight type (SST) Cu_2O/ZnO PV device prepared by only electrodeposition.

Since, the power conversion efficiency is related to the generation of minority carrier inside the p-Cu_2O layer and the transportation of minority carrier from the p-Cu_2O layer to the interface to the n-ZnO layer, the improvement in the quality and purity of the Cu_2O layer as well as the heterointerface state including the interface area of the Cu_2O/ZnO heterojunction is important to increase the efficiency close to the theoretical value. There are two types of the Cu_2O PV device of super-straight type and substrate type PV device. The thermally-prepared Cu_2O PV device was specified as the substrate-type PV device, and the components of the n-ZnO, buffer such as Ga_2O_3 and transparent conductive window layers were stacked on the Cu_2O layer. The sunlight is introduced from the upper n-ZnO side. The electrochemically prepared Cu_2O PV device was specified as the super-straight type PV device, and the Cu_2O layer was stacked on the n-ZnO and transparent conductive window layer prepared on glass substrate. The sunlight was introduced from the lower glass

substrate side.

In this thesis, I applied two device geometries and two buffer materials to overcome the low power conversion efficiency of Cu_2O-based PV devices. First, the super-straight type Cu_2O/Cl-doped ZnO PV device was prepared by electrochemical reactions in aqueous solutions, and effects of the insertion of the ZnO-nanowires and highly resistive i-ZnO buffer layer on the photovoltaic performance was investigated by considering the energy state at the heterojunction. The insertion of ZnO-nanowires alternative to the continuous ZnO layer induced the increase in the short-circuit current density but the open-circuit voltage decreased, and the further insertion of i-ZnO layer under optimized condition gave the increase in both the Jsc and Voc due to the suppressing of the recombination loss at the interface. The insertion of highly resistive buffer layer at the heterointerface is an excellent tool to improve the photovoltaic performance.

Secondly, a photo-assisted electrodeposition technique was applied to stack the ZnO layer on the Cu_2O layer for fabricating substrate-type Cu_2O-PV device, and the growth mechanism is discussed by electrochemical investigations. An optimized ZnO layer is deposited onto highly oriented <111>-p-Cu_2O layer, showed a photovoltaic performance for the first time. Stacking the aluminum-doped ZnO (AZO) onto ZnO layer leads to increase in short-circuit current density. The AZO layer plays a role to take the carrier transported through n-ZnO layer from the Cu_2O layer out. And, the highly oriented (111)-Cu_2O layer exhibited a promising candidate of absorbing layer in PV device due to the increased in diffusion length.

Thirdly, a spin-coated TiO_2 intermediate layer is developed to mitigate the interfacial defect-assisted recombination at the ZnO/Cu_2O PV device. The TiO_2 layer thickness is controlled by sol concentration and spin coating speed. The insertion of TiO_2 intermediate layer decreases the recombination at the ZnO/Cu_2O interface to some extent, resulting in increase in the open-circuit voltage. Furthermore, topping the ZnO/TiO_2/Cu_2O PV device with AZO layer shows an increase in short-circuit current density due to the increased in carrier diffusion length.

Finally, I propose an optimized Cu_2O layer to overcome short minority carrier diffusion length in Cu_2O layer by stacking directly the AZO layer onto Cu_2O layer. The AZO layer acts as a carrier transporter to take out the minority carrier from the Cu_2O layer. The optimization of the AZO layer and Cu_2O layer thickness resulted in an improvement in the photovoltaic performance with maximum conversion efficiency is obtained due to the increased in carrier diffusion length. The results demonstrated here will strongly contribute to the improvement of the photovoltaic performance of oxide photovoltaic devices prepared by the electrochemical techniques.

CONTENTS

CHAPTER 2: Super-straight type Cu_2O/ZnO photovoltaic device prepared by electrochemical reactions and the photovoltaic performance

CHAPTER 3: Substrate type <111>-Cu_2O/<0001>-ZnO photovoltaic device prepared by photo-assisted electrodeposition

CHAPTER 4: Photon-Assisted Electrochemical Construction of <111>-p-Cu_2O Photovoltaic Device with TiO_2 Intermediate Layer

CHAPTER 5: <111>-oriented Cu_2O photovoltaic device with the Al:ZnO layer and the improved performance

CHAPTER 6

CHAPTER 1

Introduction

1.1 Global environmental crises and Photovoltaics

1.1.1 Climate change

Climate change may refer to a statistical description in terms of the mean and variability of relevant quantities over a period of time ranging from months to thousands or millions of years. Human activities are believed to be contributing largely to affect the earth's energy budget by changing the emissions and resulting atmospheric concentrations of important gases and aerosols and by changing land surface properties. Figure 1.1 shows the Earth's

climate system that is powered by solar radiation.**[1]** The sun radiation reaches our atmosphere in the form of visible light part of the electromagnetic spectrum. As the earth's temperature has been relatively constant over many centuries, the incoming solar energy must be nearly in balance with the outgoing radiation. The earth's surface absorbed the incoming solar shortwave radiation (SWR), and some are reflected back to space by gases and aerosols, clouds and by the earth's surface (albedo) and some are absorbed in the atmosphere. Most of the outgoing energy flux from the earth is in the form of infrared, also referred to the longwave radiation (LWR). The LWR emitted from the Earth's surface is largely absorbed by certain atmospheric constituents consists of water vapor, carbon dioxide (CO_2), methane (CH_4), nitrous oxide (N_2O) and other greenhouse gases (GHGs) and clouds, which themselves emit LWR into all directions. The downward directed component of this LWR (Figure 1.1) adds heat to the lower layers of the atmosphere and to the earth's surface (greenhouse effect).

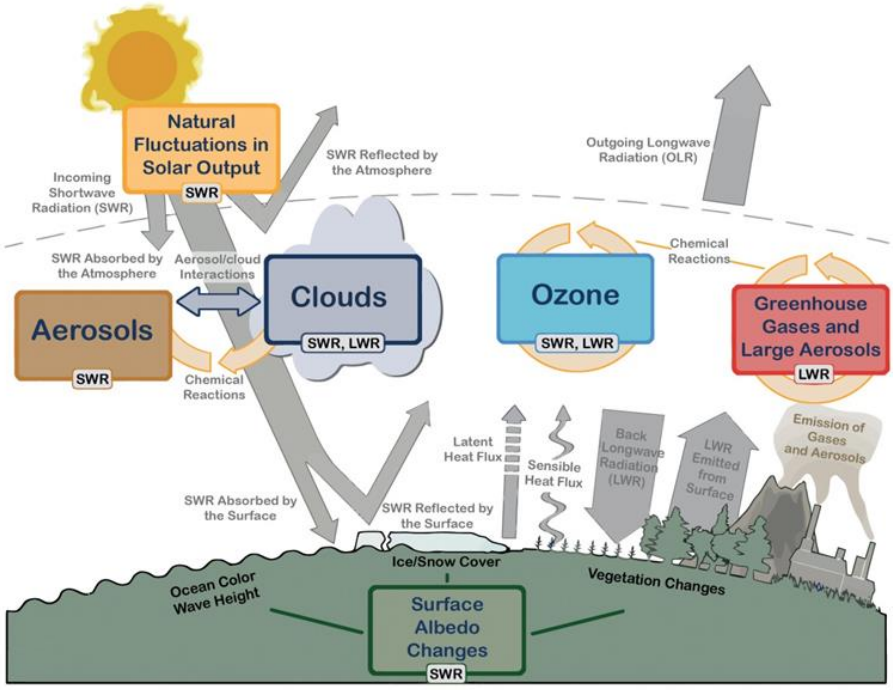

Figure 1.1 Main causes for climate change

1.1.2 Green House Gases (GHGs)

Humans enhance the greenhouse effect directly by emitting GHGs such as CO_2, CH_4, N_2O and chlorofluorocarbons (CFCs). In addition, pollutants such as carbon monoxide (CO), volatile organic compounds (VOC), nitrogen oxides (NOx) and sulphur dioxide (SO_2), which by themselves are negligible GHGs, have an indirect effect on the greenhouse effect. By acting as precursors of secondary aerosols, these GHGs alter the atmospheric chemical reactions, resulting in changes in the abundance of important gases to the amount of outgoing LWR such as CH_4 and ozone (O_3).

Since about 1850, global use of fossil fuels (coal, oil and gas) has increased to dominate energy supply, both replacing many traditional uses of bioenergy and providing new services. The rapid rise in fossil fuel combustion (including gas flaring) has produced a corresponding rapid growth in CO_2 emissions as shown in Figure 1.2.

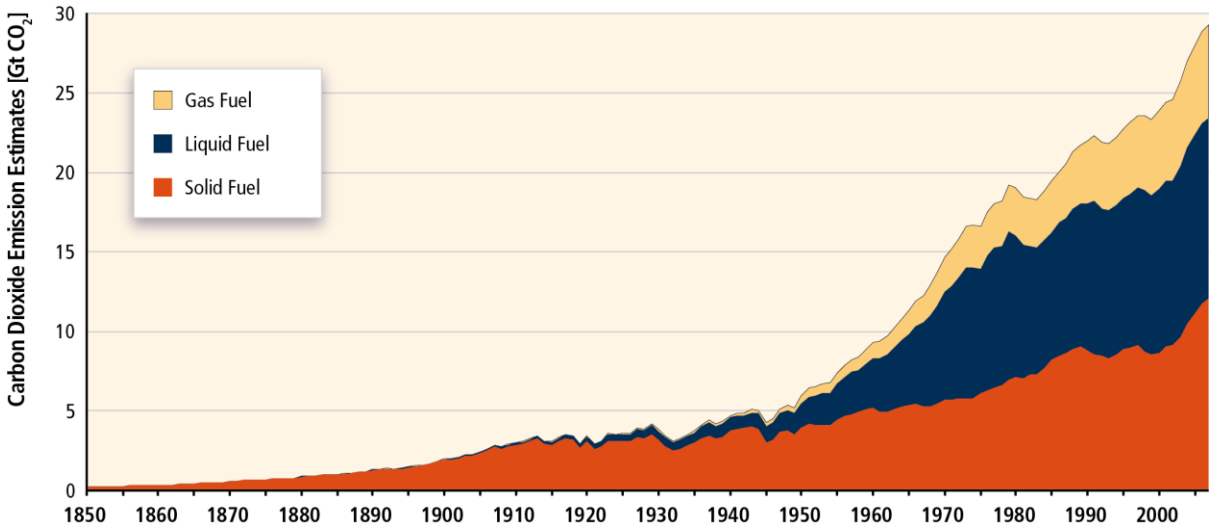

Figure 1.2 Global CO_2 emissions from fossil fuel burning, 1850 to 2007. Gas fuel includes flaring of natural gas. All emission estimates are expressed in Gt CO_2.

Table 1.1 shows the global anthropogenic CO_2 budget accumulated from 1750-2011. According to these data, given in the Intergovernmental Panel on Climate Change- Fifth Assessment Report (IPCC-TAR, 2013), prior to the Industrial Era, that began in 1750, the concentration of atmospheric CO_2 fluctuated roughly between 180 ppm and 290 ppm for at least 2.1 Myr. **[2-4]** Between 1750 and 2011, the combustion of fossil fuels (coal, gas, oil and gas flaring) and the production of cement have released 375 ± 30 PgC to the atmosphere.**[5]** Land use change activities, mainly deforestation, has released an additional 180 ± 80 PgC. This carbon released by human activities is called anthropogenic carbon. Of the 555 ± 85 PgC of anthropogenic carbon emitted to the atmosphere from fossil fuel and cement and land use change, less than half have accumulated in the atmosphere (240 ± 10 PgC). The remaining anthropogenic carbon has been absorbed by the ocean and in terrestrial ecosystems. The ocean stored 155 ± 30 PgC of anthropogenic carbon since 1750. Terrestrial ecosystems that have not been affected by land use change since 1750, have accumulated 160 ± 90 PgC of anthropogenic carbon since 1750, thus not fully compensating the net CO_2 losses from terrestrial ecosystems to the atmosphere from land use change during the same period estimated of 180 ± 80 PgC. The net balance of all terrestrial ecosystems, those affected by

Table 1.1 Global anthropogenic CO_2 budget, accumulated since the Industrial Revolution (1750-2011).**[1]**

	1750-2011 Cumulative PgC	1980-1989 PgC /yr	1990-1999 PgC /yr	2000-2009 PgC /yr	2002-2011 PgC /yr
Atmospheric increase	240 ± 10	3.4 ± 0.2	3.1 ± 0.2	4.0 ± 0.2	4.3 ± 0.2
Fossil fuel combustion and cement production	375 ± 30	5.5 ± 0.4	6.4 ± 0.5	7.8 ± 0.6	8.3 ± 0.7
Ocean-to-atmosphere flux	-155 ± 30	-2.0 ± 0.7	-2.2 ± 0.7	-2.3 ± 0.7	-2.4 ± 0.7
Land-to-atmosphere flux	30 ± 45	-0.1 ± 0.8	-1.1 ± 0.9	-1.5 ± 0.9	-1.6 ± 1.0
Partitioned as follows					
Net land use change	180 ± 80	1.4 ± 0.8	1.5 ± 0.8	1.1 ± 0.8	0.9 ± 0.8
Residual land sink	-160 ± 90	-1.5 ± 1.1	-2.6 ± 1.2	-2.6 ± 1.2	-2.5 ± 1.3

land use change and the others, is thus close to neutral since 1750, with an average loss of 30 ± 45.

From Table 1, the global CO_2 emissions from fossil fuel combustion and cement production were 7.8 ± 0.6 gC yr^{-1} on average during 2000–2009, 6.4 ± 0.5 PgC yr^{-1} during 1990–1999 and 5.5 ± 0.4 PgC yr^{-1} during 1980–1989. Global fossil fuel CO_2 emissions increased by 3.2% yr^{-1}on average during the decade 2000–2009 compared to 1.0% yr^{-1} in the 1990s and 1.9% yr^{-1} in the 1980s. The global financial crisis in 2008–2009 induced only a short-lived drop in global emissions in 2009 (–0.3%), with the return to high annual growth rates of 5.1% and 3.0% in 2010 and 2011, respectively. And fossil fuel and cement CO_2 emissions of 9.2 ± 0.8 PgC in 2010 and 9.5 ± 0.8 PgC in 2011.**[6]**

1.1.3 Renewable energy

All societies require energy services to meet basic human needs (e.g., lighting, cooking, space comfort, mobility, communication) and to serve productive processes. The quality of energy is important to the development process. For development to be sustainable, delivery of energy services needs to be secure and have low environmental impacts. Sustainable social and economic development requires assured and affordable access to the energy resources necessary to provide essential and sustainable energy services. This may mean the application of different strategies at different stages of economic development. To be environmentally benign, energy services must be provided with low environmental impacts, including GHG emissions.

Figure 1.3 shows the shares of energy sources in total global primary energy supply in 2008. On a global basis, it is estimated that renewable energy accounted for 12.9% of the total 492

EJ of primary energy supply in 2008.**[7]** The largest renewable energy contributor was biomass (10.2%), with the majority (roughly 60%) of the biomass fuel used in traditional cooking and heating applications developing countries but with rapidly increasing use of modern bio-mass as well. Hydropower represented 2.3%, whereas other renewable energy sources accounted for 0.4%.

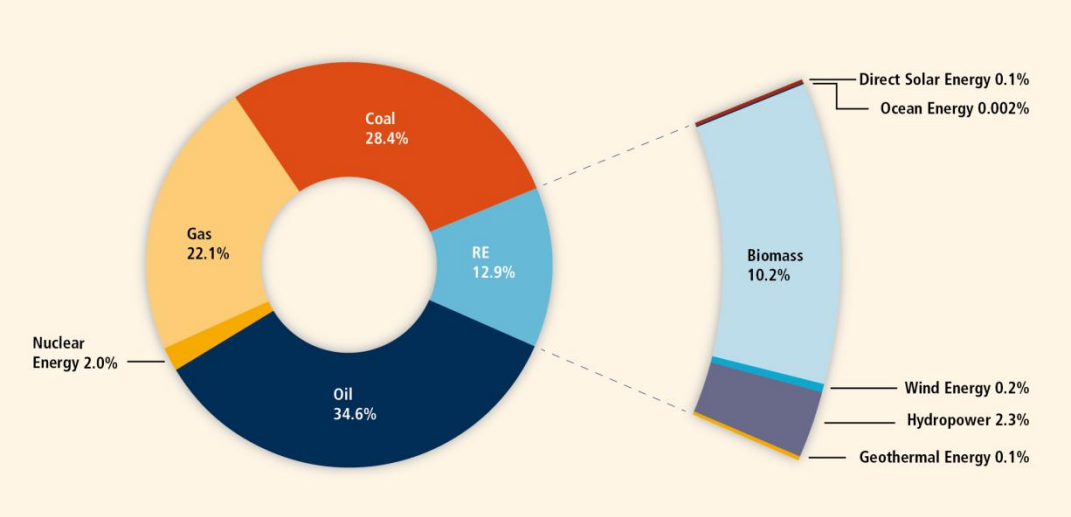

Figure 1.3 Shares of energy sources in total global primary energy supply in 2008.

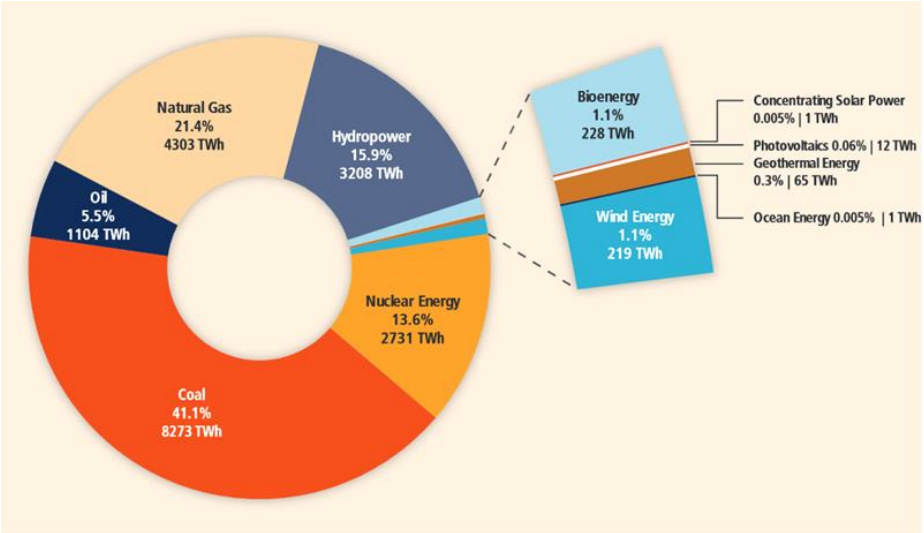

Figure 1.4 Shares of primary energy sources in world electricity generation in 2008.

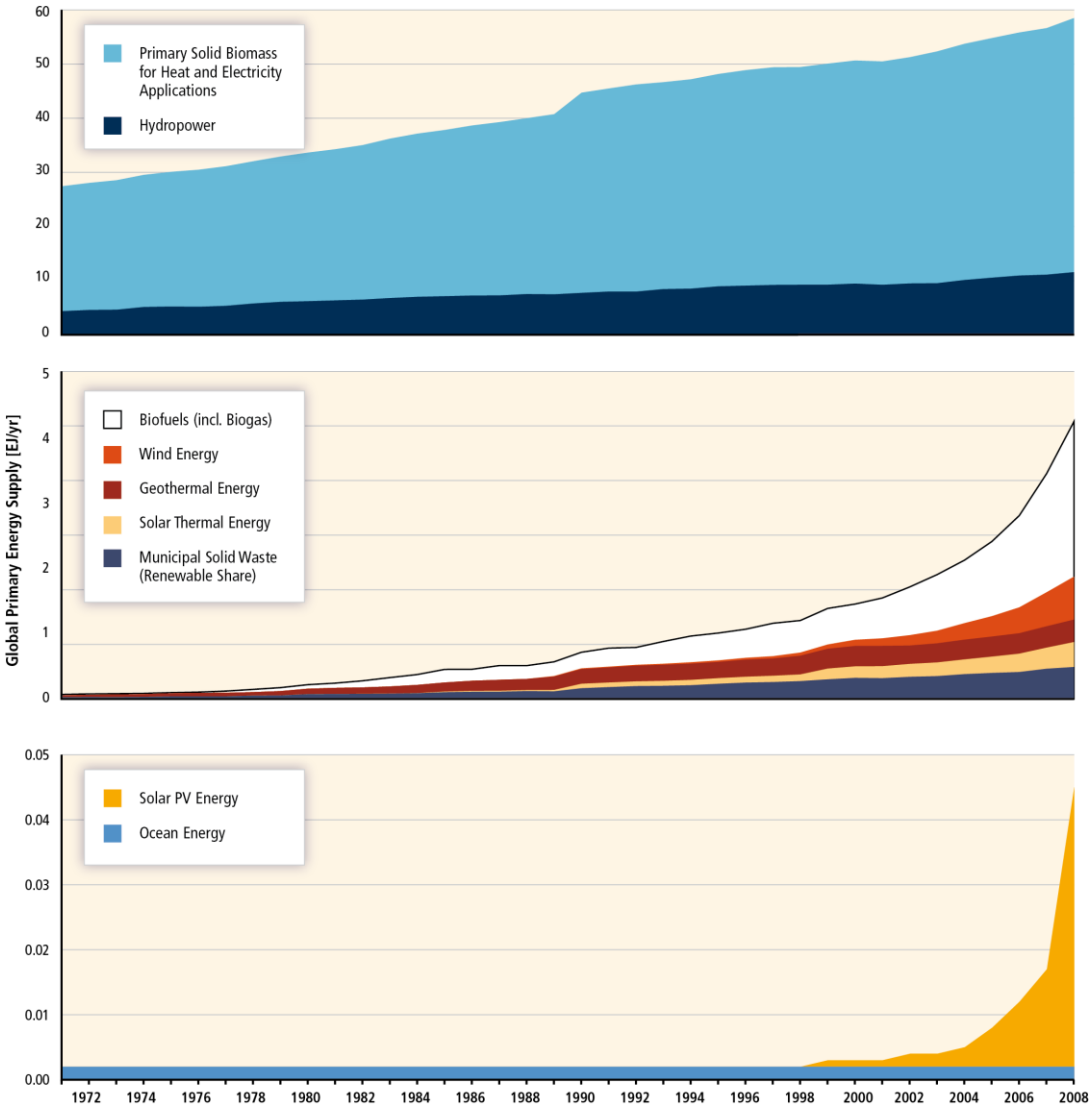

Figure 1.5 The development of global primary energy supply for renewable energy from 1971 to 2008.

The renewable energy's contribution to electricity generation is summarized in Figure 1.4. In 2008, renewable energy contributed approximately 19% of global electricity supply (16% hydropower, 3% other renewable energy). Global electricity production in 2008 was 20,181 TWh (or 72.65 EJ).**[7]** Deployment of renewable energy has been increasing rapidly in recent years. Under most conditions, increasing the share of renewable energy in the energy mix will require policies to stimulate changes in the energy system. Government policies, the

declining cost of many renewable energy technologies, changes in the prices of fossil fuels and other factors have supported the continuing increase in the use of renewable energy. While renewable energy is still relatively small, its growth has accelerated in recent years, as shown in Figure 1.5. In 2009, despite global financial challenges, renewable energy capacity continued to grow rapidly, including wind power (32%), hydropower (3%), grid-connected photovoltaics (53%), geothermal power (4%), and solar hot water/heating (21%).**[8]** Biofuels accounted for 2% of global road transport fuel demand in 2008 and nearly 3% in 2009.

1.1.4 Photovoltaic: Potential as a sustainable energy source

Due to the fast development, demands of comfort, a higher mobility and growing world population, the energy consumption is rising tremendously year by year. In the present scenario, fossil fuels as coal, oil and gas, are playing lead role to meet the energy demand. The environmental pollution is also serious problem today due to the huge use of fossil fuels. To decrease the pollution and save the environment, renewable energy technologies have good potential to meet the global energy demand.

According to Intergovernmental Panel on Climate Change report, solar energy is abundant and offers significant potential for near-term (2020) and long-term (2050) climate change mitigation.**[9]** There are a wide variety of solar technologies of varying maturities that can, in most regions of the world, contribute to a suite of energy services. Even though solar generation still only represents a small fraction of total energy consumption, markets for solar technologies are growing rapidly. Much of the desirability of solar technology is its inherently smaller environment burden and the opportunity it offer for positive social impact. The following are several significant points for photovoltaic to be a real candidate as a sustainable source.

(a) Solar energy is the most abundant of all energy resources.

The rate at which solar energy is intercepted by the Earth is about 10,000 times greater that than the rate at which humankind consumes energy. Our planet receives ~ 1.2 x 1017 W of solar power, while the rate of current worldwide energy consumption is ~1.3 x 1013 W.**[10]** This means that the Earth receives more energy in an hour than the total energy it consumes in an entire year. Although not all countries are equally endowed with solar energy, a significant contribution to the energy mix from direct solar energy is possible for almost every country.

(**b) Solar technologies offer opportunities for positive social impacts and their environmental burden is small.**

Solar technologies have low lifecycle greenhouse gas emissions, and quantification of external costs has yielded favourable values compared to fossil fuel-based energy. An important social benefit of solar technologies is their potential to improve the health and livelihood opportunities for many of the world's poorest populations; addressing some of the gap in availability of modern energy services for roughly 1.4 billion people who do not have access to electricity and the 2.7 billion people who rely on traditional biomass for home cooking and heating needs.

(c) Over the last 20 years, solar energies have seen very substantial cost reductions.

The current levelized costs of energy from solar technologies vary widely depending on the upfront technology cost. Over the two three decades, the solar industry has relied on several approaches to reduce cost, i.e, production scale-up, process improvement and raise in the conversion efficiency.**[11]**

1.2 Photovoltaic devices

1.2.1 Introduction to photovoltaic device

It is known that among renewable energy sources, solar energy is most promising and reliable energy sources in most of the countries, government is providing incentive to setup the solar energy based power plants. In order to convert solar energy in energy forms usable for human needs there are several thermodynamic pathways. In general, heat, kinetic energy, electric energy and chemical energy can be provided via solar energy conversion.

Photovoltaic (PV) is the direct conversion of radiation into electricity. Photovoltaic systems contain cells that convert sunlight into electricity. The photovoltaic effect was first observed by French physicist A. E. Becquerel in 1839.**[12]** He explained his discovery in Les Comptes Rendus de l'Academie des Sciences, "the production of an electric current when two plates of platinum or gold diving in an acid, neutral, or alkaline solution are exposed in an uneven way to solar radiation."**[13]** During the late 1800s, the discovery of a device for converting sunlight directly into electricity was brought. Called the photovoltaic (PV) cell, C. Fritts demonstrated the first solid-state solar cell by depositing a thin layer of Au on Se semiconductor.**[14]** The semiconductor acts as light absorbing layer to convert photon into hole-electrons pairs, and the internal electric field in the Au/Se Schottky junction separated the photo-excited charge carriers. The two fundamental processes, namely light absorption and charge separation, are still the basis in all inorganic solar cells. The modern silicon solar cell, attributed to Russel Ohl working at American Telephone and Telegraph's (AT&T) Bell Labs, was discovered in 1946 **[15]** and demonstrated in 1954 by Chapin, Fuller and Pearson at the same place.**[16]** Their cell employed a single-crystal Si wafer for light absorption and a p-n junction for charge separation, with an efficiency of ~ 5%.

Solar energy is the most abundant renewable energy source on earth. Our planet receives ~$1.2x10^{17}$ W of solar power, while the rate of current worldwide energy consumption is ~10,000 times smaller at $1.3x10^{13}$ W.**[17]** This means that, in just one hour, the solar energy intercepted by the Earth exceeds the world's energy consumption for the entire year. Moreover, the land requirement for solar cells is minimal. Covering 0.16% of the Earth's surface with 10% efficient cells would provide ~$2x10^{13}$ W of electricity, more than the current total energy demand of the planet.**[17]** Solar energy's potential to mitigate climate change is equally impressive. Except for the modest amount of carbon dioxide (CO_2) emissions produced in the manufacture of conversion devices, the direct use of solar energy produces very little greenhouse gases, and it has the potential to displace large quantities of non-renewable fuels.**[18]**

1.2.2 Photovoltaic devices and their current status of energy conversion efficiency

Existing photovoltaic technologies include wafer-based crystalline silicon (sc-Si) cells, as well as thin-film cells based on copper indium gallium selenide, $CuInGaSe_2$ (CIGS), cadmium telluride (CdTe), amorphous-Si (a-Si) and polycrystalline thin-film silicon (poly-Si).**[19]** Organic photovoltaic (OPV) consists of organic absorber materials and is an emerging class of solar cells. Figure 1.6 shows the type of photovoltaic devices and the conversion efficiency revolution from 1975 to 2012.

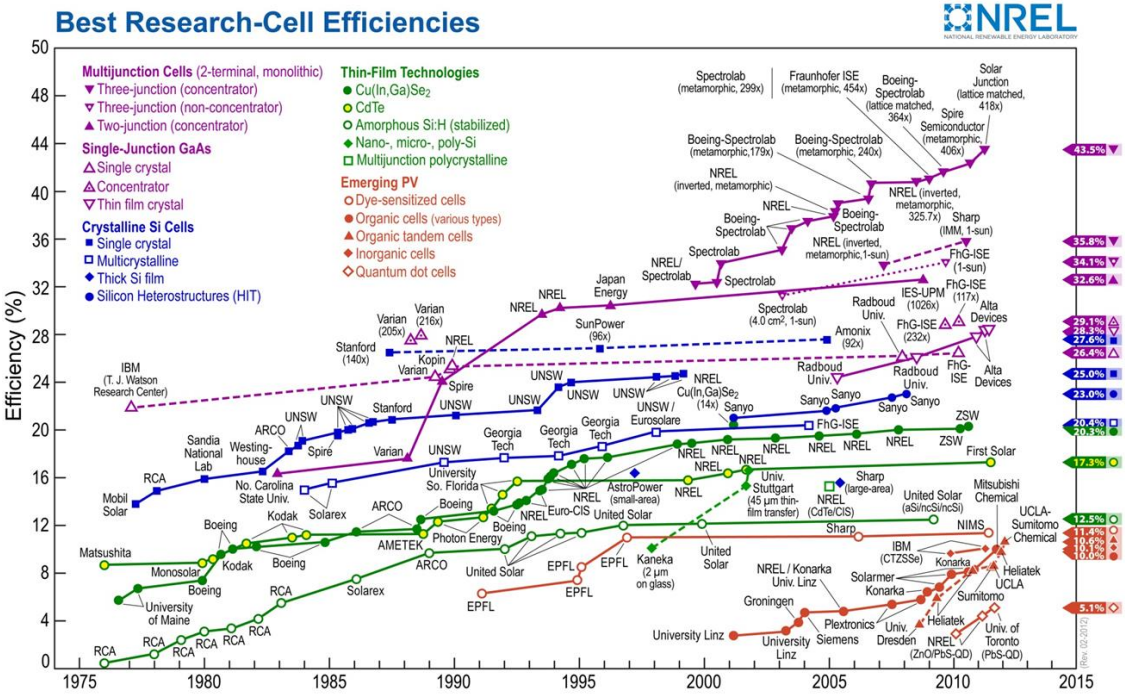

Figure 1.6 Type of photovoltaic devices and the conversion efficiency revolution from 1975 to 2012.**[20]**

The efficiency of solar cell is one of the important parameter in order to establish this technology in the market. Presently, extensive research work is going for efficiency improvement of solar cells for commercial use. The efficiency of monocrystalline silicon solar cell has showed a very good improvement year by year. It starts with only 15% in 1950s and then increased to 17% in 1970s and continuously to increase up to 28% nowadays. The polycrystalline solar cell also achieved 19.8% efficiency to this date but the commercial efficiency of polycrystalline is coming in between 12% and 15%. The monocrystalline solar cell has 24.8% efficiency, polycrystalline cells with 20.3% and thin film technology with 19.9% in 2010, respectively, under standard test conditions (i.e., irradiance of 1,000 W/m^2, AM 1.5, 25˚C). The theoretical Shockley-Queisser limit of a single-junction cell with an energy bandgap of crystalline silicon is 31% energy conversion efficiency.**[21]**

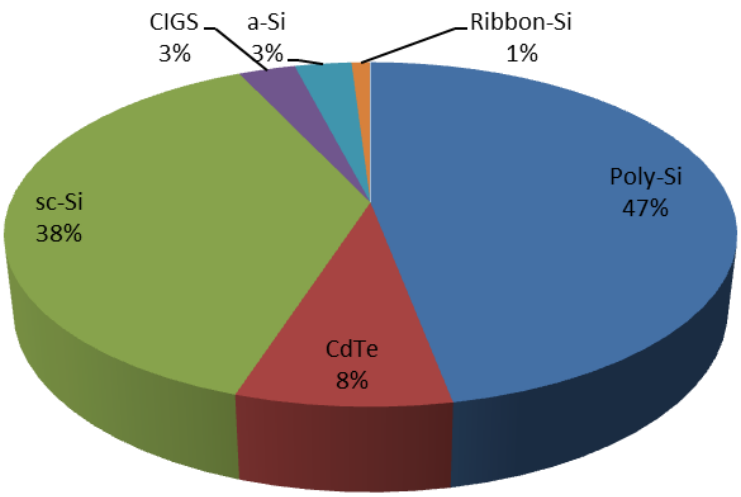

Figure 1.7 Market shares by different photovoltaic device technologies in 2011.**[22]**

From the Figure 1.6, it can be seen that GaAs has the highest efficiency among all other solar cell materials with 41.6% efficiency by so-called tandem cell. This cell stacks several pn junctions with different compositions. Each junction has a different bandgap and is responsible for light absorption in the certain portion of the solar spectrum.

The current solar cell industry is dominated by Si with nearly 90% of the market. Figure 1.7 shows the 2011 market shares by different solar cell technologies, with poly-Si leading the way at 48%, followed by sc-Si at 38%. Combination of all the thin film technologies has 14% of the market. A noticeable trend in the solar industry over the last ten years is that the market share for poly-Si cells has expended significantly, cutting into the market shares of a-Si as well as sc-Si cells.**[22]** With the shortage of Si material in recent years, the market shares of CdTe and CIGS are also expending.

1.3 Photovoltaic devices: Oxide thin film

1.3.1 Dependence of theoretical conversion efficiency on absorbing layer energy

The Shockley Queisser (SQ) Limit refers to the maximum theoretical efficiency of a perfect solar cell using a pn junction to extract electrical power. It was first calculated by William Shockley and Hans Queisser in 1961.**[21]** A solar cell's energy conversion efficiency is the percentage of power converted from sunlight to electrical energy under standard test condition. Figure 1.7 shows the relationship between theoretical energy conversion efficiency and bandgap energy of semiconductor. The modern SQ Limit calculation is a maximum efficiency of 30% for any type of single junction solar cell. The original calculation by Shockley and Queisser was 28% for a silicon solar cell.

Photovoltaic device technologies are dominated by Si by approximately 90% of the market and CIGS is also expending due to the shortage of Si material in recent years. Si and CIGS have narrow bandgap energy of 1.1 and 1.15 eV, respectively; which is suitable for single-junction solar cell with theoretical conversion efficiency about 28%. Bandgap is the most important material properties that limiting photovoltaic device power conversion efficiency, which determines the rate of photon absorption. Therefore, a higher bandgap between 1.6 and 2.1 eV is required to complement a silicon-based bottom layer in a tandem device structure theoretically capable of supporting efficiencies higher than 40%. Thus, Cu_2O is a p-type semiconductor with wide bandgap energy of 2.1 eV, which is appropriate for the application as the top layer of tandem cell (multi-junction thin film solar cell) with conversion efficiency of >40%. On the contrary, 1.4 eV-p-type semiconducting CuO show the highest theoretical conversion efficiency of 30%, suitable for the single-junction solar cell.

1.3.2 Cu_2O-based photovoltaics devices

Recently, the need for sustainable power generation has encouraged research into a variety of photovoltaic systems, which have the potential to cope with the global energy crisis in the future. Cuprous oxide (Cu_2O) is a p-type semiconductor with the band-gap energy of 2.1 eV **[23]** has received broad attention as a light-absorbing layer in a photovoltaic device, because of its non-toxicity, abundance, and theoretical conversion efficiency of 18%. Some researchers reported already that there was no homojunction PV device; PV devices have to be constructed as heterojunctions with an n-type, wide band gap window material, typically out of the family of transparent conducting oxides. The Cu_2O-based PV devices were classified into super-straight type and substrate-type structure. The super-straight type PV device consists of Cu_2O layer which is deposited on the n-ZnO and transparent conductive window layer prepared on glass substrate. The sunlight is introduced from the lower glass substrate side. On the other hand, the substrate-type PV device is PV devices with the n-ZnO transparent conductive window layers are stacked on the Cu_2O layer. The sunlight is introduced from the upper n-ZnO side. The conversion efficiency obtained up to 2015 for the Cu_2O/ZnO heterojunctions with their device structure are shown in Table 1.2. So far, the super-straight type PV device could be fabricated by only electrodeposition technique due to the difficulties in controlling the characteristic by the deposition onto n-type semiconductors. And all the Cu_2O layers used in the super-straight type PV devices were polycrystalline with a random orientation and contained some amount of impurity, and high impurities and defects in deep level such as copper and oxygen vacancies; which deteriorated the electrical characteristics and device performance. Since, the substrate-type PV device has advantage over the super-straight type PV device which is availability of annealing at elevated temperature and the ease of controlling the characteristics of the p-type semiconductors, most of the Cu_2O/ZnO heterojunction was constructed with substrate-type structure. The

substrate-type PV device has been used for the conventional compound devices such as CIGS and CdTe.

From Table 1.2, most of the research effort has therefore been focused on heterojunction PV devices, pairing Cu_2O with ZnO and its doped variations. It can be noted that the efficiencies and the open-circuit voltages of the devices varied widely depending on the synthesis method used. According to these data, the highest conversion efficiency of 6.1% has been reported for the AZO/Al-doped Ga_2O_3/Na-doped Cu_2O PV device prepared by a thermal oxidation of metallic Cu sheet in air followed by a vacuum-based pulse-laser deposition (PLD) of Ga_2O_3 and AZO layers.**[24]** In contrast, the electrodeposition process in aqueous solutions is a well-known technique due to several advantages such as low-fabrication cost, low temperature, ambient pressure processing, controllable film thickness, and possible large scale deposition. The second highest conversion efficiency of 1.28% is the randomly oriented Cu_2O/ZnO PV device prepared by only electrodeposition, previously reported in 2007 by Izaki et. al.**[25]** By using the similar procedure for the electrodeposition of Cu_2O layer, but instead of using KOH, consuming LiOH has increased the conversion efficiency of the PV device prepared only by electrodeposition to 1.43%.**[26]**

Although the Shockley-Quisser efficiency limit for Cu_2O is about 20%, the maximum efficiency realized using oxidized Cu metal foils [24] and electrodeposited Cu_2O layer [25] are significantly below the limit. This low record efficiency comes from a variety of factors that remain poorly understood in Cu_2O, including poor collection of minority carriers, un-optimized band structure in the device structure, and high surface recombination.

Table 1.2 Latest developments of Cu_2O-based PV device efficiency.

Device structure	Type of junction	PCE %	Voc (V)	p–n junction formation	Ref.
	Cu_2O-based junctions formed in vacuum				
Substrate-type	AZO/Al-Ga_2O_3/Na-Cu_2O	6.1	0.84	PLD	[24]
Substrate-type	AZO/Ga_2O_3/Cu_2O	5.38	0.8	PLD	[27]
Substrate-type	AZO/$Zn_{0.91}Mg_{0.09}O$/Cu_2O	4.31	0.73	PLD	[28]
Substrate-type	AZO/ZnO/Cu_2O	4.13	0.71	PLD	[29]
Substrate-type	AZO/Ga_2O_3/Cu_2O	3.97	1.2	ALD	[30]
Substrate-type	AZO/ZnO/Cu_2O	3.83	0.69	PLD	[31]
Substrate-type	AZO/a-ZTO/Cu_2O	2.85	0.62	ALD	[32]
Substrate-type	AZO/a-ZTO/Cu_2O	2.65	0.55	ALD	[33]
Substrate-type	AZO/Cu_2O	2.53	0.55	PLD	[27]
Substrate-type	ITO/ZnO/Cu_2O	2.01	0.6	IBS	[34]
Substrate-type	ZnO:Ga/Cu_2O	1.52	0.41	VAPE	[35]
Substrate-type	AZO/Cu_2O	1.39	0.4	dc-MSP	[35]
Substrate-type	AZO/Cu_2O	1.21	0.41	PLD	[36]
	Cu_2O-based junctions formed without vacuum				
Super-straight type	ZnO/Cu_2O	1.43	0.54	ECD	[26]
Super-straight type	ZnO/Cu_2O	1.28	0.59	ECD	[25]
Super-straight type	ZnO/Cu_2O/Cu_2O+	0.9	0.32	ECD	[37]
Super-straight type	ZnO/Cu_2O	0.47	0.28	ECD	[38]
Super-straight type	ZnO/Cu_2O	0.41	0.32	ECD	[39]
Substrate-type	ZnO/Cu_2O	1.46	0.49	AALD	[40]
Substrate-type	ITO/$Zn_{0.79}Mg_{0.21}O$/Cu_2O	2.2	0.65	AALD	[40]

1.4 Research Objective

Our research is focusing on the device structure of electrodeposited p-Cu_2O-based PV device, and, the improvement of the quality and purity of the p-Cu_2O layer which act as an absorbing layer in the p-n heterojunction is indispensable. Since the diffusion length of the photo-generated carriers is a function of mobility and relaxation time, the active region to generate the carriers in the Cu_2O layer is limited to the region at the heterointerface with the ZnO layer. The poor collection of photo-generated carriers could be due to the low mobility. The low mobility in the random-orientation of Cu_2O layer for super-straight type PV device has been changed into substrate-type PV device with highly oriented <111>-Cu_2O layer with increased mobility. The substrate-type structure has made possible to control the characteristic of p-Cu_2O layer. The final objective of this study is to construct high photovoltaic performance of Cu_2O-based PV device using various method including electrodeposition, sputtering and sol gel method, and to characterize the morphological, structural, optical and electrical properties of the PV device. The successfulness of the objectives is expected by completed the following tasks:

- To investigate the super-straight-type (SST) electrodeposited ZnO-nanowire/Cu_2O photovoltaic device with highly resistive ZnO intermediate layer.
- To investigate the growth mechanism of the substrate-type (0001)-n-ZnO layer on (111)-p-Cu_2O layer by using photo-assisted electrodeposition.
- To investigate the photo-assisted electrochemical construction of (0001)-n-ZnO/(111)-p-Cu_2O photovoltaic devices with intermediate TiO_2 layer.
- To fabricate the Aluminum-doped Zinc oxide (AZO) layer using radio frequency magnetron sputtering on (111)-p-Cu_2O photovoltaic device with electrodeposition.

1.5 Outline of this study

This study aims to overcome the photovoltaic device defects currently restricting the photovoltaic performance. In the first chapter of this thesis, the introduction including the background of the research, the effect of climate change to the increase of CO_2 concentration in atmosphere, the introduction of renewable energy and potential of the photovoltaic device as an energy generation source, the literature review of this work and finally the objective of this study is discussed. Following the introduction in this chapter, I apply different device geometries and materials in order to improve the quality including the homogeneity, thickness and energy state of the photovoltaic devices.

The first stage is the investigation of the super-straight-type (SST) Cl:ZnO/Cu_2O PV device. This is due to the low mobility of the majority carrier (1.2 $cm^2 \cdot V^{-1} \cdot s^{-1}$) for the electrodeposited Cu_2O layer,**[25]** compared to the thermally oxidized Cu_2O layer **(**90 $cm^2 \cdot V^{-1} \cdot s^{-1}$**).[41]** Therefore, 1 apply ZnO nanowires in the SST Cl:ZnO/Cu_2O PV device to expand the active region near the heterointerface, aiming to increase the generated minority carriers. In **Chapter 2**, the investigation of the SST electrodeposited-Cl:ZnO-nanowires/Cu_2O photovoltaic device with highly resistive ZnO intermediate layer is discussed. To reduce the interfacial recombination loss cause by the Cl impurity, a highly resistive ZnO layer with thickness varied from 8.5 to 32 nm is inserted in between Cl:ZnO-nws and a random orientation of Cu_2O layer by using the conventional electrodeposition technique. The structural, morphological, optical, and electrical characterizations are carried out by X-ray diffraction, X-ray photoelectron spectroscopy, scanning electron microscopy, optical absorption spectra, and Hall measurements. The insertion of the ZnO-nanowire and i-ZnO layer shows a significant enhancement in conversion efficiency by suppressing the recombination loss at the interface.

The second stage is the investigation of substrate-type ZnO/Cu_2O PV devices. It involves the chapter 3 to chapter 5. The low quality and mobility in the Cu_2O layer because of polycrystalline with a random orientation contained high impurity and defects decrease the photovoltaic performance of SST PV devices especially the Jsc. The improvement of the quality and mobility of the Cu_2O layer was realized by controlling the preferred orientation using an electrochemically heteroepitaxial growth and annealing under an optimized condition.**[42]** In **Chapter 3**, I investigate the growth mechanism of n-type semiconductor ZnO layer on the (111)-oriented-p-Cu_2O layer and discuss the correlation between ZnO microstructure and the device performance for constructing substrate-type ZnO/Cu_2O PV device. The ZnO layer is prepared by photo-assisted electrodeposition method and the (111)-oriented Cu_2O layer is prepared by conventional electrodeposition method on (111)Au/Si(100) substrate. The structural, morphological, optical, and electrical characterizations are carried out by X-ray diffraction, scanning electron microscopy, optical absorption spectra, and current density-voltage curve measurements. By controlling the deposition time, the ZnO layer is stacked on the highly oriented (111)-Cu_2O layer, and the photovoltaic performance could be obtained under AM 1.5 G illuminations.

Chapter 4 discussed the investigation of the insertion of TiO_2 intermediate layer in the substrate-type ZnO/(111)-Cu_2O PV device. Since, the photo-assisted electrodeposited ZnO layer consist of pores, the TiO_2 intermediate layer is developed to mitigate the interfacial defect-assisted recombination at the ZnO/(111)-Cu_2O PV device. The TiO_2 intermediate layer is prepared by sol gel method. And, the TiO_2 layer thickness is controlled by sol concentration and spin coating speed. The structural, morphological, optical, and electrical characterizations are carried out by X-ray diffraction, scanning electron microscopy, optical absorption spectra, and current density-voltage curve measurements. The insertion of TiO_2 layer decreases the recombination loss at the ZnO/(111)-Cu_2O interface. Moreover, stacking

the ZnO/TiO_2/(111)-Cu_2O PV device with AZO layer, shows an increase the short-circuit current density.

In **Chapter 5**, I develop Cu_2O-based photovoltaic devices comprising AZO/(111)-Cu_2O PV device and discuss the Cu_2O layer thickness on device performance. Due to the existence of pores in the electrodeposited ZnO layer and restriction in the baking temperature for TiO_2 layer, the AZO layer is directly deposited onto the (111)-Cu_2O layer. The AZO layer acts as a carrier transporter to take out the minority carrier from the Cu_2O layer. The Aluminum-doped ZnO (AZO) is prepared on Cu_2O layer by sputtering technique. The structural, morphological, optical, and electrical characterizations are carried out by X-ray diffraction, X-ray photoelectron spectroscopy, scanning electron microscopy, optical absorption spectra, and Hall measurements. By controlling the Cu_2O layer thickness, the carrier diffusion length and optical depth are tuned to create an optimum minority carrier, resulted in maximum value in the device short-circuit current density.

In the last which is **Chapter 6**, the summary of all results obtained was made.

REFERENCES

[1] Intergovernmental Panel on Climate Change report (IPCC), 2014.

[2] Hönisch, B., N. G. Hemming, et al. Atmospheric carbon dioxide concentration across the Mid-Pleistocene transition, Science, 324 (5934), 1551 (2009).

[3] Lüthi, D., M. Le Floch, et al. 2008. High-resolution carbon dioxide concentration record 650,000-800,000 years before present, Nature, 453, (7193), 379 (2008).

[4] Petit, J. R., J. Jouzel, et al. Climate and atmospheric history of the past 420,000 years from the Vostok ice core, Antartica, Nature, 399 (6735), 429 (1999).

[5] Boden, T., G. Marland, et al. Global CO_2 emissions from fossil-fuel burning, cement manufacture, and gas flaring: 1751-2008. U. S. Department of Energy, Carbon Dioxide Information Analysis Center (2011).

[6] Peters, G. P., M. Andrew, et al. The challenge to keep global warming below 2 ˚C, Nature Climate Change, 3 (1), 4-6 (2013).

[7] International Energy Egency (IEA), 2010.

[8] Renewable Energy Policy Network for the 21st century, REN 21, 2010.

[9] Special report on renewable energy source and climate change mitigation (SRREN), IPCC (2011).

[10] U.S. Department of Energy, Basic Research Needs for Solar Energy Utilization (2005).

[11] Meng Tao, The Electrochemical Society Interface (Winter), 2008.

[12] E. Becquerel, Comptes, 9 (144), 561 (1839).

[13] Palz, Wolfgang, Power for the World - The Emergence of Electricity from the Sun. Belgium: Pan Stanford Publishing. p. 6 (2010).

[14] C. E. Fritts, American Journal of Science, 26, 465 (1883).

[15] R. Ohl, U. S. Patent 2, 402, 662 (1946).

[16] D. Chapin, C. Fuller, and G. Pearson, J. Appl. Phys., 25 (5), 676 (1954).

[17] U. S. Department of Energy, Basic Research Needs for Solar Energy Utilization (2005).

[18] G. Tsilingiridis, G. Martinopoulos, and N. Kyriakis, Renewable Energy, 29 (8), 1277 (2004).

[19] 「太陽電池の基礎と応用」小長井　誠、山口　真史、近藤　道雄、培風館、2010.

[20] National Renewable Energy Laboratory, NREL.

[21] W. Shockley, H. J. Queisser, J. Appl. Phys., 32(3), 510 (1961).

[22] Paula Mints, Navigant consulting PV services program.

[23] K. Mizuno, M. Izaki, K. Murase, T. Shinagawa, M. Chigane, M. Inaba, A. Tasaka, Y. Awakura, J. Electrochem. Soc., 152, C179 (2005).

[24] T. Minami, Y. Nishi, T. Miyata, Appl. Phys. Express, 8, 022301 (2015).

[25] M. Izaki, T. Shinagawa, K. T. Mizuno, Y. Ida, M. Inaba, A. Tasaka, J. Phys. D: Appl. Phys., 40, 3326 (2007).

[26] K. Fujimoto, T. Oku, T. Akiyama, Appl. Phys, Express, 6, 086503 (2013).

[27] T. Minami, Y. Nishi, T. Miyata, Appl. Phys. Express, 6, 044101 (2013).

[28] T. Minami, Y. Nishi, T. Miyata, S. Abe, ECS Trans., 2886 (2012).

[29] Y. Nishi, T. Miyata,T. Minami, Thin Solid Films, 528, 72 (2013).

[30] Y. S. Lee, D. Chua, R. E. Brandt, S. C. Siah, J. V. Li, J. P. Mailoa, S. W. Lee, R. G. Gordon, T. Buonassisi, Adv. Mater., 26, 4704 (2014).

[31] T. Minami, Y. Nishi, T. Miyata, J. Nomoto, Appl. Phys. Express 4, 062301 (2011).

[32] S. W. Lee,Y. S. Lee, J. Heo, S. C. Siah, D. Chua, R. E. Brandt, S. B. Kim, J. P. Mailoa, T. Buonassisi, R. G. Gordon, Adv. Energy Mater., 1301916 (2014).

[33] Y. S. Lee, J. Heo, S. C. Siah, J. P. Mailoa, R. E. Brandt, S. B. Kim, R. G. Gordon, T. Buonassisi, Energy Environ. Sci., 6, 2112 (2013).

[34] A. Mittiga, E. Salza, F. Sarto, M. Tucci, R. Vasanthi, Appl. Phys. Lett., 88, 163502 (2006).

[35] T. Minami, T. Miyata, K. Ihara, Y. Minamino, S. Tsukada, Thin Solid Films, 494, 47 (2006).

[36] T. Minami, H. Tanaka, T. Shimakawa, T. Miyata, H. Sato, J. Appl. Phys., 43, L917 (2004).

[37] A. T. Marin, D. Munoz-Rojas, D. C. Iza, T. Gershon, K. P. Musselman, J. L. MacManus-Driscoll, Adv. Functional Mater., 23, 3413 (2013).

[38] K. P. Musselman, A. Wisnet, D. C. Iza, H. C. Hesse, C. Scheu, J. L. MacManus-Driscoll, L. Schmidt-Mende, Adv. Mater., 22, E254 (2010).

[39] S. S. Jeong, A. Mittiga, E. Salza, A. Masci, S. Passerini, Eletrochimica Acta, 53, 2226 (2008).

[40] Y. Ievskaya, R. L. Z. Hoye, A. Sadhanala, K. P. Musselman, J. L. MacManus-Driscoll, Solar Energy Materials & Solar Cells, 135, 43 (2015).

[41] H. Tanaka, T. Shimakawa, T. Miyata, H. Sato, T. Minami, Thin Solid Films, 469, 80 (2004).

[42] T. Shinagawa, M. Onoda, B. M. Fariza, J. Sasano, M. Izaki, J. Mater. Chem. A, 9182 (2013).

CHAPTER 2

Super-straight type Cu_2O/ZnO photovoltaic device prepared by electrochemical reactions and the photovoltaic performance

2.1 Introduction

Due to difficulties in doping Cu_2O to n-type semiconductor, the most common approach to construct PV device is using a ZnO/Cu_2O heterojunction structure. The Cu_2O layer for photovoltaic applications has been prepared by the thermal oxidation of a metallic Cu sheet in air at 1273 K,**[2]** sputtering,**[3]** and electrodeposition in an aqueous solution.**[4]** The record

efficiencies of the photovoltaic devices, however, still remain low. The conversion efficiency of 6.1 % has been reported for a substrate-type AZO/Al:Ga_2O_3/Na:Cu_2O PV device with the Cu_2O layer prepared by thermal oxidation with ZnO and Ga_2O_3 layers prepared by a pulse-laser deposition technique.**[5]** In contrary, solution chemical processes, including the electrodeposition, have several advantages over the thermal ones, and the conversion efficiencies of 3.97 % has been reported for the substrate-type AZO/ Ga_2O_3/ Cu_2O PV device with the Cu_2O layer prepared by electrodeposition with Ga_2O_3 and ZnO layers prepared by an atomic layer deposition.**[6,7]** The conversion efficiency, however, is limited, up to now, to 1.28% for the super-straight type ZnO/Cu_2O photovoltaic device prepared only by electrodeposition.**[4]**

In this chapter, an approach to reduce the impact of interface defects on the performance of Cu_2O-based PV device is demonstrated. By inserting a thin highly resistive ZnO layer between the absorber and the transparent conducting oxide layer, the photovoltaic performance of the Cl:ZnO-nws/Cu_2O PV device has been successfully improved.

2.2 Subjects in the Cu_2O/ZnO PV device and the challenge for the improvements

High mobility of the minority carriers in the Cu_2O layer can increase the carrier's diffusion length and the photovoltaic device conversion efficiency. The mobility of the majority carrier was reported to be 1.2 $cm^2 \cdot V^{-1} \cdot s^{-1}$ for the electrodeposited Cu_2O layer,**[8]** and the value was much lower than 90 $cm^2 \cdot V^{-1} \cdot s^{-1}$ reported for the thermally oxidized Cu_2O layer.**[9]** Since the diffusion length of the generated carriers by light irradiation is a function of the mobility and relaxation time, the active region to generate the carrier in the Cu_2O layer is limited to the region near the heterointerface with the ZnO layer. Musselman and co-workers have shown the advantage of using ZnO nanowires to expand the active region around the ZnO-nws.**[10]**

Moreover, electrodeposited Cl-doped ZnO-nws (Cl:ZnO-nws) can be used for this purpose due to its low resistivity.**[11]**

Despite of the low resistivity originates from the Cl impurity incorporated in the ZnO semiconductor;**[12]** there are challenges to dope ZnO-nanowires with Cl, that is impurities. The impurities present near the heterointerface act as recombination sites, resulting in a decrease in the photovoltaic performance. Fortunately, our previous report has demonstrated that the recombination loss is strongly reduced by inserting a highly resistive ZnO layer between the n- ZnO and phthalocyanine layers in the layered hybrid photovoltaic device.**[13]**

2.3 Objective of this study

In this study, we show the preparation of a super-straight type Cl:ZnO-nws/Cu_2O photovoltaic device by electrodeposition in aqueous solutions and effects of the insertion of the highly resistive ZnO (i-ZnO) layer on the photovoltaic performance. The Cl:ZnO-nws and i- ZnO layer were prepared in a zinc chloride aqueous solution saturated with a molecular oxygen precursor and a simple zinc nitrate aqueous solution, respectively. The i-ZnO layer was directly deposited on the Cl:ZnO-nws and suppressed the deposition of the Cu_2O layer on the Cl:ZnO-nws. They favored a bottom-up growth, starting from the near F-doped SnO_2-coated glass substrate (FTO) region.

2.4 Experimental procedures

The Cl:ZnO-nws layer was prepared on an FTO substrate (AGC Fabritech Co., Ltd., Type DU) by electrodeposition in an aqueous solution containing 0.2 mmol/L zinc chloride hydrate and 0.1 mol/L KCl at 353 K using a potentiostat (AUTOLAB PGSTAT30).**[14]** The solution

was saturated with molecular oxygen, and O_2 bubbling was maintained during the electrodeposition.**[15]** The FTO substrate was fixed and connected to a rotating disk electrode (RDE), and the rotation was carried out at a constant rotation speed of 300 rpm.**[16]** The electrodeposition was performed for 3600 s in a three-electrode cell at a potential of −1.0 V referenced to the saturated calomel electrode (SCE). The i-ZnO layer was prepared by electrodeposition at −1.0 to −1.2 V referenced to a Ag/AgCl electrode for 5−20 s in an aqueous solution containing 0.08 mol/L zinc nitrate hydrate **[17]** at 333 K using a potentiostat (Hokuto Denko, HA-501) connected to a coulomb meter (Hokuto Denko, HF-201). The Cu_2O layer was prepared by electrodeposition at 313 K in an aqueous solution containing a 0.4 mol/L copper (II) acetate hydrate and 3 mol/L lactic acid. The solution pH was adjusted to 12.5 with a KOH aqueous solution. The electrodeposition was carried out at −0.4 V referenced to a Ag/AgCl electrode using a potentiostat (Hokuto Denko, HABF-501A). The solutions were prepared with reagent-grade chemicals and distilled water purified by a Millipore Elix Advantage system.

Before the electrodeposition of the Cl:ZnO-nws, the FTO substrate was successively cleaned in acetone and ethanol for 6 min each in an ultrasonic bath. These FTO substrates were immersed in an HNO_3 aqueous solution for 2 min, rinsed with distilled water, and then used for the experiment. After the Cu_2O deposition, a Au electrode with a size of 3 mm×3 mm was deposited on top of the Cu_2O layer by vacuum evaporation (ULVAC, VPC-260F system).

An X-ray photoelectron spectroscopy (XPS) analysis was performed using an ULVAC-PHI Model 5700MC with monochromated Al Kα radiation at a pressure of around 1.6×10^{-8} Pa. Binding energies were corrected by referencing the C 1s signal of the adventitious contamination hydrocarbon to 284.8 eV. The electron pass energy in the analyzer was set at 11.75 eV corresponding to 0.57 eV of full width at half-maximum (FWHM) of the Ag 3d5/2

peak at 368.35 eV. The Ar sputtering was carried out for 1 min at 1 kV by a differential pumping type ion etching gun. The X-ray diffraction patterns were recorded by a θ/2θ scanning technique with monochromated Cu Kα radiation operated at 40KV and 200 mA using a Rigaku RINT2500. The optical absorption spectra were measured using a UV−vis−near- infrared spectrophotometer (Hitachi, U4100) with reference to the bare substrate. Electron microscopy observations were carried out using afield-emission scanning electron microscope (FE-SEM, Hitachi, SU8000). The electrical characterization was carried out by the van der Pauw method using a Hall effect measuring system (Toyo Technica, Resitest 8310) in air at ambient temperature and 0.3 T magnetic field. The samples were prepared by mechanically splitting them off from the glass substrate followed by fastening in epoxy resin (Araldite 2091). Four in electrodes were prepared on the ZnO samples using the vacuum evaporation system. The electrical characteristic was estimated by recording the current density−voltage curves in dark and under AM1.5G illumination with a 100 $mW \cdot cm^{-2}$ power (Bunko Keiki, OTENTO-SUN III solar simulator system) by a Keithley 2400 source meter.

2.5 Results and discussion

2.5.1 Morphological characteristic of Cl:ZnO-nws layer on FTO substrate with i-ZnO

The FE-SEM images of the side and top surface of the Cl:ZnO-nws before and after the electrodeposition of i- ZnO for 5, 10, and 20 s are shown in Figure 2.1. The Cl:ZnO-nws grew straight from the FTO substrate, and the bare surface of the FTO substrate could be observed between the Cl:ZnO-nws. The mean length and width of the Cl:ZnO-nws were estimated to be 1.13 μm and 85 nm, respectively, and the hexagonal facets corresponding to the (0001) planes could be observed on the top views.**[18]** The ZnO nuclei deposited during

the initial stage of the growth possessed a random orientation due to the random orientation of the SnO_2 polycrystalline layer of the FTO substrate, and then the ZnO nuclei grew in the direction of the ⟨0001⟩ orientation due to the lowest surface energy in the wurtzite structure, resulting in the formation of tilted Cl:ZnO-nws.**[19]** Both the side and top surfaces of the Cl:ZnO-nws were very smooth. The electrodeposition of the i-ZnO for the deposition time of 5 to 20 s did not affect the length and orientation of the Cl:ZnO-nws. Isolated small grains of approximately 15.5 nm in size could be observed on both the side and top surfaces of the Cl:ZnO-nws after the electrodeposition for 5 s, and after 20 s, the grains with a size of approximately 22.5 nm were deposited over the entire side and top surfaces of the Cl:ZnO-nws (Figure 1d). The width of the Cl:ZnO-nws increased with an increase in the deposition

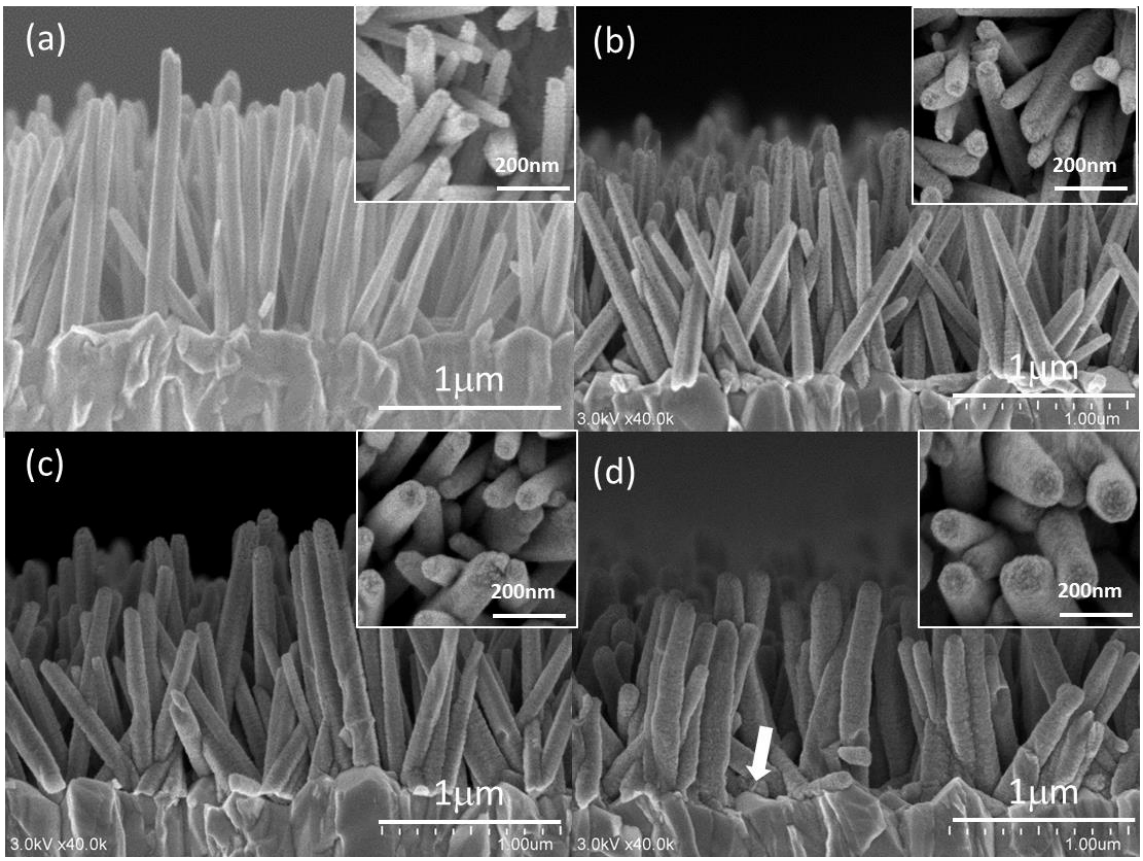

Figure 2.1 Cross-sectional structures and surface morphology (inset) of Cl-doped ZnO nanowires (a) before and after coating with highly resistive i-ZnO layer for (b) 5 s, (c) 10 s, and (d) 20 s.

time and was estimated to be 102, 120, and 149 nm at 0, 5, 10, and 20 s, respectively. The thickness of the i-ZnO layer calculated from the difference in the wire width before and after the electrodeposition of i-ZnO was 8.5, 17, and 32 nm for 5, 10, and 20 s, respectively. The thickness (d, nm) linearly varied with the deposition time (t, s) according to d= 1.67t. The thickness of the i-ZnO layer was smaller than the grain size for the deposition times shorter than 10 s. This suggests the imperfect coverage of Cl:ZnO-nws with the i-ZnO grains. It was as denoted by the white arrows in Figure 2.2a. Some Cu_2O grains were directly deposited on the FTO substrate, but the bare surface of the FTO substrate could be clearly observed

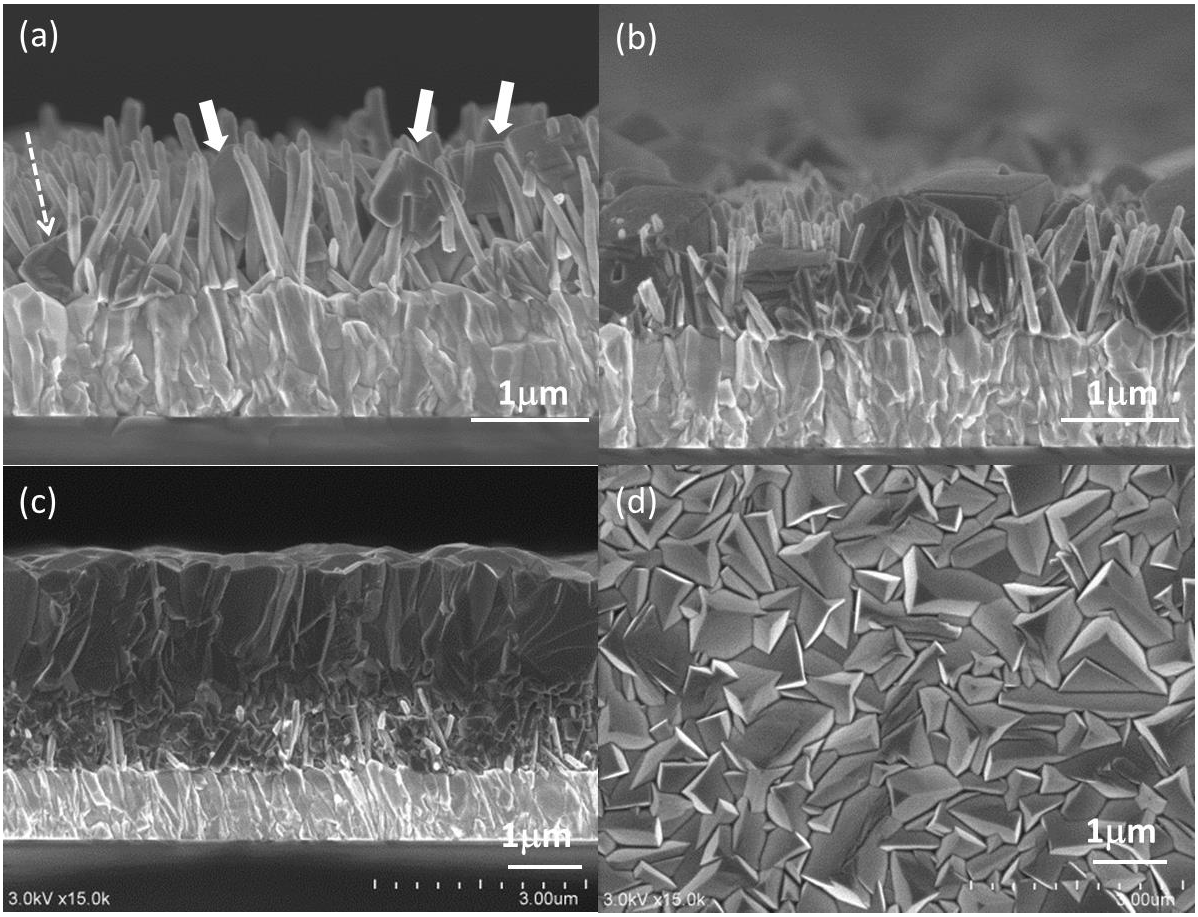

Figure 2.2 Cross-sectional structures of Cu_2O layers deposited on Cl-doped ZnO nanowires for electric charges of (a) 0.4, (b) 0.65, and (c) 1.7 $C \cdot cm^{-2}$. (d) The surface morphology of the Cu_2O layer.

between the Cl:ZnO-nws. The Cu_2O layer deposited for 0.65 $C \cdot cm^{-2}$ was a heterogeneous mixture of two types of grains and possessed an irregular surface due to the existence of the top edge of the Cl:ZnO-nws and of the flat surface of large Cu_2O grains (Figure 3b). Cu_2O grains with the size of 0.5−0.6 μm could be observed near the substrate, and some Cl:ZnO-nws were embedded in the Cu_2O grains, resulting from the growth of Cu_2O grains deposited on the FTO substrate at 0.4 $C \cdot cm^{-2}$. Moreover, large cubic Cu_2O grains with a size over 1.2μm were separately observed on the layer's outer part and originated from the Cu_2O grains deposited on the Cl:ZnO-nws. The Cl:ZnO-nws were embedded inside the Cu_2O layer, and no damage, such as fracture, could be observed. However, bare surface areas of the FTO substrate were still observed between the Cu_2O grains. A continuous Cu_2O layer with a thickness of 3.3 μm was formed at 1.7 $C \cdot cm^{-2}$, and the surface was very smooth (Figure 3c,d).

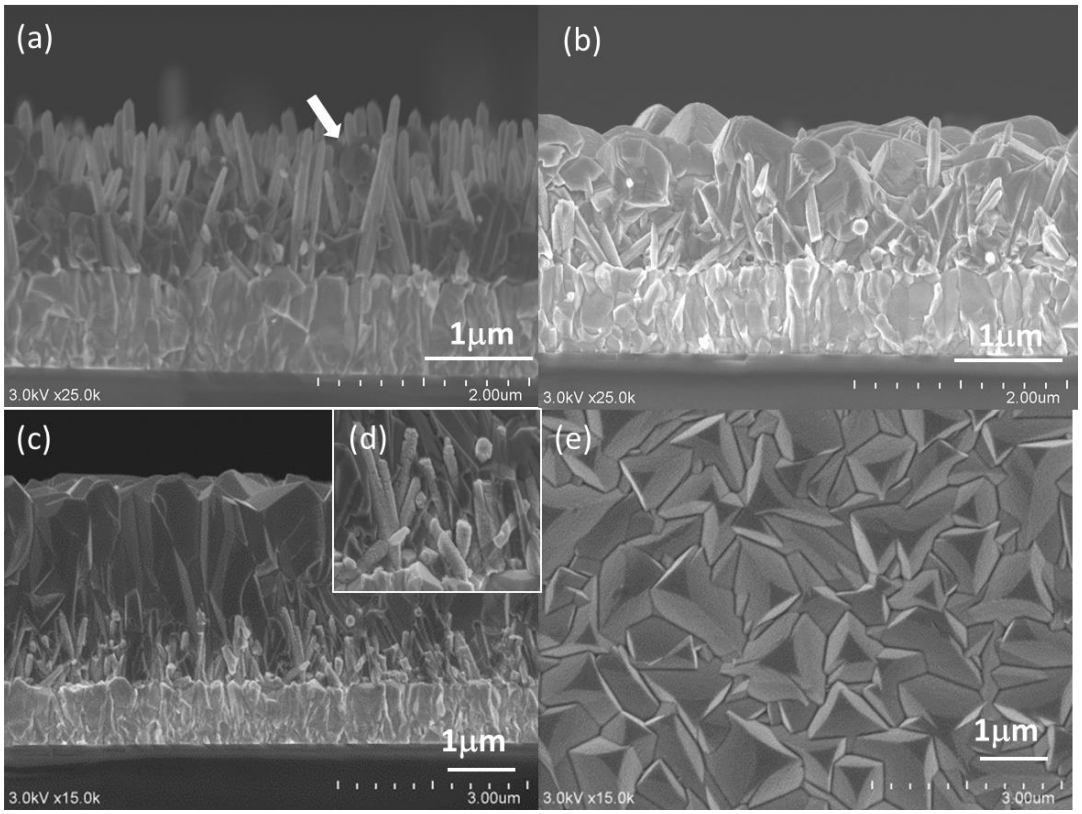

Figure 2.3 Cross-sectional structures of Cu_2O layers deposited on Cl-doped ZnO nanowires/i-ZnO for electric charges of (a) 0.4, (b) 0.65, and (c, d) 1.7 C·cm−2 . (e) The surface morphology of the Cu_2O layer.

No defects, such as pores, could be found throughout the layer thickness, and the space observed between the Cu_2O grains at 0.65 $C \cdot cm^{-2}$ disappeared, filled with the Cu_2O grains. The Cu_2O layer was composed of a mixture of granular crystallites with a size of~0.3 μm and upper columnar grains of ~2 μm in length and 1 μm in width. The small Cu_2O crystallites were observed at a thickness below approximately 1.3 μm corresponding to the length of the Cl:ZnO-nws. The columnar Cu_2O grains were formed at a thickness over 1.3 μm and grew in the direction normal to the surface. The surface of the resultant Cu_2O layer was composed of aggregated angular grains with a size of approximately 1.0 μm, and no defects, such as pores, could be observed on the surface (Figure 2.2d).

Figure 2.3 shows the cross-sectional structures of the Cu_2O layers deposited on the Cl:ZnO-nws/i-ZnO for the electric charges of 0.4, 0.65, and 1.7 $C \cdot cm^{-2}$ and the surface morphology of the resultant Cu_2O layer. The i-ZnO layer was deposited at −1.1 V for 20 s. Almost all the Cu_2O grains with a size of approximately 0.35μm were directly deposited on the FTO substrate, and the Cu_2O grains deposited on the Cl:ZnO-nws/i-ZnO was rarely observed, as denoted by the white arrows in Figure 2.3a. The surface of the FTO substrate between the Cl:ZnO-nws/i-ZnO was covered with the deposited Cu_2O grains. No change in the length and width of the Cl:ZnO-nws could be observed before and after the Cu_2O deposition. After 0.65 $C \cdot cm^{-2}$ of electric charge exchanged (Figure 2.3b), the Cu_2O grains embedded the Cl:ZnO-nws/i-ZnO, and the space between the Cl:ZnO-nws/ i-ZnO was perfectly filled by the Cu_2O phase. Defects, such as pores, were not observed throughout the Cu_2O layer. For an electric charge exchange of 1.7 $C \cdot cm^{-2}$ (Figure 4c−e), the Cu_2O layer was composed of aggregated columnar Cu_2O grains grown in direction normal to the surface. No defects, such as pores, were observed throughout the layer thickness. The thickness of the Cu_2O layer was estimated to be approximately 1.4 μm (0.65 $C \cdot cm^{-2}$) and 3.3 μm (1.7 $C \cdot cm^{-2}$) corresponding to the value theoretically calculated from the electric charge with the assumption of a 100% current

efficiency. The surface of the resultant Cu_2O layer was composed of aggregates of angular grains without any pores (Figure 2.3e). Also, small i-ZnO grains could be observed on the Cl:ZnO-nws even after the Cu_2O electrodeposition (Figure 2.3d).

2.5.2 Electrochemical stacking of ZnO-nanowires prepared by electrochemical reaction

The electrodeposition of the i-ZnO layer induced the suppression of the Cu_2O deposition on the Cl:ZnO-nws and the preferential bottom-up growth starting from the FTO substrate. This resulted in the formation of the Cu_2O layer embedding the Cl:ZnO-nws/i-ZnO. The cathodic electrodeposition of the Cu_2O layer from the alkaline aqueous solution containing the cupric lactate complex is described as follows:**[22]**

$$Cu^{2+} + 2L^{-} \rightarrow [Cu^{II} - L_2] \quad (1)$$

with $[Cu^{II} - L_2]$:cupric lactate complex

$$[Cu^{II} - L_2] + e^{-} \rightarrow Cu^{+} + 2L^{-} \quad (2)$$

$$Cu^{+} + OH^{-} \rightarrow [Cu^{I}OH] \quad (3)$$

$$2[Cu^{I}OH] \rightarrow Cu_2O + H_2O \quad (4)$$

The electrons needed for the formation of the Cu_2O deposition were supplied from both the FTO substrate and Cl:ZnO-nws, and the supplement from the Cl:ZnO-nws was suppressed by the i-ZnO layer. The Cl:ZnO-nws contained a certain amount of a Cl^{-} impurity originating from the zinc chloride and potassium chloride in the solution, and the Cl^{-} impurity acted as a donor in the ZnO semiconductor.**[23]**

The continuous Cl:ZnO layer prepared from a 5 mmol/L zinc chloride solution with a saturated molecular oxygen was electrically characterized with the van der Pauw method and

showed a resistivity of 4.4×10^{-2} Ω·cm with a 1.5×10^{19} cm^{-3} carrier concentration and a mobility of 9.57 $cm^2 \cdot V^{-1} \cdot s^{-1}$. The carrier concentration nearly agreed with 6.2×10^{19} cm^{-3} reported for the Cl:ZnO-nws prepared in the same manner.**[24]** The resistivity on the order of 10^8 Ω·cm was obtained for the 1 μm thick i-ZnO layer prepared at −1.1 V by the van der Pauw method; however, the carrier concentration and mobility could not be estimated because of the high layer resistivity originating from the small grain size and defects incorporated into the ZnO layer.**[25]** The change in the growth of the electrodeposited Cu_2O layer by the insertion of the i-ZnO layer was attributed to the high resistivity of the i-ZnO layers. The bottom-up growth was reported for the Cu_2O electrodeposition on ZnO-nanorods and for the ZnO seed layer prepared in a zinc nitrate aqueous solution used for the preparation of the i-ZnO layer.**[26]**

2.5.3 Structural characteristic of Cl:ZnO-nws layer on FTO substrate with i-ZnO

Figure 2.4 shows the Zn 2p, O 1s, and Cl 2p electron spectra for the Cl:ZnO-nws before and after the electrodeposition of the i-ZnO layer for 20 s. The escaping depth of an electron was approximately 3−4 monolayers due to the electron energy ranging from 194 to 1026 eV. The incident Al Kα radiation was irradiated at an angle of 45° in the direction normal to the sample surface, and the hemispherical analyzer was set at a direction normal to the sample surface. The electron spectra recorded here reflected the region near the top surface of the Cl:ZnO-nws with and without the i-ZnO layer. Both Zn 2p spectra showed a peak at the binding energy of 1022 eV, which corresponded to the Zn^{2+} state in ZnO.**[20]** The bare Cl:ZnO-nws showed a shoulder at ~531.2 eV in addition to the peak at 530 eV. The O^{2-} state in ZnO and the OH^- state in $Zn(OH)_2$ possessed binding energies of 530 and 531.2 eV, respectively.**[19]** The shoulder at 531.2 eV decreased by depositing the i-ZnO layer for 20 s,

while keeping the peak energy at 530 eV. The Ar sputtering was carried out to remove the surface contamination of the Cl:ZnO-nws using an ion etching gun prior to the measurements. Since the ion etching gun was placed in the analyzer chamber in a direction different from the incident X-ray source and analyzer, it was impossible to perfectly remove the surface contamination including $Zn(OH)_2$. The bare Cl:ZnO-nws showed a peak at 199 eV on the Cl2p electron spectrum, and the energy agreed with that for the Cl^- state in $ZnCl_2$.**[21]** The compound of ClO_4^- was reported to have a binding energy of around 208 eV.**[20]** The existence of the Cl 2p peak at 199 eV suggested that the Cl impurity incorporated into the ZnO was bound to the Zn cation. The Cl content calculated using the sensitivity factor **[20]** was estimated to be approximately 1% for the bare Cl:ZnO-nws. Also, the Cl content can be controlled by adjusting the preparation conditions such as the solution formulation, current density, and solution temperature.**[12]** The Cl 2p peak disappeared by depositing the i-ZnO layer for 20 s.

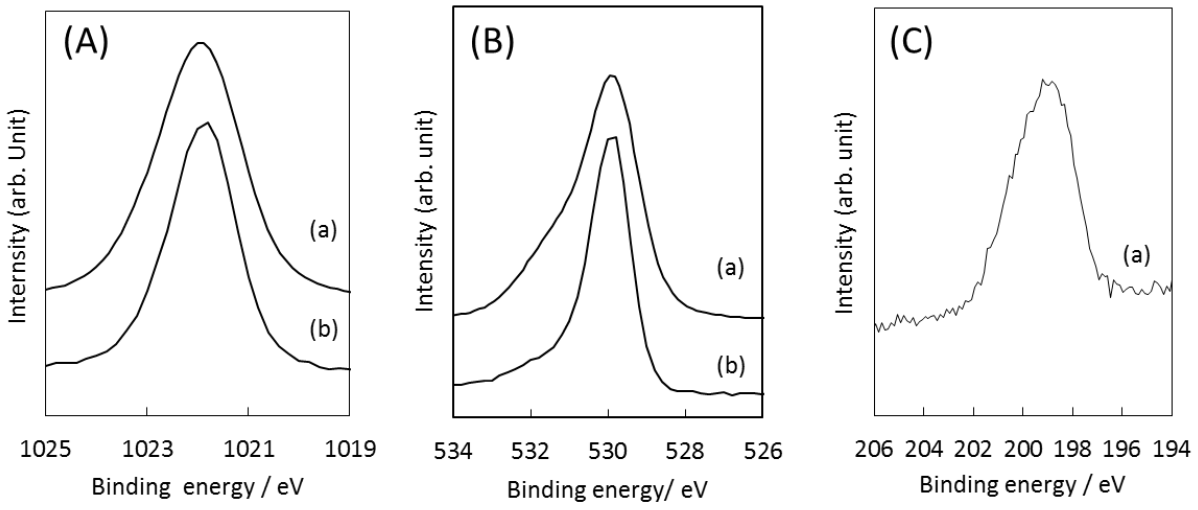

Figure 2.4 (A) Zn 2p, (B) O 1s, and (C) Cl 2p electron spectra for Cl-doped ZnO nanowires (a) before and (b) after electrodeposition of the i-ZnO layer for 20 s.

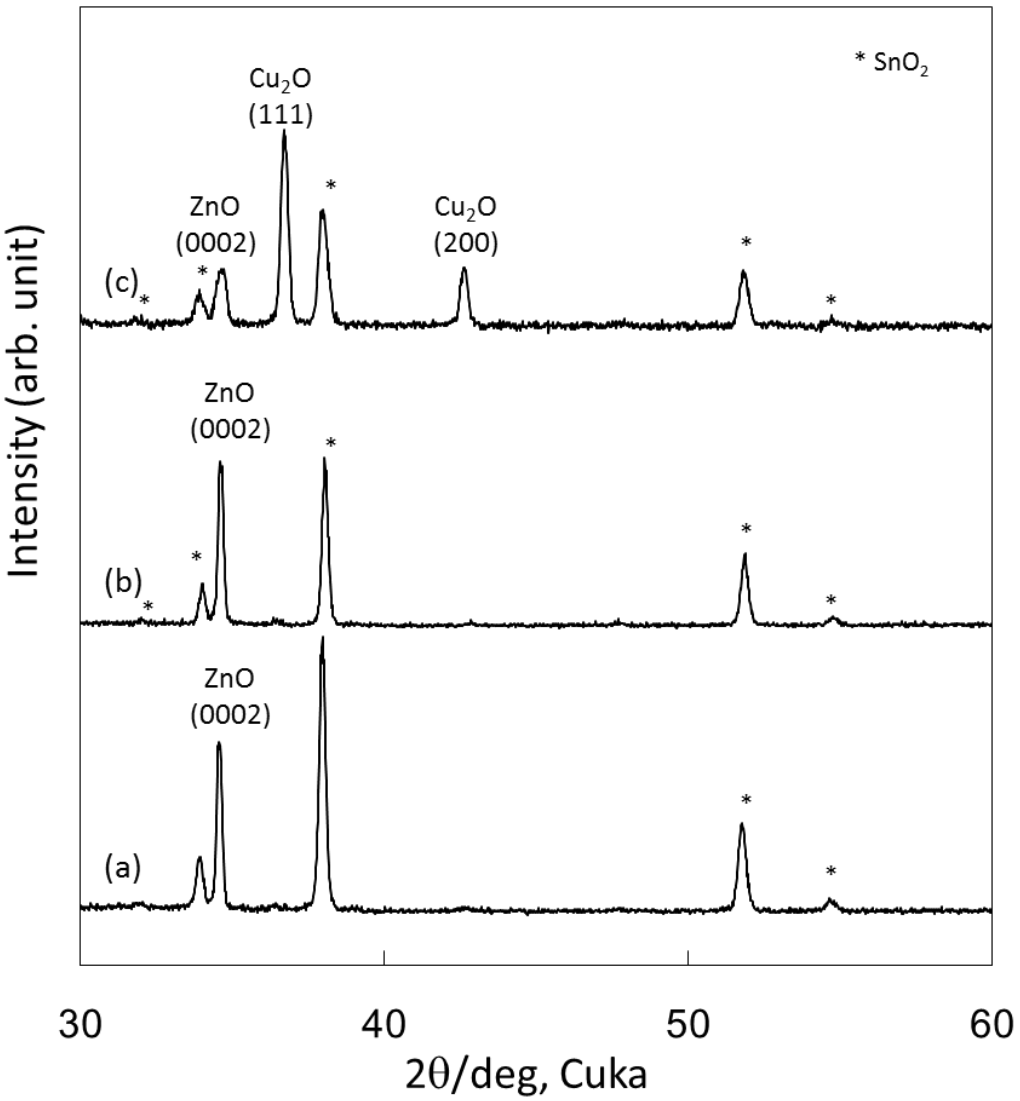

Figure 2.5 X-ray diffraction patterns of (a) Cl-doped ZnO nanowire, (b) Cl-doped ZnO nanowire/i-ZnO, and (c) Cl-doped ZnO nanowire/i-ZnO/Cu_2O structures.

Figure 2.5 shows X-ray diffraction patterns for Cl:ZnO-nws, Cl:ZnO-nws/i-ZnO, and Cl:ZnO-nws/i-ZnO/ Cu_2O. The X-ray diffraction patterns for the i-ZnO/ZnO-nws and Cu_2O /i-ZnO/ ZnO-nws structures were almost the same in profile and peak angles, irrespective of the deposition time of the i-ZnO. The Cl:ZnO-nws showed only one peak assigned to the reflection of the (0002) planes of the wurtzite ZnO crystal **[27]** in addition to those originating from the SnO_2 **[28]** of the FTO substrate, indicating the formation of a (0001)

preferred orientation. The electrodeposition of the i-ZnO layer had no effect on the intensity and angles of the diffraction X-ray pattern due to the thinness. The electrodeposition of the Cu_2O layer added two peaks assigned to the (111) and (200) planes of Cu_2O that are characteristic of the cubic cupric lattice **[29]** in addition to those originating from the ZnO and SnO_2. The X-ray diffraction pattern of the Cu_2O layer was almost the same in peak intensity and angle irrespective of the existence of the i-ZnO layer and electric charge of the Cu_2O deposition. The Cu_2O layer possessed a slight (111) preferred orientation from the peak intensity ratio compared to that tabulated on the International Centre for Diffraction Data (ICDD) card **[21]** and almost agreed with that of a Cu_2O layer prepared on a two-dimensional continuous ZnO layer.**[1]** The lattice constant calculated from the peak angles was estimated at 0.4234 nm, which is smaller than 0.4269 nm listed on the ICDD card **[29]** and 0.4261 nm for an unconstrained Cu_2O layer prepared on the continuous ZnO layer.**[1]** We note that the strain-induced lattice parameter changes have been previously described, for instance, in the case of a nanoporous ZnO layer electrodeposited between arrayed ZnO-nws.**[30]**

Figure 2.6 shows the correlation between the light absorption coefficient and photon energy for the Cl:ZnO-nws, Cl:ZnO-nws/i-ZnO, and Cu_2O layer prepared on the Cl:ZnO-nws/i- ZnO. The band-gap energy was estimated by extrapolating the linear part with the assumption of a direct optical transition for both ZnO and Cu_2O. The band-gap energy was 3.31 eV for the Cl:ZnO-nws and changed to 3.26 eV after deposition of the i- ZnO layer. These values were consistent with those already reported for the Cl:ZnO-nws and i-ZnO layer.**[24]** The band-gap energy was estimated to be 2.02 eV for the Cu_2O layer, irrespective of the electric charge.

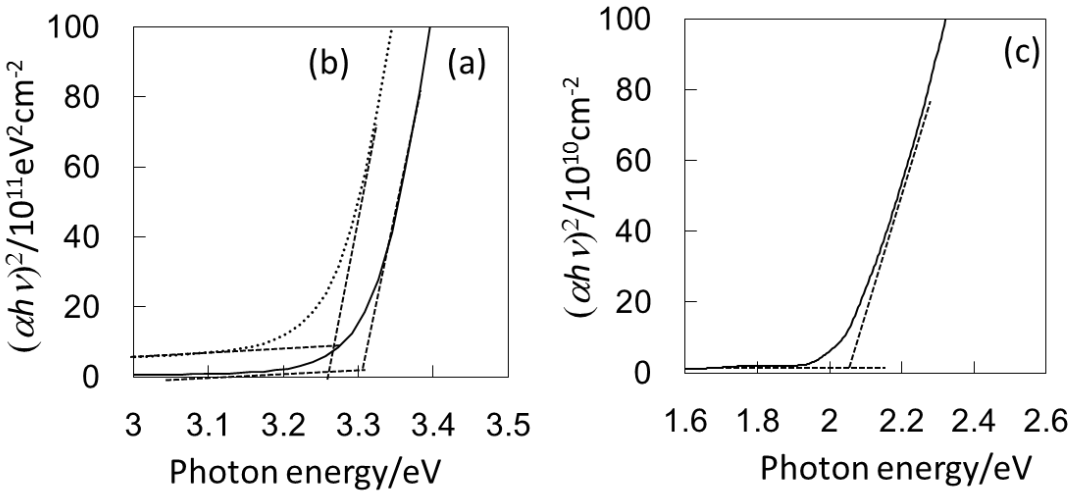

Figure 2.6 Correlations between absorption coefficient and photon energy for Cl-doped ZnO nanowire (a) before and after electrodeposition of i-ZnO layer for (b) 20 s, and (c) Cu_2O layer.

2.5.4 The effects of the i-ZnO intermediate layer on the electrical characteristic of ZnO-nanowire/Cu_2O photovoltaic devices

Figure 2.7 shows the current density−voltage curves of the Cl:ZnO-nws/ Cu_2O photovoltaic (PV) devices prepared with and without the i-ZnO layer. All the Cl:ZnO-nws/ Cu_2O PV devices generated electricity under the AM1.5G illumination. The i-ZnO-free Cl:ZnO-nws/ Cu_2O PV device showed a conversion efficiency of 0.40% with a 0.23 V open circuit voltage (Voc), 5.3 $mA\cdot cm^{-2}$ short circuit current density (Jsc), and 0.33 fill factor (FF). The performance was nearly close to 0.47% already reported for the PV devices prepared in a similar manner.**[31]** The insertion of the i-ZnO layer induced an improvement in the photovoltaic performance. The FF and Voc were improved by the increasing deposition time, and the maximum values of 0.34 and 0.52 V were obtained for 20 s. Jsc increased to 7.56 $mA\cdot cm^{-2}$ with increasing the deposition time at 10 s and then slightly decreased to 7.09 $mA\cdot cm^{-2}$ for 20 s. The conversion efficiency was improved with the increasing deposition time, and the maximum conversion efficiency of 1.26% was achieved for 20 s. As discussed

earlier, the thickness of the i-ZnO layer was linearly proportional to the deposition time. The grain size of the i-ZnO layer deposited on the Cl:ZnO-nws ranged from 15 to 23 nm, and the thickness was smaller than the grain size for deposition times below 10 s. This comparison suggests a noncontinuous i-ZnO layer with separated grains deposited on the Cl:ZnO-nws and the existence of an exposed area of Cl:ZnO-nws between the i- ZnO grains. However, the exact morphology of the surface could not be determined by the FE-SEM imaging. The defects located at the surface of the Cl:ZnO-nws act as recombination sites,**[32]** resulting in a decreased photovoltaic performance. A deposition time of 20 s was needed to cover all the surface of the Cl:ZnO-nws with the i-ZnO layer. The electrodeposition of Cu_2O grains preferentially occurred on the FTO substrate at 20 s for the i-ZnO deposition, and a continuous Cu_2O layer could be formed by the growth. Although the formation of the i-ZnO layer could not be confirmed by the FE-SEM observation, the improvement in the photovoltaic performance indicated that the deposited i-ZnO layer suppressed the electrical shorting between the Cu_2O layer and FTO substrate.

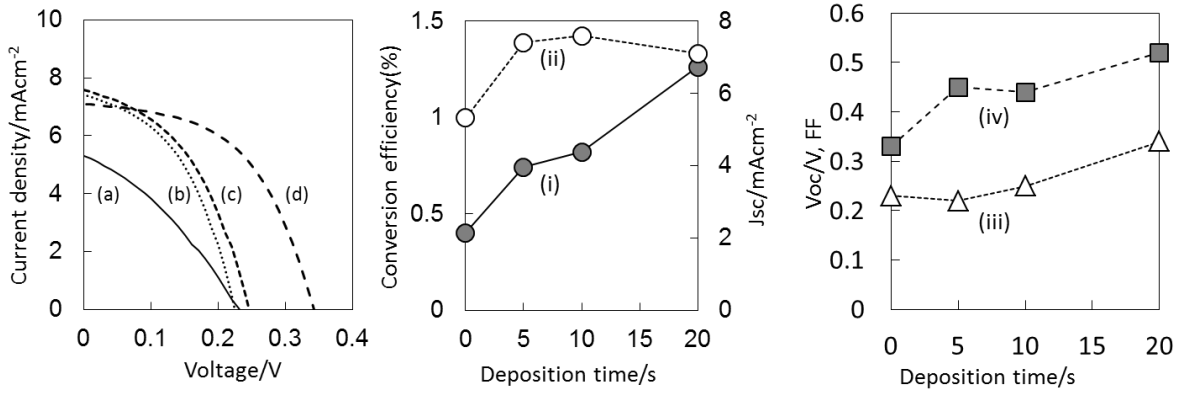

Figure 2.7 Current density−voltage curves for Cl-doped ZnO nanowire/Cu_2O photovoltaic devices with i-ZnO layers deposited for (a) 0, (b) 5, (c) 10, and (d) 20 s, and the relation of (i) conversion efficiency, (ii) short circuit current density (Jsc), (iii) open circuit voltage (Voc), and (iv) FF to the deposition time.

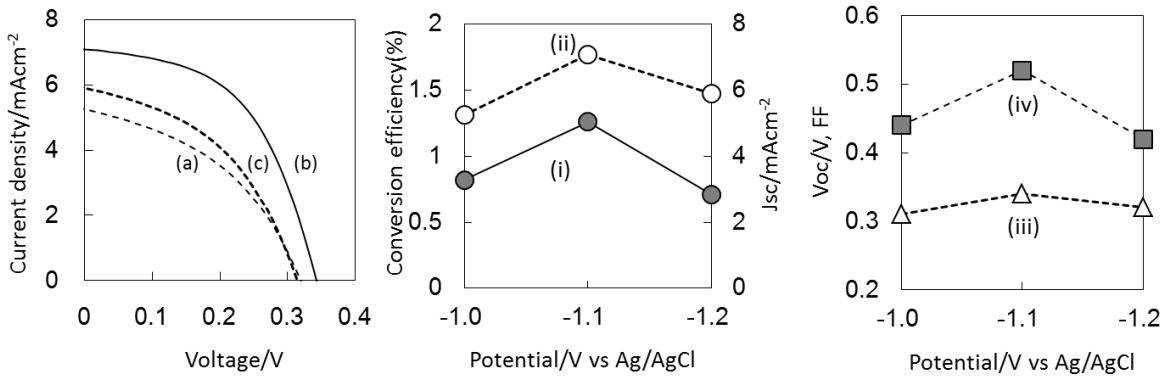

Figure 2.8 Current density−voltage curves for Cl-doped ZnO nanowire/Cu 2 O photovoltaic devices with i-ZnO layers deposited at (a)−1.0, (b)−1.1, and (c)−1.2 V, and the relation of (i) conversion efficiency, (ii) short circuit current density(Jsc), (iii)open circuit voltage (Voc), and (iv) FF to the potential.

Figure 2.8 shows the effects of the deposition potential of the i- ZnO layer on the photovoltaic performance of Cl:ZnO-nws/i- ZnO/ Cu_2O PV devices. The deposition time was fixed at 20 s. The maximum conversion efficiency of 1.26% was achieved at −1.1 V, and all the photovoltaic parameters decreased at both −1.0 and −1.2 V. The electrical properties of resistivity, carrier concentration, and mobility changed depending on the preparation conditions of the cathodic potential and current density for the electrodeposited ZnO layers.**[25]** The i-ZnO layers prepared at a potential ranging from −1.0 to −1.2 V possessed a very high resistivity on the order of 10^8 Ω·cm, with an unknown carrier concentration. It is speculated from the results already reported on the electrical characteristics that the carrier concentration is on the order of 10^{11} cm^{-3} (Nc,i-ZnO) and decreased with the shift in the potential to the negative side.**[25]** The carrier concentration of the Cl:ZnO-nws was 1.5×10^{19} cm^{-3} (Nc,Cl:ZnO-nws) as already estimated in this study. The location of the Fermi level (E_F) is closely related to the carrier concentration. The energy difference (ΔE_c) between the

conduction band energy minimum (CBM) and Fermi level (E_F) is estimated for n-type semiconductors by the following equation:**[33]**

$$\Delta E_c = \mathrm{CBM} - E_F = kT \log_e (N_c / n) \quad (5)$$

Where k, T, and N_c are the Boltzmann constant, temperature, and effective density of state in the conduction band. The energy difference (ΔE_c) decreased with increasing the carrier concentration corresponding to the donor density until the donor density reached the effective density of state (N_c). The energy differences for i-ZnO ($\Delta E_{c,i\text{-}ZnO}$) and Cl:ZnO-nws ($\Delta E_{c,Cl:ZnO\text{-}nws}$) were calculated according to equation 5, and the difference of $\Delta E_{c,i\text{-}ZnO} - \Delta E_{c,Cl:ZnO\text{-}nws}$ could be calculated to be approximately 0.5 eV.

The energy difference (ΔE_v) between the valence band maximum (VBM) and Fermi level (E_F) could be estimated for the p- Cu_2O layer by the following equation:**[33]**

$$\Delta E_v = E_F - \mathrm{VBM} = kT \log_e (N_V / p) \quad (6)$$

The carrier concentration (p) corresponding to the acceptor density was reported to be 1.9×10^{14} cm^{-3} for a Cu_2O layer prepared in the same manner.**[1]** The energy difference (ΔE_v) was calculated to be approximately 0.3 eV with the assumption for the effective density of state in the valence band (N_V) to be on the order of 10^{19} cm^{-3} . A cliff-type conduction band offset **[34]** was formed at the heterointerface between the Cl:ZnO-nws and Cu_2O layer, and the defects that originated from the high carrier concentration act as a recombination site **[32]** near the interface. The i-ZnO layer possessed a Fermi level lower by approximately 0.5 eV than that for the Cl:ZnO-nws, and the concentration of defects, which act as a donor in the ZnO semiconductor, was relatively low. The insertion of the i-ZnO layer between the Cl:ZnO-nws and Cu_2O layer could play a role in suppressing the recombination loss due to the decrease in the conduction band offset and increase in the depletion layer. Moreover, the

observed change in the photovoltaic performance with the i-ZnO deposition cathodic potential indicates the importance of the value of the conduction band offset, which is determined by the ionization energy as demonstrated for Cu(InGa)Se_2/Zn(OS)/ZnO solar cells.**[34]** The change in the carrier concentration somewhat affects the ionization energy, but further investigation with an inverse photoemission spectroscopy is needed to accurately illustrate the conduction band offset at the heterointerface.

The continuous ZnO layer/ Cu_2O PV devices prepared only by electrodeposition showed the best conversion efficiency of 1.28% with a 0.59 V in Voc , 3.8 $mA \cdot cm^{-2}$ in Jsc , and 0.58 in FF.**[4]** The use of the Cl:ZnO-nws alternative to the continuous ZnO layer produced a major improvement in the Jsc from 3.8 to 7.56 $mA \cdot cm^{-2}$ due to the increase in the active region expanded along the Cl:ZnO-nws, but the Voc decreased from 0.59 V **[4]** to 0.35 V. This suggested the imperfect control of the quality of the i-ZnO layer, such as the homogeneity, thickness, and electrical characteristics. The maximum conversion efficiency of 5.38% has been reported for an Al-doped ZnO(AZO)/Ga_2O_3/Cu_2O PV device prepared by the thermal oxidation of a metallic Cu sheet followed by a pulse-laser deposition of Ga_2O_3 and AZO layers.**[5]** The Voc changed from 0.55 to 0.80 V depending on the oxide material inserted between the Cu_2O and AZO layers, **[35,36]** and the best value was achieved with a Ga_2O_3 buffer layer. Also, a 1.2 V Voc has been reported for the electrodeposited Cu_2O photovoltaic device with Ga_2O_3 prepared by an atomic layer deposition.**[6]** The Jsc value obtained in this study was slightly lower than that for the AZO/Ga_2O_3/Cu_2O PV device, and the Voc was half that for the AZO/Ga_2O_3/Cu_2O PV device. Further investigation on controlling the heterointerface state and the electrical property of the Cu_2O layer is indispensable for improving the photovoltaic performance.

2.6 Conclusions

In summary, super-straight type Cl-doped ZnO-nanowire (Cl:ZnO-nws)/Cu_2O PV devices have been prepared by electrodeposition, and the effects of the insertion of a highly resistive ZnO layer (i-ZnO) on the photovoltaic performances has been investigated. The Cl:ZnO-nws and i-ZnO layer were prepared in a zinc chloride aqueous solution with saturated molecular oxygen and in a zinc nitrate aqueous solution, respectively. The Cu_2O layer was prepared in an alkaline aqueous solution containing a copper (II) acetate hydrate and lactic acid. The i-ZnO grains were directly deposited on the Cl:ZnO-nws, and the thickness increased with the increasing deposition time. The direct deposition of the Cu_2O layer on the Cl:ZnO-nws was suppressed by the deposited i-ZnO layer with a high resistivity. The insertion of the i-ZnO layer between the Cl:ZnO-nws and Cu_2O layer produced an improvement in the photovoltaic performance depending on the deposition potential and time. The conversion efficiency was boosted from 0.40 to 1.26% by inserting the i-ZnO layer prepared at −1.1 V for 20 s due to the reduction in the recombination loss at the heterointerface. The application of ZnO-nanowire and i-ZnO layer induced the increase in Jsc to 7.68 $mAcm^{-2}$ from 3.8 $mAcm^{-2}$ for bilayer ZnO/Cu_2O PV device because the increase in the active region of Cu_2O and suppressing of the recombination loss at the heterointerface. However, the random orientation of Cu_2O layer in the Cl-doped ZnO-nws/Cu_2O PV device restrict the increase in Jsc due to low mobility corresponding to the short diffusion length of carriers. Preparation of single orientation of Cu_2O layer could be a solution to the poor mobility of minority carriers inside Cu_2O layer.

REFERENCES

[1] K. Mizuno, M.Izaki, K. Murase, T. Shinagawa, M. Chigane, M.Inaba, A.Tasaka, Y.Awakura, J. Electrochem. Soc., 152, C179 (2005).

[2] A. Mittiga, E. Salza, F. Sarto, M. Tucci, R. Vasanthi, Appl. Phys. Lett., 88, 163502/1 (2006).

[3] G. K. Paul, R. Ghosh, S. K. Bera, S. Bandyopadhyay, T. Sakurai, K. Akimoto, Chem. Phys. Lett., ,463, 117 (2008).

[4] M. Izaki, T. Shinagawa, K. Mizuno, Y. Ida, M. Inaba, A. Tasaka, J. Phys. D: Appl. Phys., 40, 3326 (2007).

[5] T. Minami, Y. Nishi, T. Miyata, Appl. Phys. Express, 6, 4101/1 (2013).

[6] Y. S. Lee, D. Chua, R. E. Brandt, S. C. Siah, J. V. Li, J. P. Mailoa, S. W. Lee, R. G. Gordon, T. Buonassisi, Adv. Mater., 26, 4704 (2014).

[7] S. W. Lee,Y. S. Lee, J. Heo, S. C. Siah, D. Chua, R. E. Brandt, S. B. Kim, J. P. Mailoa, T. Buonassisi, R. G. Gordon, Adv. Energy Mater., 1301916 (2014).

[8] T. Shinagawa,; M.Onoda, B. M. Fariza,; J. Sasano, M. Izaki, J. Mater. Chem. A, 1, 9182 (2013).

[9] H. Tanaka, T. Shimakawa, T. Miyata, H. Sato, T. Minami, Thin Solid Films, 469, 80 (2004).

[10] K. P. Musselman, A. Wisnet, D. C. Iza, H. C. Hesse, C. Scheu, J. L. MacManus-Driscoll, L. Schmidt-Mende, Adv. Mater., 22, E254 (2010).

[11] J. Fan, F. Gueell, C. Fabrega, A. Shavel, A. Carrete, T. Andreu, M. J. Ramon, A. Cabot, Appl. Phys. Lett., 99, 262102/1 (2011).

[12] T. Pauporte,´ E. Jouanno, F. Pelle,´ B. Viana, P. Aschehoug, J. Phys. Chem. C, 113, 10422 (2009).

[13] M. Izaki, R. Chizaki, T. Saito, K. Murata, J. Sasano, T. Shinagawa, ACS Appl. Mater. Interfaces, 5, 9386 (2013).

[14] O. Lupan, T. Pauporte,´ J. Cryst. Growth, 312, 2454 (2010).

[15] A. Goux, T. Pauporte,́ D. Lincot, Electrochim. Acta, 51, 3168 (2006).

[16] P. Mandin, T. Pauporte,́ P. Fanouiliere, D. Lincot, J. Electroanal. Chem., 565, 159 (2004).

[17] M. Izaki, T. Omi, Appl. Phys. Lett., 68, 2439 (1996).

[18] H. Elbelghiti, T. Pauporte, D. Lincot, Phys. Status Solidi A, 205, 2360 (2008).

[19] T. Pauporte,́ G. Bataille, L. Joulaud, F. J. Vermersch, J. Phys. Chem. C, 114, 194 (2010).

[20] Chastain, J.Handbook of X-ray Photoelectron Spectroscopy;Perkin-Elmer Corporation: Waltham, MA, 1992.

[21] J. C. Klein, D. M. Hercules, Surface Characterization of Model Urushibara Catalysts. J. Catal., 82, 424 (1983).

[22] T. Shinagawa, Y. Ida, K. Mizuno, S. Watase, M. Watanabe, M. Inaba, A. Tasaka, M. Izaki, Cryst. Growth Des., 13, 53 (2013).

[23] I. Mora-Sero, F. Fabregat-Santiago, B. Denier, J. Bisquert, R. Tena-Zaera, J. Elias, C. Levy-Clement, Appl. Phys. Lett., ,89, 203117/1 (2006).

[24] J. Rousset, E. Saucedo, D. Lincot, Chem. Mater., 21, 534 (2009).

[25] T. Shinagawa, M. Chigane, K. Murase, M. Izaki, J. Phys. Chem. C, 116, 15925 (2012).

[26] J.-W. Chen, D.-C. Perng, J.-F. Fang, Sol. Energy Mater. Sol. Cells, 95, 2471 (2011).

(27) Joint Committee on Powder Diffraction Standards.Powder Diffraction File;International Centre for Diffraction Data: Newtown Square, PA, 1992; pp 41−1445.

[28] Joint Committee on Powder Diffraction Standards.Powder Diffraction File;International Centre for Diffraction Data: Newtown Square, PA, 1992; pp 36−1451.

[29] Joint Committee on Powder Diffraction Standards.Powder Diffraction File;International Centre for Diffraction Data: Newtown Square, PA, 1992; pp 5−667.

[30] V. M. Guerin, T. Pauporte,́ Energy Environ. Sci., 4, 2971 (2011).

[31] K. P. Musselman, A. Marin, A. Wisnet, C. Sheu, J. L. MacManus- Driscoll, L. Schmidt-Mende, Adv. Funct. Mater., 21, 573 (2011).

[32] A. Luqua, A. Marti, Chapter 4. In Handbook of Photovoltaic Science and Enineering; A. Luqua, S. Hegedus, Eds.; Wiley: Chichester, West Sussex, 2003; pp 120−124.

[33] S. M. Sze, K. K. Ng, Physics of Semiconductor Devices, 3rd ed; Wiley: Hoboken, NJ, 2007.

[34] N. Terada, R. T. Widodo, K. Itoh, S. H. Kong, H. Kashiwabara, T. Okuda, K. Obara, S. Niki, K. Sakurai, A.Yamada, S. Ishizuka, Thin Solid Films, 480, 183 (2005).

[35] T. Minami, Y. Nishi, T. Miyata, J. Nomoto, Appl. Phys. Express, 4, 062301/1 (2011).

[36] Y. Nishi, T. Miyata, T. Minami, Thin Solid Films, 528, 72 (2013).

CHAPTER 3

Substrate type <111>-Cu_2O/<0001>-ZnO photovoltaic device prepared by photo-assisted electrodeposition

3.1 Introduction

Most of the Cu_2O-based photovoltaic devices were classified into substrate-type device; which has been used for the conventional compound devices such as CIGS and CdTe, because of the ease of controlling the characteristics of the p-type semiconductors including Cu_2O act as the absorbing layer. On the other hand, super-straight type structure; that is difficult to control the characteristic by the deposition onto n-type semiconductors. And all

the Cu_2O layers used in the photovoltaic devices were polycrystalline with a random orientation and contained some amount of impurity, and high impurities and defects in deep level such as copper and oxygen vacancies; which deteriorated the electrical characteristics and device performance.

The Cu_2O layers for the photovoltaic application have been prepared by several techniques such as the thermal oxidation of a metallic Cu sheet,**[3]** RF magnetron sputtering,**[4]** radical oxidation,**[5]** sol-gel spin coating **[6]** and electrodeposition.**[7]** The ZnO layers have been prepared by electrodeposition in an aqueous solution containing either zinc nitrate **[8]** or zinc chloride **[9,10]** as well as gas-phase deposition techniques such as sputtering,**[11]** molecular beam epitaxy, and laser ablation techniques. The conversion efficiency of 6.1% has been reported for the substrate-type AZO/Al:Ga_2O_3/Na:Cu_2O photovoltaic device prepared by the thermal oxidation of metallic a Cu sheet in air followed by the gas-phase deposition of Ga_2O_3 and ZnO layers.**[12]** A 3.97%-efficiency has been reported for the electrodeposited substrate-type Cu_2O photovoltaic device with a Ga_2O_3 layer prepared by an atomic layer deposition (ALD).**[13]** The conversion efficiency, however, was limited to 1.28% for the randomly oriented super-straight type Cu_2O/ZnO photovoltaic device prepared only by electrodeposition.**[14]** And, our previous work reported that the crystallinity and mobility of (111)-Cu_2O layer prepared on (111)-Au/Si wafer improved by heteroepitaxial growth and annealing under an optimized condition.**[15]**

Therefore, in this chapter, an approach to reduce impurity and defects of the Cu_2O layers and construction of substrate type Cu_2O-based photovoltaic device is demonstrated. By stacking a photo-assisted electrodeposited-ZnO layer onto the (111)-Cu_2O/(111)-Au/Si substrate, the photovoltaic performance of the substrate type Cu_2O/ZnO PV device could be obtained only by electrodeposition.

3.2 Obstacles of electrochemical deposition of (0001)-ZnO layer deposition on (111)-Cu_2O layer

The highly oriented Cu_2O layer is a candidate as the light-absorbing layer in the substrate-type PV device, but the Cu_2O layer was reduced during the electrodeposition of n-ZnO to construct the photovoltaic device. Based on the pH-potential diagram of Cu-water system, the potential for the ZnO electrodeposition was within the electrochemical stable region of metallic the Cu.**[16]** Since the range for depositing ZnO layer on Cu_2O layer was very narrow and located between -0.08 and +0.09 V Vs Ag/AgCl, therefore, the photo-assisted electrodeposition was carried out at the potential of -0.06 V Vs Ag/AgCl within the stable region for the Cu_2O. Due to the very low applied potential during the ZnO electrodeposition, the ZnO grains could not be growth on the Cu_2O layer. Therefore, supplying electrons by light from an outside source at a wavelength below the absorption edge for the Cu_2O, enabled the electrodeposition of the ZnO layer onto the Cu_2O layer without any reduction of the Cu_2O layer.**[17]**

3.3 Experimental design

The (111)-Cu_2O layer was prepared on (111)-Au/Si substrate due to the significantly low lattice mismatch of 4.7% as reported in our previous work.[18] The possibility to deposit the (111)-Cu_2O layer on (111)-Au/Si substrate by using electrodeposition by comparing the mismatch value was predicted. The mismatch calculation was done using the formation of the lattice parameters of both materials and the atomic arrangement between (111)-Cu_2O and (111)-Au at the interface. There are heteroepitaxial relations of (1x1)(111)<110>Cu_2O//(1x1)(111)<110>Au with a lattice mismatch of 4.7%. Therefore, it is

predicted the high possibility of the heteroepitaxial growth of (111)-Cu_2O layer on (111)-Au substrate.

The (111)-oriented Cu_2O layer was deposited on a (111)-oriented Au/Si(100) substrate by a conventional electrodeposition method. Then, the (0001)-oriented ZnO layer was stacked on the Cu_2O layer by photo-assisted electrodeposition to construct the (111)-Cu_2O/(0001)-ZnO PV device. It is predicted that the current density is very low and not sufficient for depositing the ZnO layer because of the applied potential significantly more positive than that in conventional electrodeposition method. The irradiation of light at photon energy higher than the bandgap energy of the Cu_2O induced the excitation of the electrons from the valence band to the conduction bands, resulting in an increase in amount of the minority carrier of electrons.

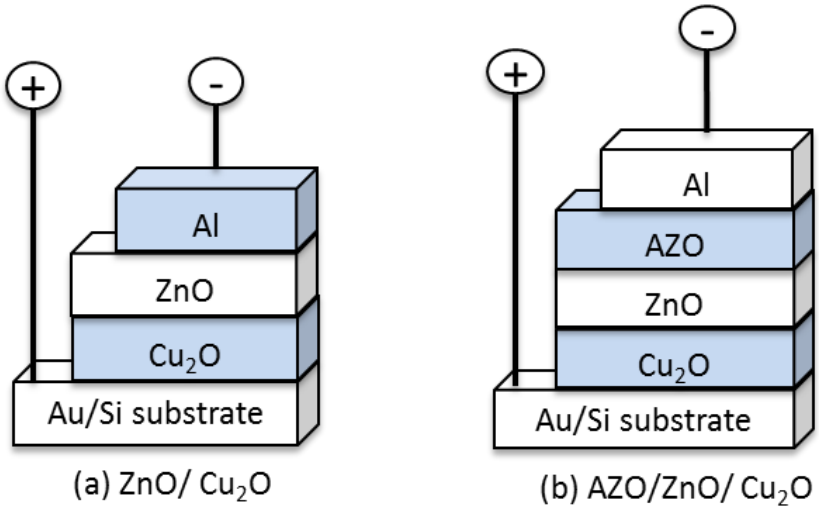

Figure 3.1 Schematic illustration of the cell configuration of (111)-Cu_2O/(0001)-ZnO (a) and (111)-Cu_2O/(0001)-ZnO/AZO (b) PV devices.

As for the comparison, the aluminum-doped ZnO (AZO) layer with thickness approximately 100 nm was also stacked by using radio-frequency magnetron sputtering on Cu_2O layer. The schematic structures of the cell configuration of (111)-Cu_2O/(0001)-ZnO and (111)-Cu_2O/(0001)-ZnO/AZO PV devices are as shown in Figure 3.1.

3.4 Principle of ZnO layer deposition on Cu_2O layer using photo-assisted electrodeposition method

The schematic illustration of the change in the electronic state during the electrodeposition of the ZnO layer on the Cu_2O layer by light irradiation is shown in Figure 3.2. We have proposed a tentative mechanism for the ZnO deposition on the p-Cu_2O layer by the light irradiation based on the band diagram in the solution containing zinc nitrate.**[17]** The generally accepted reaction schemes for the electrodeposition of the ZnO layer in a zinc nitrate aqueous solution are as follows:**[19]**

$$Zn(NO_3)_2 \longrightarrow Zn^{2+} + 2NO_3^- \quad (1)$$

$$NO_3^- + H_2O + 2e^- \longrightarrow NO_2^- + 2OH^- \quad (2)$$

$$Zn^{2+} + 2OH^- \longrightarrow Zn(OH)_2 \quad (3)$$

$$Zn(OH)_2 \longrightarrow ZnO + H_2O \quad (4)$$

Since the Cu_2O layer is a p-type semiconductor material with the conduction band minimum (CBM) at -3.3 eV and valence band maximum at -5.4 eV, the electrons needed for the ZnO deposition are minority carriers and located inside the valence band in the absence of any external excitation. When the Cu_2O/electrolyte interface is irradiated by light at a photon energy greater than the bandgap energy of Cu_2O (2.1 eV), electrons are excited to the conduction band from the valence band. The electrons diffuse inside the Cu_2O layer, while some of them are swept down to the interface to the solution by the electric field formed at the interface to the solution. The electrons cause the reduction reaction of the nitrate ions followed by the formation of the ZnO (reaction 3). The pH in the vicinity of the substrate surface before the light irradiation locates at near critical value inside the Zn^{2+} stable region

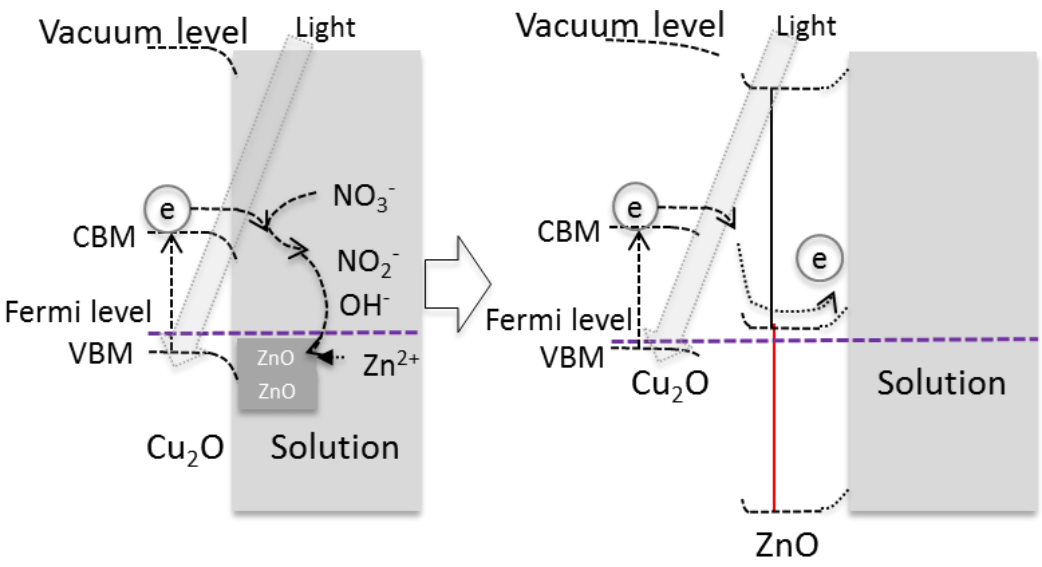

Figure 3.2 Photo electrochemical designs of the ZnO deposition (a) and dissolution (b) during the photo-assisted electrodeposition process.

in the potential–pH diagram, but the irradiated light induces an increase in the pH value in the vicinity of the substrate to the ZnO stable region by reduction of the nitrate ions, resulting in the stacking of the ZnO layer on the Cu_2O layer (Fig. 3.2a). Once the ZnO nuclei are deposited on the p-Cu_2O layer, the successive growth continued at the applied potential. The deposited ZnO layer formed a p-n heterojunction with the p-Cu_2O layer, and the depletion layer was formed at the heterointerface. The thickness of the depletion layer (W) is closely related to the donor density (N_D) and acceptor density (N_A) for the ZnO and Cu_2O layer, respectively, according to the following equation: **[20]**

$$W=\left[\frac{2\varepsilon_s}{q}\left(\frac{N_A+N_D}{N_A\ N_D}\right)V_{bi}\right]^{1/2} \quad (a) \qquad ,V_{bi}=\frac{kT}{q}ln\frac{N_AN_D}{ni^2} \quad (b) \qquad (5)$$

where q, n_i and V_{bi} are the elementary charge (1.6×10^{-19} C), effective density of state, and the built-in voltage, respectively. The carrier concentration corresponding to the acceptor density was reported to be $1.5x10^{14}$ cm^{-3} for the Cu_2O layer,**[15]** and the ZnO layer deposited

at -0.30 $mAcm^{-2}$ was reported to be $8x10^{16}$ cm^{-3}.**[21]** The V_{bi} and W at 300 K were calculated to be 0.66 eV and 690 nm, respectively. The thickness of the depletion layer was smaller than that of the resultant ZnO layer shown in Fig. 3.6. The band alignment changed from Fig. 3.4 (a) to 3.4 (b) during the growth of the ZnO layer. It is predicted that the electron generated by the light irradiation swept out from the Cu_2O to the solution during the initial stage of the ZnO electrodeposition, and then the electron were confined inside the ZnO layer due to the energy barrier formed at the interface between the ZnO layer and solution. The pH value closely related to the number of electrons swept down to the solution, and the formation of the energy barrier reduces the number of electrons, resulting in the decreased local pH value and then returning to the Zn^{2+} state region in the potential-pH diagram. This is the reason for the change in the ZnO thickness with the deposition time.

3.5 Objective of this study

In this study, we report the preparation of the substrate-type <0001>ZnO/<111>-Cu_2O photovoltaic (PV) device by the photo-assisted electrodeposition process without reduction reaction from Cu_2O to Cu during the ZnO deposition. First, the (111)-oriented p-Cu_2O layer was deposited on a (111)-oriented Au/Si(100) substrate, then the (0001)-oriented n-ZnO layer was stacked on the Cu_2O layer by photo-assisted electrodeposition method. The transparent conductive window (TCO) of Al:ZnO (AZO) layer was stacked on the ZnO layer by a radio frequency magnetron sputtering.

The structural, optical, and electrical characteristics investigated with X-ray diffraction (XRD), scanning electron microscopy (FE-SEM) observations, and measurements of electrical properties including the photovoltaic performance.

3.6 Experimental procedures

The Cu_2O layer was potentiostatically deposited at −0.5 V referenced to the Ag/AgCl electrode on the Au(111)/Si(100) substrate at an electric charge of 1.7 coulomb cm^{-2} with a potentiostat (Hokuto Denko, HABF-501A) in an alkaline aqueous solution containing a 0.4 M copper(II) acetate monohydrate ($Cu(CH_3COO)_2.H_2O$, Nacalai Tesque, Inc.) and 3 M lactic acid (Kanto Chemical, Co., Inc.) at 328 K. The solution was prepared with deionized water purified by an Elix-UV system (Millipore), and KOH was added for the pH adjustment to 12.5. The Au(111)/Si(100) (Kobelco Research Inst. Inc.) was used as the substrate, and prior to the electrodeposition, the Au(111)/Si(100) substrate was rinsed with acetone, polarized in 1 M NaOH and rinsed with distilled water. A Pt plate was used as the counter electrode. The ZnO layer was stacked on the Cu_2O layer at a potential of −0.06 V referenced to Ag/AgCl for the deposition time up to 5 hours in a simple aqueous solution containing 0.08 M zinc nitrate hydrate at 336 K. The potential used in this study was determined in a previous study [18]. The photons needed for the ZnO electrodeposition was supplied to the Cu_2O layer by irradiating at a light wavelength longer than 380 nm with a filter in the direction normal to the surface of the Cu_2O layer using a high pressure mercury lamp (USHIO Optical Modulex, SH-UI250HQ, 500 W).**[17]** The light intensity was estimated to be 33 mW/cm^2. For comparison, the ZnO layer was deposited on a Cu_2O layer without light irradiation. The photovoltaic device of the ZnO/Cu_2O heterojunction was fabricated with and without AZO deposition by radio-frequency magnetron sputtering (ULVAC, RFS-200) at room temperature with sputtering power of 100 W, deposition time of 5 min and pressure up to 10^{-4} Pa followed by stacking a 100-nm-thick-Al electrode by vacuum evaporation (ULVAC, VPC-260F) on the top of the (0001)-ZnO/(111)-Cu_2O heterostructures.

X-ray Diffraction (XRD) patterns were recorded by a θ /2 θ scanning technique with monochromated Cu Kα radiation operated at 20 kV and 10 mA using a Rigaku RINT 2500. Observation of the surface and cross-sectional morphology of the layers was carried out using a field emission scanning electron microscope (FE-SEM, Hitachi High Technology SU8000) at an operating voltage of 3 kV. The optical absorption spectra were recorded using a UV-Vis-NIR spectrophotometer (Hitachi High-Technology UV-4100) with an integrating sphere. The current density-voltage curve in the dark and under AM1.5 illumination with a 100 $mWcm^{-2}$ power was recorded using a solar simulator (Bunko Keiki, OTENTOSUN-III) and a Keithley 2400 source meter.

3.7 Results and Discussion

The deposition was carried out at a potential inside the stable region of Cu_2O in the potential-pH diagram of the Cu-water system to inhibit the reduction reaction from Cu_2O to Cu during the ZnO deposition. Fig. 3.3 shows the current density-potential curves for electrodeposition of the ZnO layer on the Cu_2O/Au substrate with and without the light irradiation. During the ZnO deposition without light irradiation, the current density slightly decreased when the potential was changed from the immersion potential of +0.09 to -0.35 V and then decreased with an increased gradient to -0.13 $mAcm^{-2}$ at -0.6 V. The decrease in current density was attributed to the reduction reaction of nitrate ion to nitrite ion, because the equilibrium potential for depositing metallic Zn was approximately -0.96 V referenced to the Ag/AgCl electrode. The current density was very low at the potential of -0.06 V, at which the Cu_2O phase is electrochemically stable in agreement with to the potential-pH diagram for the Cu-water system.**[22]** In the case of the ZnO electrodeposition with light irradiation, the immersion potential slightly shifted to +0.13 V. The current density decreased to -0.14

$mAcm^{-2}$ when the potential was changed to the negative side from the immersion potential to the potential of -0.08 V and was five-fold that without light irradiation. The current density significantly decreased with the shift in the potential to the negative side, and the current density reached -1.0 $mAcm^{-2}$ at the potential of -0.14 V. The electrons were supplied by excitation of electrons from the valence band to the conduction band in the Cu_2O layer by irradiating light at a wavelength below the absorption edge of the Cu_2O semiconductor and by sweeping down to the solution side by the electric field formed at the interface to the solution.

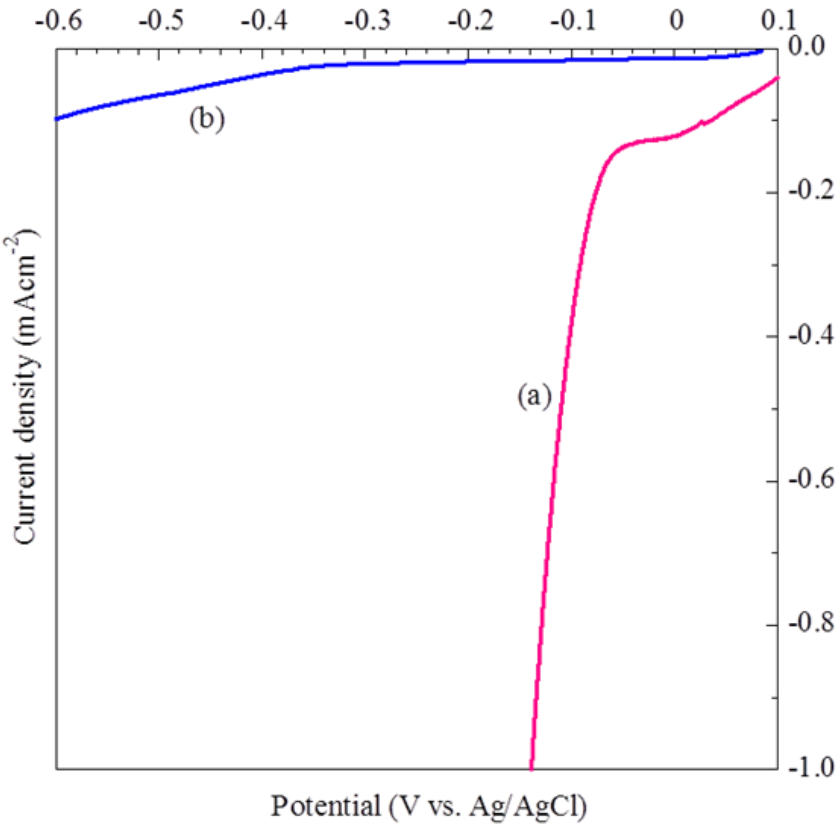

Figure 3.3 Cyclic voltammogram for the ZnO electrodeposition on the Cu_2O/Au/Si substrate with (a) and without (b) the light irradiation in a solution containing 0.08 M $Zn(NO_3)_2$ at the solution temperature of 336 K.

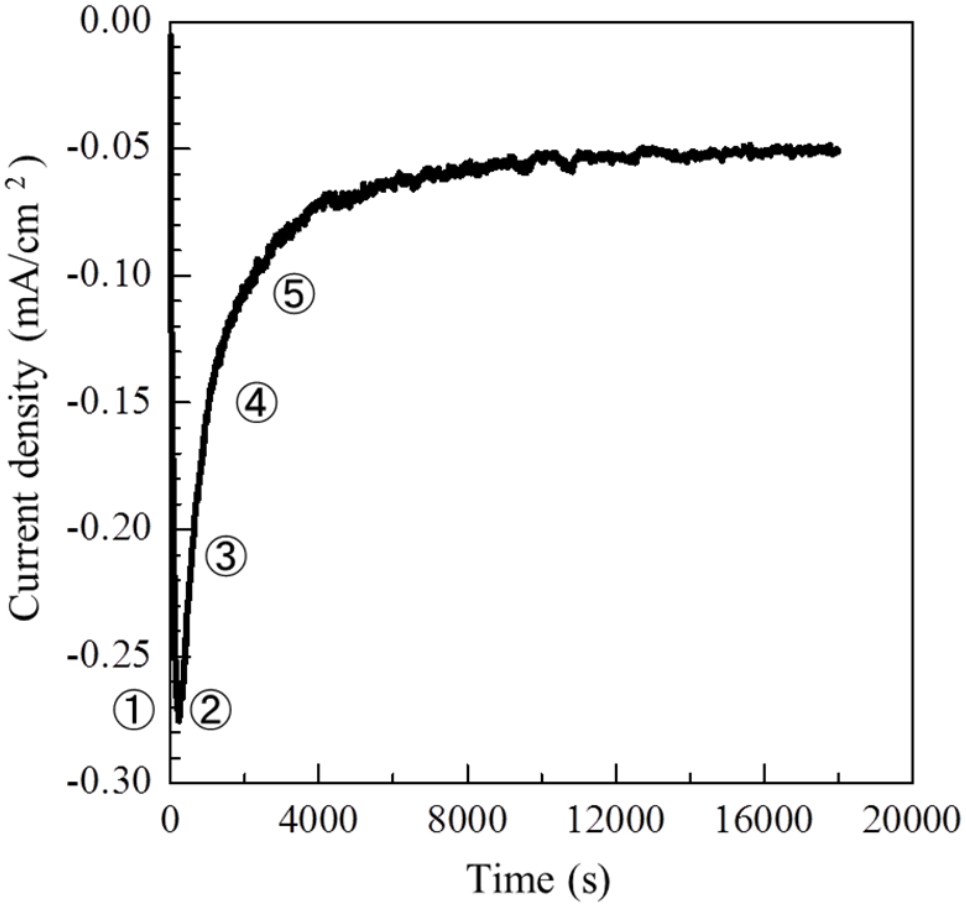

Figure 3.4 Current density-time curves for the ZnO electrodeposition on the Cu_2O/Au substrate in a solution containing 0.08 M $Zn(NO_3)_2$ at bath temperature of 336K.

The current density-time curves during the ZnO electrodeposition at -0.06 V with light irradiation is shown in Fig. 3.4. The current density for the ZnO deposition without light irradiation showed a very low value of approximately -6 μA/cm^2 (not shown), irrespective of the deposition time. During light irradiation, the current density rapidly decreased just after applying the potential at -0.06 V and reached a maximum value of -0.275 mA/cm^2 at 250 sec. The current density gradually increased and reached a plateau region at approximately -0.05 mA/cm^2. The current density corresponds to the number of electrons that reached the surface of the substrate, and the number of electrons excited from the valence band to the conduction band in the Cu_2O semiconductor would be constant, because the absorption by the deposited

ZnO layer was negligible at the wavelength of light, suggesting that the change in the current density was attributed to the change in the electric field formed at the interface to the solution by forming the ZnO layer. Five deposition times of 1200, 1800, 2400, and 3000 s were selected for investigating the structure of the deposited ZnO layer.

3.7.1 Structural characteristic of photo-assisted electrodeposited ZnO layer on (111)Cu_2O layer

Fig. 3.5 shows X-ray diffraction patterns of the Cu_2O layer before and after stacking the ZnO layer by electrodeposition with light irradiation. Only two peaks assigned as the Cu_2O(111) and Au(111) planes could be observed on the XRD pattern before stacking the ZnO layer. Only one peak assigned as the (0002) plane of ZnO with the characteristic wurtzite lattice structure could be observed after the ZnO deposition in addition to the two peaks originating from the Cu_2O and Au layers, indicating the formation of the (0002) out-of-plane orientation of the ZnO layer, as predicted from the lattice relationship of (1×1)(111)[1$\underline{1}$0]Cu_2O//(1×1)(0001)[11$\underline{2}$0]ZnO with the lattice mismatch of 7.6%, which is lower than 12.7% for the (0001)ZnO//(111)Au combination.**[23]** There are no other peaks identified as metallic Cu and monoclinic CuO on both XRD patterns. The unit cell parameter in the c-axis calculated for the ZnO layer showed the almost constant value of 0.521 nm irrespective of the deposition time and nearly agreed with the 0.5207 nm tabulated on the ICDD card **[24]** as shown in the inset (B).

The penetration depth of the incident X-ray was greater than the thickness of the deposited ZnO layer based on the existence of diffracted X-ray peaks of the Cu_2O layer. The intensity of the (111) Cu_2O peak decreased after stacking the ZnO layer, due to absorption of the incident X-ray. The intensity ratio of the (0001) ZnO to the (111) Cu_2O peaks, which was

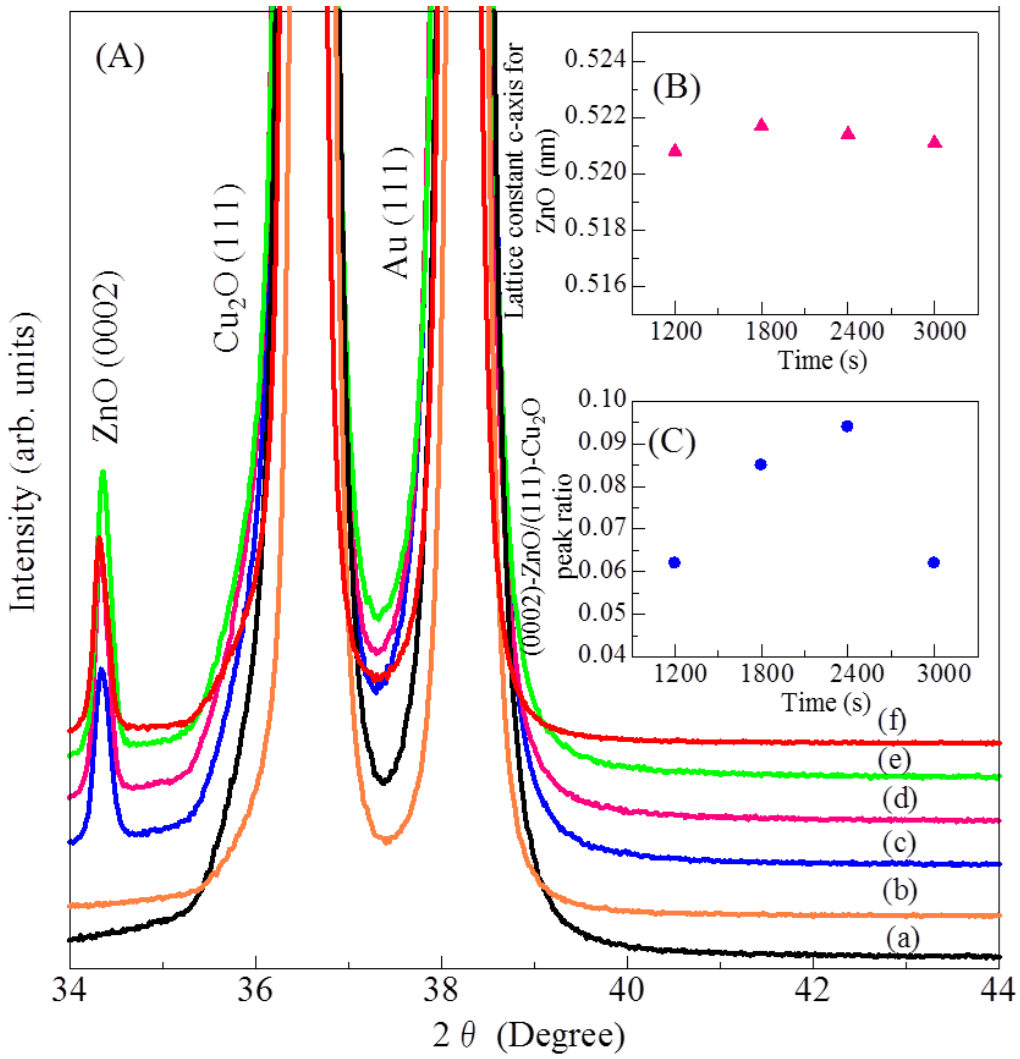

Figure 3.5 XRD patterns (A) for the Cu_2O/Au substrate before (a) and after stacking ZnO layers at deposition time of 24 (b), 1200 (c), 1800 (d), 2400 (e), and 3000 s (f), and relation of the lattice constant c-axis for ZnO (B) and the peak intensity ratio of (0002)-ZnO/(111)-Cu_2O to the deposition time (C).

proportional to the volume of the deposited ZnO layer, increased with an increase in the deposition time till 2400 s and then decreased, as shown in the inset (C), indicating the change in the ZnO thickness. The ZnO layer thickness decreased at the deposition time of

3000 s due to dissolution of the grains because of the pH changes in the vicinity of the substrate surface as explained in Fig. 6 (b).

3.7.2 Morphological characteristic of photo-assisted electrodeposited ZnO layer on (111)Cu_2O layer

Fig. 3.6 shows FE-SEM images of the Cu_2O layers before and after stacking the ZnO layer for 24 to 3000 s with light irradiation. The Cu_2O layers deposited on the Au(111) layer were composed of aggregates of the columnar grains grown in direction perpendicular to the Au(111) substrate surface, and the thickness was estimated to be about 2.4 μm. The triangular facet corresponding to the (111)-plane of the Cu_2O crystal was obviously observed in the plan-view FE-SEM image, and the surface morphology was similar to the typical pyramidal-shape-Cu_2O layer prepared on a conductive glass substrate as already reported.**[14]** No ZnO grains could be observed on both the surface and cross-sectional images after the electrodeposition for 24 s with light irradiation. The low density-isolated hexagonal columnar ZnO grains with the width and height of approximately 150 and 160 nm, respectively, grew in the direction normal to the surface, and hexagonal facets corresponding to the (0001) plane were clearly observed on the surface image after the electrodeposition for 1200 s with light irradiation. The bare surface of the Cu_2O layer, however, still could be observed between the ZnO grains. The hexagonal columnar ZnO grains with an average width of 150 nm were deposited on the entire surface of the Cu_2O layer at the deposition time for 1800 s. Some vacancies could be observed between the ZnO grains, but the bare Cu_2O surface could not be observed. The thickness of the ZnO layer was estimated to be about 160 nm from the cross-sectional images. The width of the ZnO grains increased to 180 nm with an increase in the deposition time to 3000 s, and the vacancies between the ZnO grains remained. The ZnO layer showed an increased surface roughness compared to that formed at 1800 s.

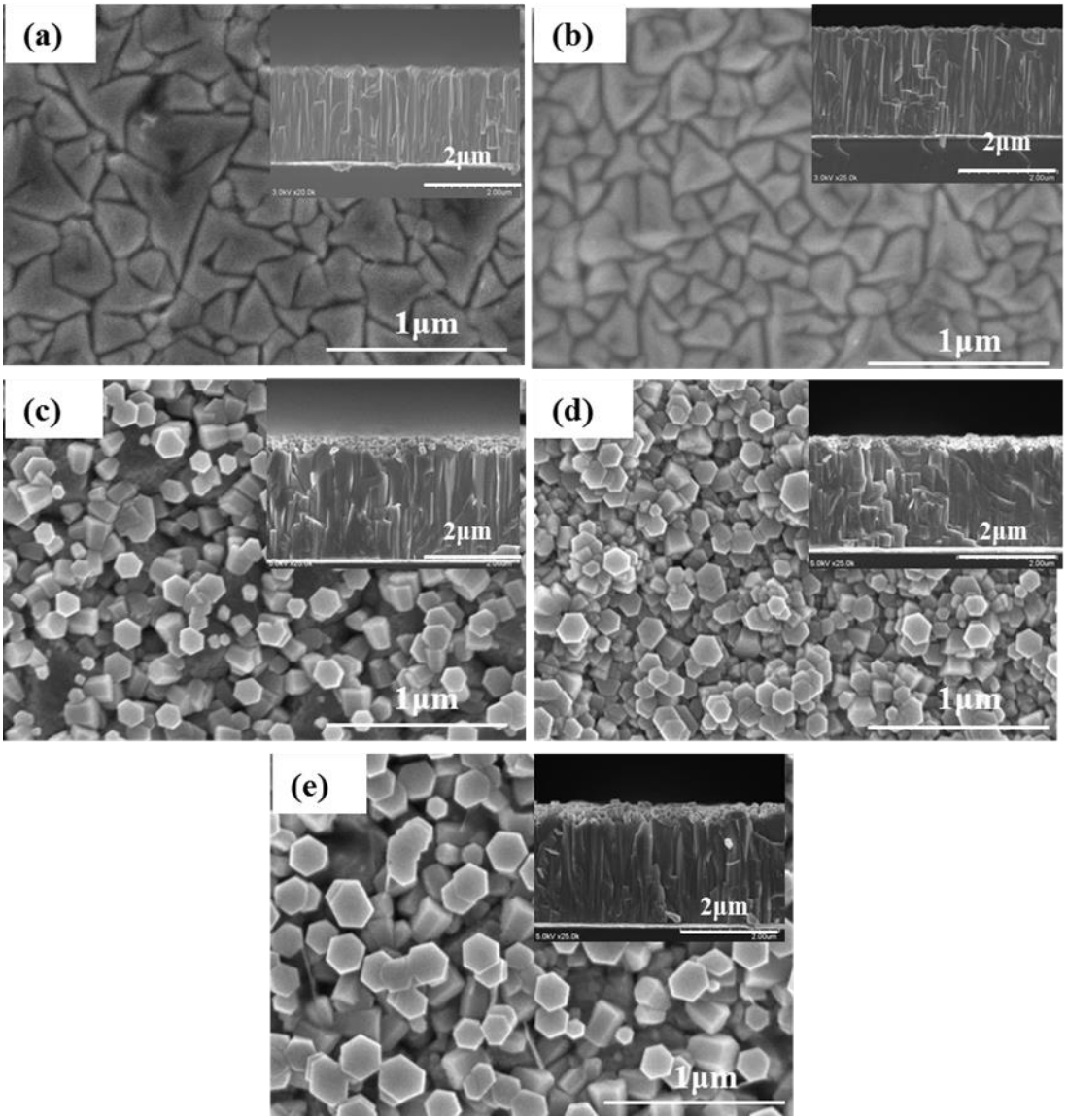

Fig. 3.6 Surface and cross-sectional FESEM images of the Cu_2O/Au/Si substrate before (a) and after stacking ZnO layers at electrodeposition time of 24 (b), 1200 (c), 1800 (d), and 3000 s (e).

3.7.3 Optical characteristic of photo-assisted electrodeposited ZnO layer on (111)Cu_2O layer

Fig. 3.7 shows the optical absorption spectra for the Cu_2O layer after depositing ZnO layers for 24 to 3000 s with light irradiation. The Cu_2O layer showed an absorption edge around 600 nm, and the interference fringe pattern was obviously observed at a wavelength less than 600 nm, indicating the formation of a homogeneous Cu_2O layer with the characteristic bandgap energy of 2.1 eV. An absorption edge was also observed at a wavelength around 380 nm that originated from the ZnO layer for 1200 to 2400 s in addition to that for the Cu_2O

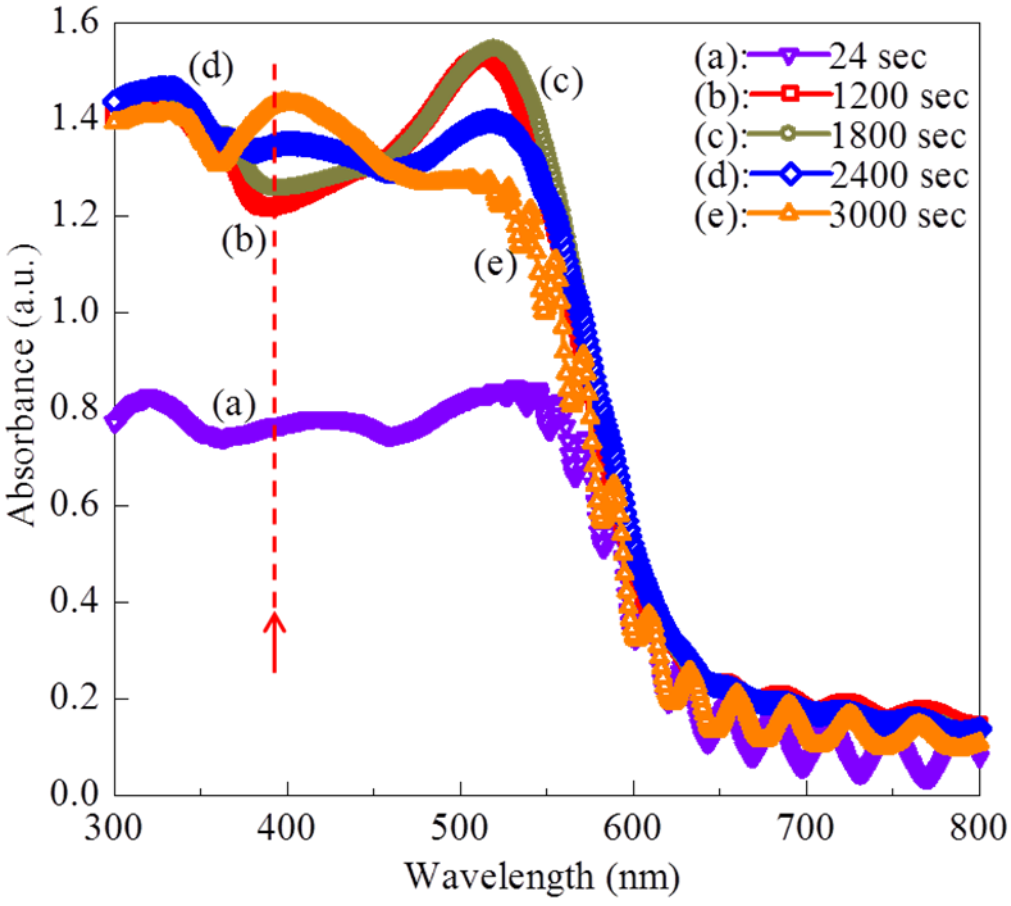

Fig. 3.7 Absorption spectra for ZnO/Cu_2O heterostructures prepared at the electrodeposition time of 24 (a), 1200 (b), 1800 (c), 2400 (d), and 3000 s (e).

layer as denoted by the arrow. The absorbance for the ZnO layer is proportional to the amount of the deposited ZnO layer when the absorption coefficient was constant. The absorption that originated from the ZnO layer could be observed at the deposition time ranging from 1200 to 3000 s and increased with the increase in the deposition time to 3000 s. The absorption edge remained increase at 3000 s because of the scattering effect even the ZnO layer underwent some deterioration due to the dissolution as supported by the weakened diffraction X-ray peak in Fig. 3 (inset C)

3.7.4 Electrical characteristic of photo-assisted electrodeposited ZnO layer on (111)Cu_2O layer

Fig. 3.8 shows the current density-voltage curves for ZnO/Cu_2O PV devices with and without the AZO layer under AM 1.5 illumination. Both the ZnO/Cu_2O and AZO/ZnO/Cu_2O PV devices were prepared at 1800 s for the ZnO deposition. The ZnO/Cu_2O PV devices prepared at 24, 1200, 2400, and 3000 s exhibit low photovoltaic performance irrespective of the AZO layer due to the existence of pores located between the n-ZnO grains. The ZnO/Cu_2O PV device without the AZO layer showed the best photovoltaic performance of 0.06% in conversion efficiency with the short-circuit current density of 2.55 $mAcm^{-2}$ and open-circuit voltage of 0.08 V. And the AZO/ZnO/Cu_2O PV device showed a relatively low photovoltaic performance of 0.015% with the short-circuit current density of 5.87 $mAcm^{-2}$ and open-circuit voltage of 0.01 V compared to the ZnO/Cu_2O PV device. However, stacking the AZO layer induced the increase in Jsc to 5.87 $mAcm^{-2}$. Since the absorption edge originating from the Cu_2O layer did not change by stacking the AZO layer, the range of the wavelength for generating carriers is almost the same for the n-ZnO/ Cu_2O PV devices with and without the AZO layer, indicating that the AZO layer played a role to take the carriers transported

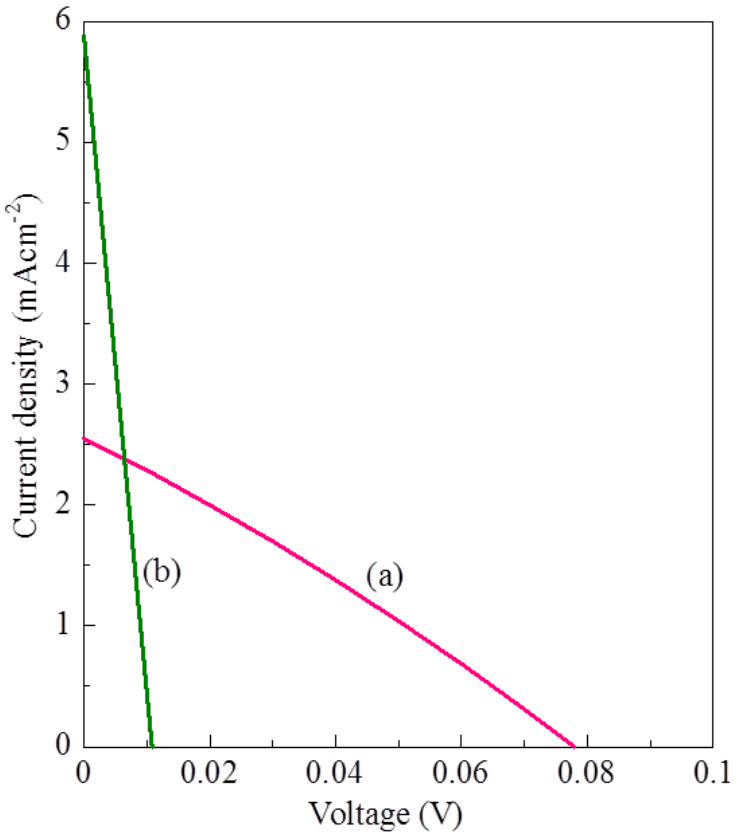

Fig. 3.8 Current density-voltage curves for ZnO/Cu_2O (a) and AZO/ZnO/Cu_2O (b) photovoltaic devices at the electrodeposition time of 1800 s.

through n-ZnO layer from the Cu_2O layer out. By stacking the AZO layer onto the ZnO/Cu_2O PV device closes the gap or vacancy between the ZnO grains. This would lead to the increase in the interfacial area between the p-n heterojunction, and as a result, the Jsc would also increase.

The short-circuit current density of 3.8 $mAcm^{-2}$ was obtained for the randomly oriented Cu_2O/ZnO PV devices prepared by electrodeposition.**[14]** The <111>-oriented Cu_2O layer used in this study showed an improved mobility of approximately 20 cm^2/Vs compared with 1.2 cm^2/Vs for the randomly oriented Cu_2O layer, indicating the longer diffusion length of carrier in the <111>-oriented Cu_2O layer.**[18]** This will be the reason for the increased Jsc. The open-circuit voltage (Voc) was very low irrespective of the existence of the AZO layer,

compared with those already reported. The low Voc might be due to the leakage current and interface state, resulting in recombination loss at the ZnO/Cu_2O interface. The Voc value strongly depended on the heterointerface state including the band alignment, and the Voc up to 1.20 V **[13]** was reported depending on the oxide buffer layer **[25]** inserted between the n-ZnO and p-Cu_2O layer. Further improvement of the quality including the homogeneity and energy state at the heterointerface is indispensable to raise the photovoltaic performance.

3.8 Conclusions

We have successfully demonstrated the construction of the substrate-type <0001>-ZnO/<111>-Cu_2O photovoltaic (PV) device by electrodeposition of the <111>-p-Cu_2O layer on an Au (111)/Si wafer substrate followed by stacking the <0001>-n-ZnO layer by photo-assisted electrochemical growth in aqueous solutions. The <0001>-oriented ZnO layer was stacked on the Cu_2O layer by electrodeposition at -0.06 V vs. Ag/AgCl electrode, which was located inside the stable region of Cu_2O in the potential-pH diagram, in a zinc nitrate solution with the light irradiation at wavelength shorter than the adsorption edge of the Cu_2O semiconductor with the bandgap energy of 2.1 eV. The PV device was fabricated by stacking the Al:ZnO-transparent conductive window by radio-frequency magnetron sputtering and the top Al electrode by an evaporation. The thickness increased with the deposition time up to 1800 s and then decreased by the dissolution of the ZnO layer during the photo-assisted electrodeposition process. And the pores could be observed for the ZnO layer at the deposition time over 1800 s. The PV device showed a photovoltaic performance under AM1.5 illumination, and the stacking the AZO layer induced the short-circuit current density from 2.55 to 5.87 $mAcm^{-2}$, which was about 1.5 fold that for randomly oriented Cu_2O PV device (3.8 $mAcm^{-2}$). The existence of pores in the resultant ZnO layer increased the leakage current at the p-n heterojunction interface, resulted in decrease of the photovoltaic performance. A buffer layer could be inserted in between Cu_2O layer and ZnO layer to mitigate the leakage current and increase the photovoltaic performance.

REFERENCES

[1] J. J. Lofeski, J. Appl. Phys., 27, 777 (1956).

[2] M. A. Green, M. Keevers, J. Prog. Photovoltaics, 3, 189 (1995).

[3] J. Herion, E. A. Niekisch, G. Scharl, Solar Energy Mater., 4, 101 (1980).

[4] V. F. Drobny, D. L. Pulfrey, Thin Solid Films, 61, 89 (1979).

[5] Z. Zhigang, N. Atsushi, T. Jiro, Optic Express, 21, 11448 (2013).

[6] D. S. C. Halin, I. A. Talib, A. R. Daud, M. A. A. Hamid, Int. J. of Photoenergy, 352156 (2014).

[7] T. D. Golden, M. G. Shumsky, Y. Zhou, R. F. VanderWerf, R. A. Van Leeuwen, J.A. Switzer, Chem. Mater., 8, 2499 (1996).

[8] M. Izaki, T. Omi, Appl. Phys. Lett., 68, 2439 (1996).

[9] S. Peulon, D. Lincott, Adv. Mater., 8, 166 (1996).

[10] M. Izaki, T.Omi, J. Electrochem. Soc., 144, L3 (1997).

[11] N. Fujimura, T. Nishihara, S. Goto, J. Xu, T. Ito, J. Cryst. Growth, 130, 269 (1993).

[12] T. Minami, Y. Nishi, T. Miyata, Thin Solid Films, 549, 65 (2013).

[13] Y. S. Lee, D. Chua, R. E. Brandt, S. C. Siah, J. V. Li, J. P. Mailoa, S. W. Lee, R. G. Gordon, T. Buonassisi, Adv. Mater., 26, 4704 (2014).

[14] M. Izaki, T. Shinagawa, K. Mizuno, Y. Ida, M. Inaba, A. Tasaka, J. Phys. D: Appl. Phys., 40, 3326 (2007).

[15] T. Shinagawa, M. Onoda, B. M. Fariza, J. Sasano, M. Izaki, J. Mater. Chem. A, 1 9182 (2013).

[16] B. M. Fariza, J. Sasano, T. Shinagawa, H. Nakano, S. Watase, M. Izaki, J. Electrochem. Soc., 158, D621 (2011).

[17] B. M. Fariza, J. Sasano, T. Shinagawa, S. Watase, M. Izaki, Thin Solid Films, 520, 2261 (2012).

[18] M. Izaki, S. Sasaki, M. B. Fariza, T. Shinagawa, T. Ohta, S. Watase, J. Sasano, Thin Solid Films, 520, 1779 (2012).

[19] M. Izaki, T. Omi, J. Electrochem. Soc., 143, L53 (1996).

[20] S.M. Sze, K.K. Ng, Physics of Semiconductor Devices, Wiley-Interscience, New Jersey, 2007, pp.126.

[21] T. Shinagawa, M. Chigane, K. Murase, M. Izaki, J. Phys. Chem. C, 116, 15925 (2012).

[22] M. Pourbaix, Atlas of Electrochemical equilibria in Aqueous Solutions, National Association of Corrosion engineering, Houston, 1974, pp. 387.

[23] M. Izaki, S. Watase, H. Takahashi, Adv. Mater., 15, 2000 (2003).

[24] Joint Committee on Powder Diffraction Standards 1992, Powder Diffraction File (Swarthmore, PA: International Data for Diffraction Data); 1992, pp 36-1451.

[25] M. Izaki, T. Ohta, M. Kondo, T. Takahashi, M. B. Fariza, M. Zamzuri, J. Sasano, T. Shinagawa, T. Pauporte, ACS Appl. Mater. Interface, 6, 13461 (2014).

CHAPTER 4

Photo-Assisted Electrochemical Construction of <0001>-n-ZnO/<111>-p-Cu_2O Photovoltaic Devices with Intermediate TiO_2 Layer

4.1 Introduction

To develop efficient PV devices, proper band alignment throughout the entire device structure is necessary to minimize energy losses from non-ideal interfaces. In Chapter 2, Cl-doped ZnO-nanowire has been deposited on the random orientation of Cu_2O layer. A highly resistive ZnO layer was inserted in between the Cl-doped ZnO-nws and Cu_2O layer. The deposition of the ZnO-nanowire and insertion of the i-ZnO layer showed a significant enhancement in conversion efficiency by expanding the active region and suppressing the

recombination loss at the interface. But, the low mobility in the random orientation of the Cu_2O layer restricted the generation of minority carriers resulted in low Jsc. The problem of low mobility in the random orientation of the Cu_2O layer has been solved by construction of heteroepitaxial growth of (111)-oriented Cu_2O layer on (111)-Au/Si as discussed in Chapter 3.

In Chapter 3, a photo-assisted electrodeposited-ZnO layer has been stacked onto the (111)-Cu_2O/(111)-Au/Si substrate, and the photovoltaic performance of the substrate type Cu_2O/ZnO PV device was obtained only by electrodeposition. By stacking an AZO layer on the top of the (111)-Cu_2O/ZnO PV device, induced an increase in the short-circuit current density (5.87 mA cm^{-2}) about 1.5 fold than that for randomly oriented Cu_2O PV device (3.8 $mAcm^{-2}$). But, the existence of pores in the resultant ZnO layer increased leakage current at the p-n heterojunction interface, resulted in decrease of the photovoltaic performance especially the Voc.

To mitigate the voltage loss mechanism due to a low built-in voltage and leakage current at the interface, a buffer layer could be introduced in between the (111)-Cu_2O layer and ZnO layer. This layer serves as an electron-blocking layer and reducing the magnitude of the recombination current at the (111)-Cu_2O/ZnO interface. And, to achieve maximum benefit, this layer needs to be thin enough to avoid significant optical absorption or resistive loss. One of the promising candidates to be used as buffer layer or electron transporting layer in between the (111)-Cu_2O/ZnO PV devices is TiO_2. This is because of its low work function, high electron mobility and optical transparency, as well as their ease of synthesis.

4.2 Objective of this study

In this study, we show the preparation of a (0001)-ZnO/(111)-Cu_2O photovoltaic device by electrodeposition in aqueous solutions and effects of the insertion of the TiO_2 layer on the photovoltaic performance. The (0001)-ZnO and (111)-Cu_2O layer were prepared by photo-assisted electrodeposition and conventional electrodeposition in aqueous solutions,

respectively. The TiO_2 layer was directly deposited on the Cu_2O by a sol-gel process composed of a spin coating and baking, and suppressed the deposition of the ZnO layer on the Cu_2O layer as well as improved the growth of ZnO layer. An AZO layer was also stacked on the top of the (0001)-ZnO/TiO_2/(111)-Cu_2O PV device by sputtering method. Since the photo-assisted electrodeposition of ZnO layer produced ZnO layer with pores, the insertion of TiO_2 and stacking AZO is a way to construct a homogenous and compact ZnO layer. The AZO layer prepared by sputtering method produced a thin and compact layer, and is relatively low resistivity compared to the ZnO layer. As discussed in Chapter 3, the stacking of the AZO layer could also induce an increase in the short-circuit current density. The structural, optical, and electrical characterization of the substrate type (0001)-ZnO/(111)-Cu_2O PV device were carried out by X-ray diffraction (XRD), scanning electron microscopy (SEM) observations, optical absorption, and electrical measurements.

4.3 Insertion of TiO_2 intermediate layer and Al:ZnO transparent conductive window in in ZnO/Cu_2O PV device

4.3.1 Experimental procedures

The Cu_2O layer was deposited potentiostatically at −0.5 V referenced to Ag/AgCl electrode on the Au(111)/Si(100) substrate at an electric charge of 1.7 coulomb cm^{-2} with a potentiostat (Hokuto Denko, HABF-501A) in an alkaline aqueous solution containing a 0.4 M copper(II) acetate monohydrate ($Cu(CH_3COO)_2.H_2O$, Nacalai Tesque, Inc.) and 3 M lactic acid (Kanto Chemical, Co., Inc.) at 328 K. KOH was added for the pH adjustment to 12.5. Prior to the electrodeposition, the Au(111)/Si(100) substrate was rinsed with acetone, polarized in 1 M NaOH and rinsed with distilled water. A Pt plate was used as the counter electrode. The TiO_2 layer was deposited on the Cu_2O by a sol-gel process composed of spin coating of 3% and

5% of mixed titanium tetra-isopropoxide (TTIP), anyhydrous 2-propanol (IPA) and diethalamine (DEA) solution at 3500 and 5000 rpm followed by a baking at 423K in air for 10 min. Then, the ZnO layer was stacked on the TiO_2 layer at a potential of −0.06 V referenced to the Ag/AgCl for the deposition time of 1800 s in a simple aqueous solution containing 0.08 M zinc nitrate hydrate at 336 K. For comparison, the TiO_2-free-ZnO/Cu_2O heterojunction diode was fabricated. The AZO layer was sputtered on the ZnO layer by using radio frequency (rf) magnetron sputtering (ULVAC, RFS-200) with AZO target (99%). The substrate temperature was 25˚C, pressure chamber of 1.0 Pa, and the rf power of 100 W for 60 sec. The photovoltaic device was fabricated by stacking 100-nm-thick-Al electrode with a vacuum evaporation (ULVAC, VPC-260F) on the top of the the (0001)-ZnO/TiO_2/(111)-Cu_2O heterostructures.

Structural characterization was carried out by X-ray Diffractometer (XRD, Rigaku RINT 2500) operated at 20 kV and 10 mA using Cu Kα radiation. The observation of surface and cross-sectional morphology of the layers was carried out with a field emission scanning electron microscope (FE-SEM, Hitachi High Technology SU8000) at an operating voltage of 3 kV. Optical absorption spectra were recorded using a UV-Vis-NIR spectrophotometer (Hitachi High-Technology UV-4100) with an integrating sphere. The current density-voltage curve in the dark and under AM1.5 illumination with 100 $mWcm^{-2}$ in power was recorded using a solar simulator (Bunko Keiki, OTENTOSUN-III) with Keithley 2400 source meter.

4.3.2 Results and discussion

4.3.2.1 Structural characteristic of ZnO/TiO_2/Cu_2O PV device

The X-ray diffraction patterns of the for ZnO/Cu_2O heterojunction structure before and after inserting the TiO_2 layer at spin coating speed of 3500 and 5000 rpm is shown in Figure 4.1.

There are three peaks seen in X-ray diffraction pattern could be assigned to the (111) plane of Au with a face-centered cubic lattice, (111) plane of Cu_2O with the characteristic cubic cupric structure, and (0002) plane of ZnO with the hexagonal structure before and after inserting the TiO_2. The X-ray diffraction patterns for the (111)-Cu_2O layer, (111)-Au and (0002)-ZnO were almost the same in profile and peak angles, irrespective of the insertion of the TiO_2 layers. And, the X-ray diffraction pattern for the ZnO layer decreased in peak intensity as the spin coating speed decrease due to the increase in TiO_2 layer thickness. However, the TiO_2 layers possessed either an amorphous or thin thickness, because that no obvious peaks identified as the TiO_2 could be observed.

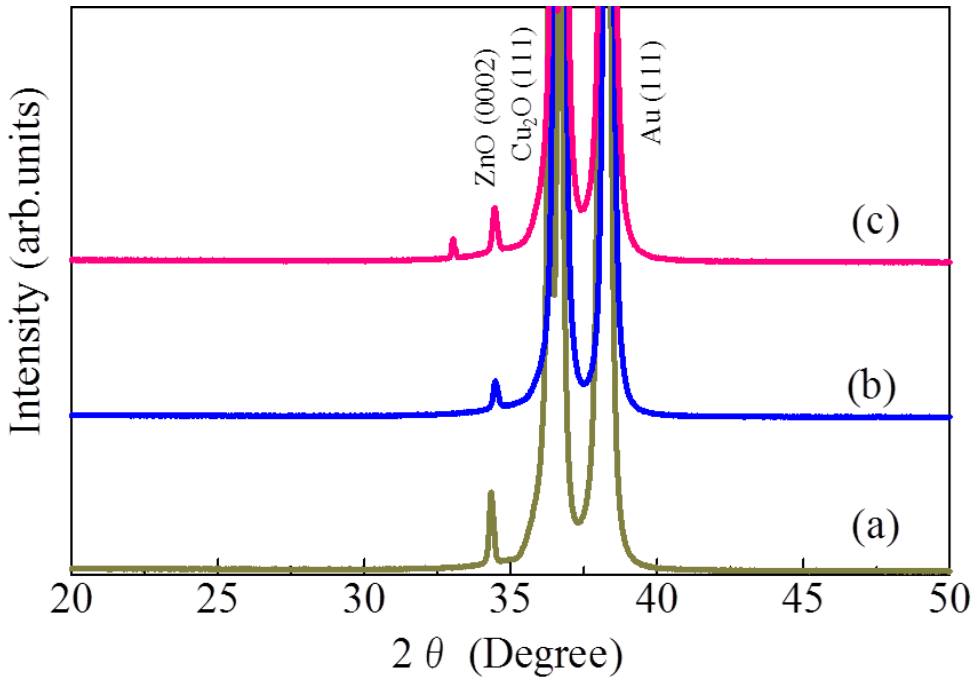

Figure 4.1 XRD patterns for ZnO/Cu_2O PV devices on Au substrate before (a) and after inserting TiO_2 layers at spin coating speed of 3500 rpm (b) and 5000 rpm (c).

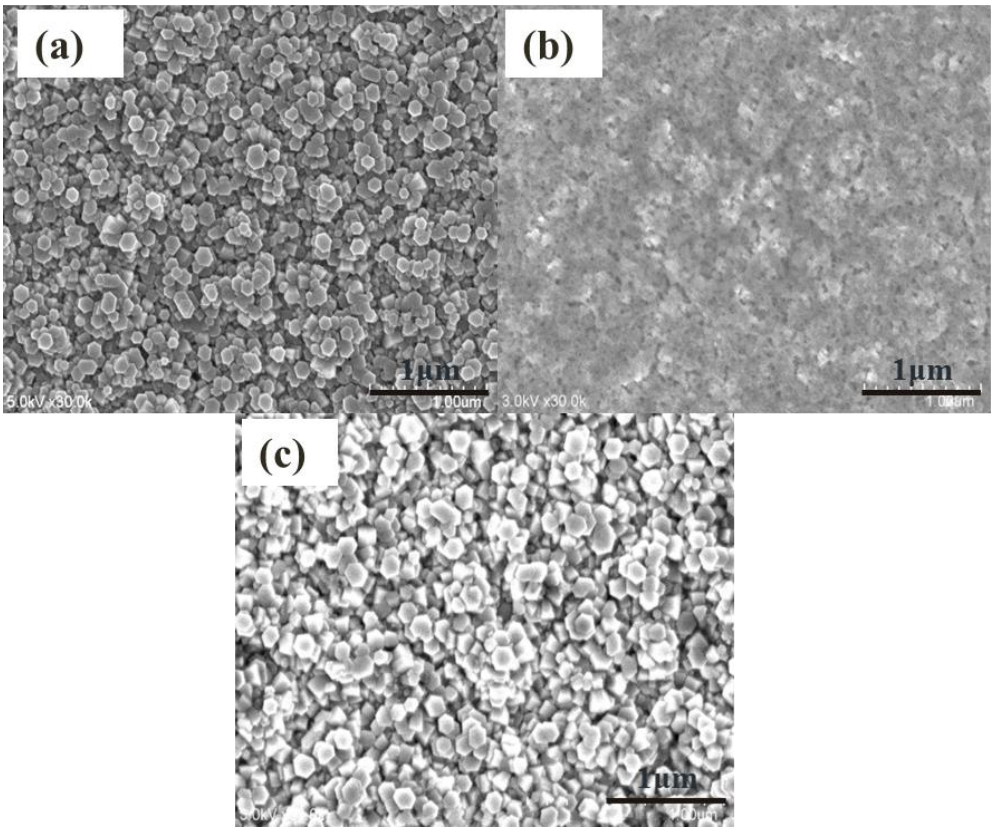

Figure 4.2 FESEM images of ZnO layer prepared without (a) and with TiO_2 layers at spin coating speed of 3500 (b) and 5000 rpm (c).

Figure 4.2 shows FE-SEM images of the ZnO layers before and after stacking the TiO_2 layer for 3500 and 5000 rpm. The Cu_2O layers deposited on the Au(111) layer were composed of aggregates of hexagonal columnar grains grown in direction perpendicular to the Au(111) substrate surface, and the thickness was estimated to be about 2.4 μm. The hexagonal columnar ZnO grains with the width of approximately 150 nm grew in the direction normal to the surface and hexagonal facets corresponding to the (0001) plane was observed clearly on the surface image before inserting TiO_2 layer. After inserting the TiO_2 layer at 3500 rpm, ZnO grains could be seen rarely on the TiO_2 layer and was consistent with the weakened diffraction peak on the XRD patterns as shown in Figure 4.2, the hexagonal columnar ZnO grains could be seen with the width of approximately 90 nm grown in the direction normal to the surface, after inserting the TiO_2 layer at 5000 rpm as shown in Figure 4.2 (c). Some pores

could be observed between the ZnO grains. The TiO_2 layer thickness estimated from FE-SEM cross-sectional image was to be about 140 nm at 5000 rpm and increased at 3500 rpm. The thickness of the ZnO layer was estimated to be around 200 nm.

4.3.2.2 Optical characteristic of ZnO/TiO_2/Cu_2O PV device

Figure 4.3 shows the absorption spectra for ZnO/Cu_2O photovoltaic devices after depositing TiO_2 layer at 3500 and 5000 rpm. The Cu_2O film showed an absorption edge at 600 nm, and the interference fringe pattern was obviously observed at a wavelength less than 600 nm, indicating the formation of Cu_2O layer with the characteristic bandgap energy of 2.1 eV. An

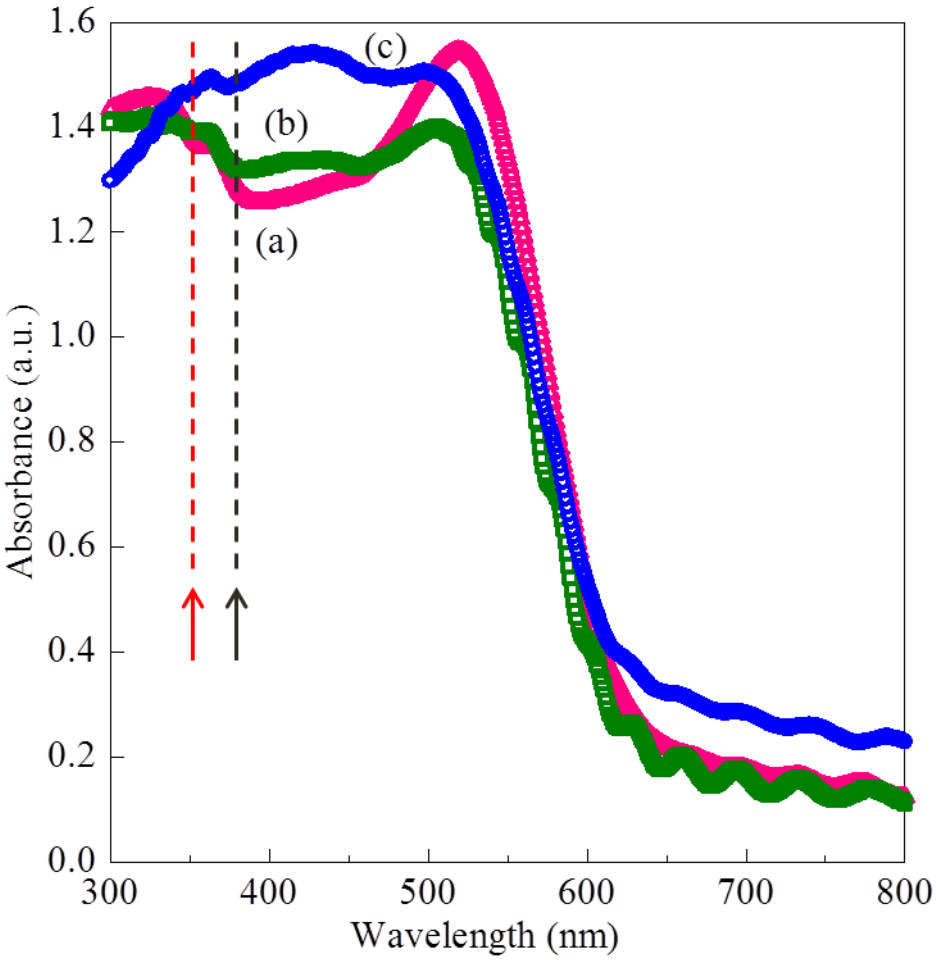

Figure 4.3 Absorption spectra for ZnO/Cu_2O PV devices without (a) and with the TiO_2 layer at 3500 (b) and 5000 rpm (c).

absorption edge was also obviously observed at a wavelength around 380 nm originated from the ZnO layer in addition to that for the Cu_2O layer as represented by black arrow. An absorption edge assigned as the TiO_2 layer also observed at a wavelength around 350 nm corresponding to the characteristic bandgap energy of 3.5 eV as represented by red arrow. The decrease in the absorbance at 350 nm was consistent with the change in the TiO2 thickness.

4.3.2.3 Electrical characteristic of ZnO/TiO_2/Cu_2O PV device

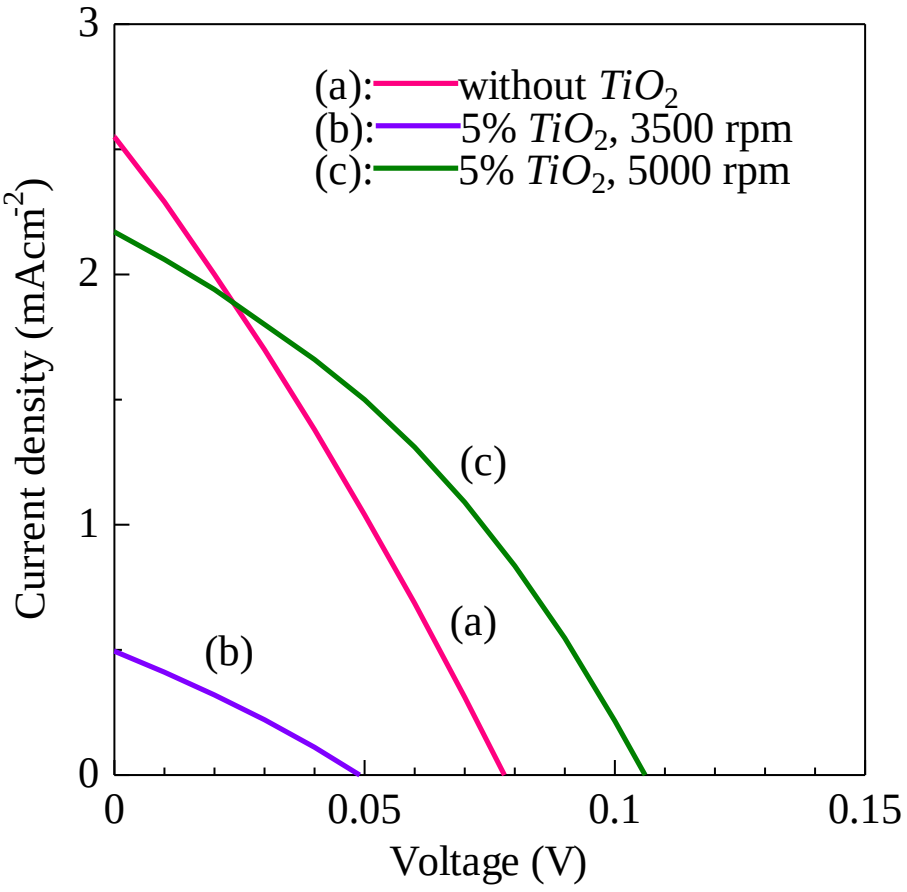

Figure 4.4 Current-voltage characteristic of the ZnO/Cu_2O PV cells without (a) and with the TiO_2 layer at 3500 (b) and 5000 rpm (c).

The current density-voltage curves for the Cu_2O/ZnO PV cells with and without TiO_2 layers are acquired under AM 1.5G illumination (100 $mWcm^{-2}$), as shown in Figure 4.4. The PV device without TiO_2 exhibited a conversion efficiency of 0.06 % with the open current voltage (Voc), short-circuit current (Jsc) and fill factor (FF) of 78 mV, 2.55 $mAcm^{-2}$, and 0.28. The performance of ZnO/TiO_2/Cu_2O PV devices strongly depended on spin coating speed closely relating to the TiO_2 layer thickness and the resultant ZnO layer. The ZnO/TiO_2/Cu_2O PV device prepared at 5000 rpm showed an increase in Voc to 0.1 V and conversion efficiency to 0.08 %, although the Jsc decreased slightly. The slight increase in Voc is made by inserting the TiO_2 layer in between ZnO/Cu_2O heterointerface, where the band-alignment was improved and interface defects was reduced. However, further improvement of the quality including the homogeneity and energy state is indispensable to raise the photovoltaic performance.

4.4.2.4 Structural characteristic of AZO/ZnO/TiO_2/Cu_2O PV device

Figure 4.5 shows X-ray diffraction patterns of ZnO/Cu_2O heterojunction structure before and after inserting the TiO_2 sol concentration of 3% and 5%. Three diffraction peaks assigned as the ZnO(0002),**[11]** Cu_2O(111),**[12]** and Au(111) planes could be observed on the XRD pattern before and after inserting the TiO_2. No obvious peaks identified as the TiO_2 could be observed on the XRD patterns. The ZnO peak intensity decreased as the TiO_2 sol concentration increased.

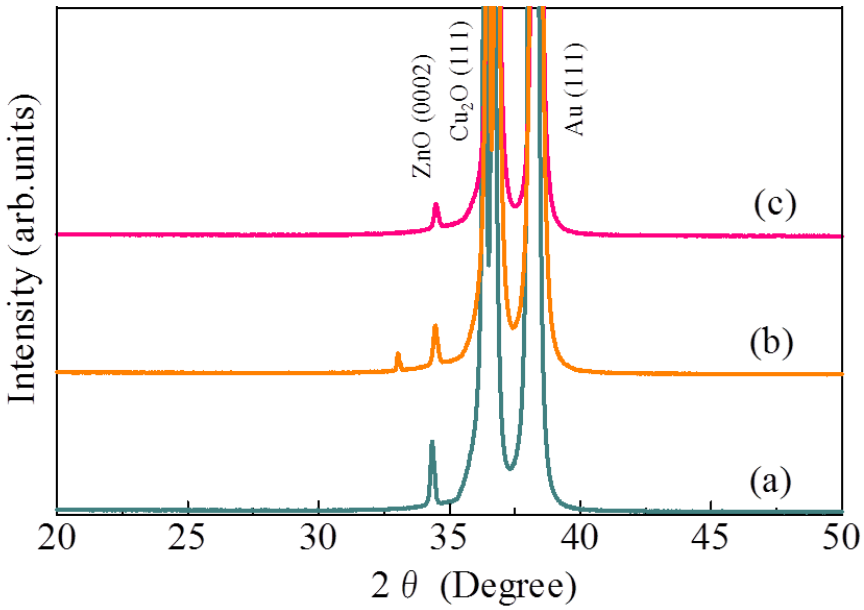

Figure 4.5 XRD patterns for AZO/ZnO/Cu_2O PV devices on Au substrate before (a) and after inserting TiO_2 layers at 3% (b) and 5% sol (c).

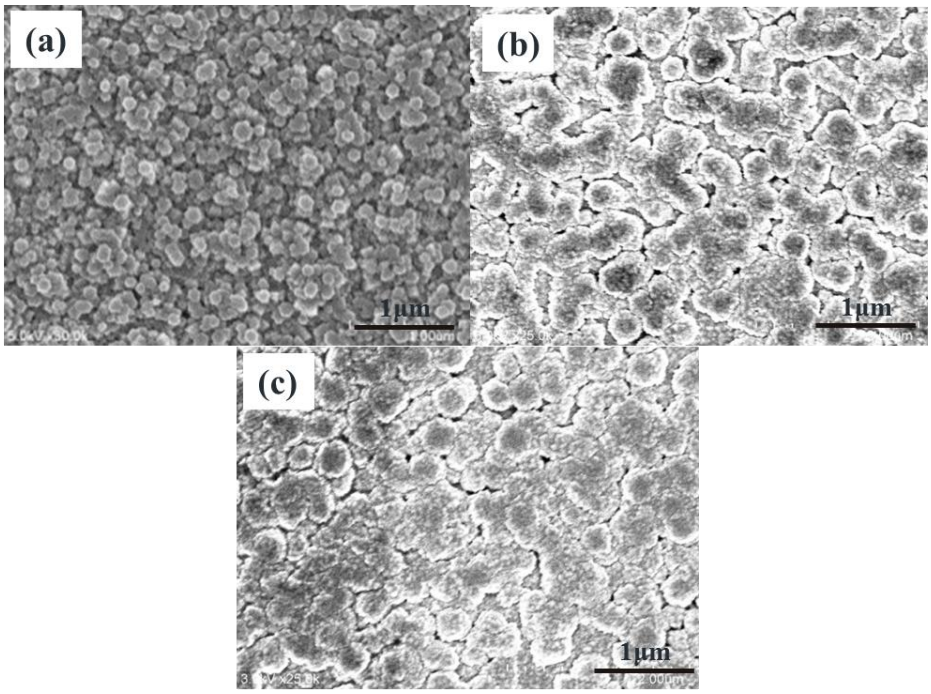

Figure 4.6 FESEM images of AZO/ZnO/Cu_2O PV device prepared without (a) and with TiO_2 layers with 3% (b) and 5 % sol (c).

Figure 4.6 shows FE-SEM images of the ZnO layers before and after stacking the TiO_2 layer with sol concentrations of 3% and 5%. The Cu_2O layers deposited on the Au(111) layer were composed of aggregates of hexagonal columnar grains grown in direction perpendicular to the Au(111) substrate surface, and the thickness was estimated to be about 2.4 μm. The hexagonal columnar ZnO grains with the width of approximately 150 nm grew in the direction normal to the surface and hexagonal facets corresponding to the (0001) plane was observed on the surface image without the TiO_2 layer. The TiO_2 layer thickness was estimated to be about 100 nm at 5% TiO_2 sol and decreased at 3% TiO_2 sol. For the TiO_2 layer prepared at 5%, ZnO grains with the width of approximately 90 nm were grown in the direction normal to the surface, and some pores could be observed between the ZnO grains. The width changed to 110 nm at 3% as shown in Fig. 4.6 (b). The thickness of the ZnO layer was estimated to be around 200 nm. The deposition of AZO layer on the ZnO layer decreased the pores between the ZnO grains.

4.4.2.5 Optical characteristic of AZO/ZnO/TiO_2/Cu_2O PV device

Figure 4.7 shows the absorption spectra for AZO/ZnO/Cu_2O PV devices after depositing TiO_2 layer with 3% and 5% TiO_2 sol. The Cu_2O film showed an absorption edge at 600 nm, and the interference fringe pattern was observed at a wavelength less than 600 nm, indicating the formation of Cu_2O layer with the characteristic bandgap energy of 2.1 eV. An absorption edge was also observed at a wavelength around 380 nm originated from the ZnO layer in addition to that for the Cu_2O layer. An absorption edge assigned as the TiO_2 layer also observed at a wavelength around 350 nm corresponding to the characteristic bandgap energy of 3.5 eV.

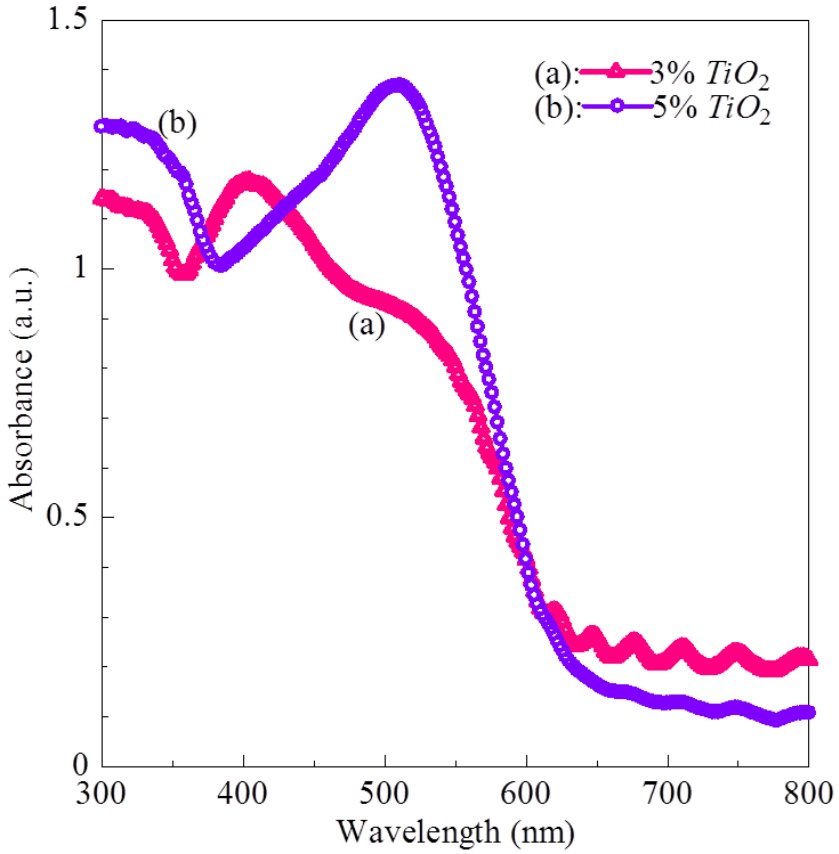

Figure 4.7 Absorption spectra for AZO/ZnO/Cu_2O PV devices with inserting the TiO_2 layer of 3% (a) and 5% sol (b).

4.4.2.6 Electrical characteristic of AZO/ZnO/TiO_2/Cu_2O PV device

To demonstrate the effect of the TiO_2 buffer layer on ZnO/Cu_2O PV cell performance, we fabricate ZnO/Cu_2O PV cells by inserting 3% and 5% TiO_2 layer. Figure 4 shows the current density-voltage curves for the AZO/ZnO/Cu_2O PV cells with and without TiO_2 layers under AM 1.5G illumination (100 $mWcm^{-2}$). The PV device without TiO_2 exhibited a conversion efficiency of 0.004 % with 0.01 V open current voltage (Voc) and 5.87 $mAcm^{-2}$ short-circuit current (Jsc). The performance of AZO/ZnO/TiO_2/Cu_2O PV devices strongly depended on TiO_2 sol concentration which closely relating to the TiO_2 layer thickness and the resultant ZnO layer.

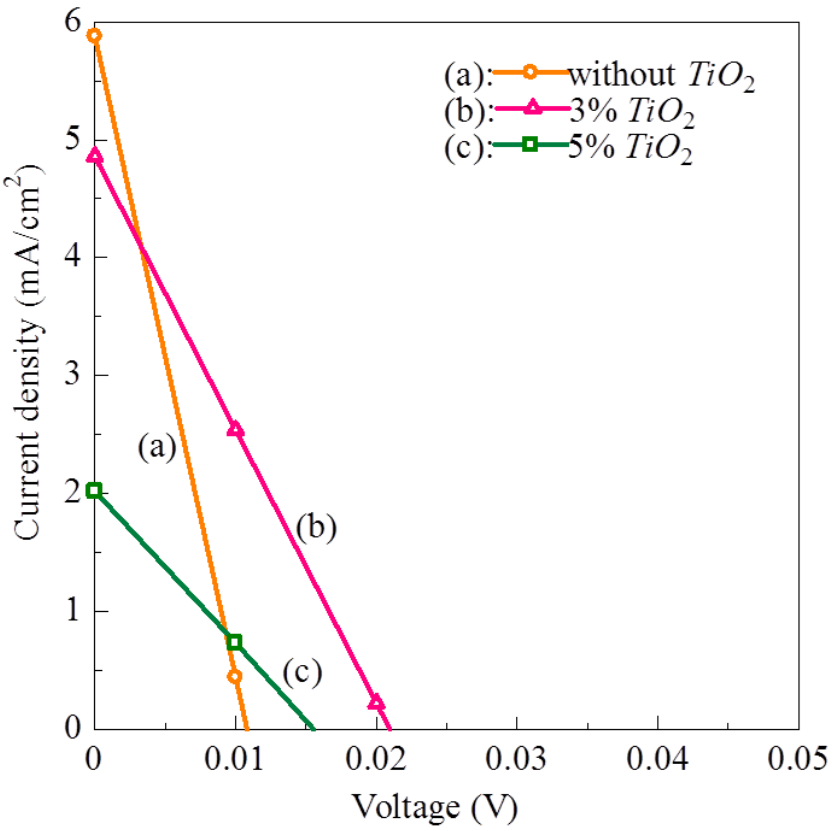

Figure 4.8 I-V curves of the AZO/ZnO/Cu_2O PV cells without (a) and with inserting the TiO_2 layer of 3% (b) and 5% sol (c).

The AZO/ZnO/TiO_2/Cu_2O PV device prepared at 3% TiO_2 sol showed an improved conversion efficiency of 0.03 %, although the Jsc decreased slightly. The Jsc was highest with PV device without TiO_2 layer, indicated that the TiO_2 layer decreased the active region resulted in decrease in Jsc. The low Voc suggested the electrical shorting thorough the pores between the deposited ZnO grains. Further improvement of the quality including the homogeneity and energy state is indispensable to raise the photovoltaic performance.

4.5 Conclusions

We have demonstrated the construction of substrate-type ZnO/TiO_2/Cu_2O PV devices and the effects of the inserted TiO_2 layer at the ZnO/Cu_2O heterointerface on the photovoltaic performance. The <111>-oriented Cu_2O layer was prepared by heteroepitaxial conventional electrodeposition, and the ZnO layer was grown by a photon-assisted electrodeposition. The PV device was fabricated by stacking the top Al electrode by evaporation. The thickness of TiO_2 layer was controlled by changing the sol concentration and spin coating speed. ZnO/TiO_2/<111>-Cu_2O PV devices showed photovoltaic performance under AM1.5 illumination, and the performance changed depending on the TiO_2 layer thickness, and the resultant ZnO layer. The insertion of the TiO_2 layer in the ZnO/(111)-Cu_2O PV device by a sol-gel process resulted in the improvement of the photovoltaic performance to 0.08% with Voc of 0.1 V, Jsc of 2.17 $mAcm^{-2}$, and FF of 0.34. And the dilution of sol gel concentration to 3% in the AZO/ZnO/TiO_2/<111>-Cu_2O PV device resulted in the improvement of the photovoltaic performance to 0.03% with Voc of 0.02 V, Jsc of 4.86 $mAcm^{-2}$, and FF of 0.25. By stacking the sputtered AZO layer on the top of the ZnO/<111>-Cu_2O PV device has increased the surface contact at the heterointerface resulting an increase in short-circuit current density. The TiO_2 layer used in this study could not be full functionalized due to the low baking temperature. After the TiO_2 sol was deposited on the Cu_2O layer, the baking process in air took place. Since the formation of undesired CuO with a sponge-like structure was detected on the surface of Cu_2O annealed in air at 400 $^{\circ}$C,[1] the TiO_2 sol has been baked with temperature of 150 $^{\circ}$C much lower than the temperature needed for proper baking which is around 500 $^{\circ}$C. Thus, that is the reason for the TiO_2 layer prepared by sol gel method is not viable as a buffer layer in the AZO/ZnO/TiO_2/<111>-Cu_2O PV device prepared on (111)-Au/Si substrate.

REFERENCES

[1] T. Shinagawa, M. Onoda, B. M. Fariza, J. Sasano, M. Izaki, J. Mater. Chem. A, 1 9182 (2013).

CHAPTER 5

<111>-oriented Cu_2O-electrodeposit and the photovoltaic device with improved performance

5.1 Introduction

In this chapter, an AZO layer has been prepared on the (111)-oriented Cu_2O/(111)-Au/Si by sputtering method. The problem of low mobility in the random orientation of the Cu_2O layer has been solved by construction of heteroepitaxial growth of (111)-oriented Cu_2O layer on (111)-Au/Si substrate as discussed in Chapter 3. High mobility of the minority carriers in the Cu_2O layer could increase the carrier's diffusion length and the photovoltaic device conversion efficiency. And, the photovoltaic performance of the substrate-type (111)-

Cu_2O/ZnO PV device was obtained for the first time by stacking the ZnO layer onto the (111)-Cu_2O/(111)-Au/Si substrate only by electrodeposition. Furthermore, stacking an AZO layer on the top of the (111)-Cu_2O/ZnO PV device, induced an increase in the short-circuit current density (5.87 mA cm^{-2}) about 1.5 fold than that for randomly oriented Cu_2O PV device (3.8 $mAcm^{-2}$). However, the existence of pores in the resultant ZnO layer increased the leakage current at the p-n heterojunction interface, resulted in decrease of the photovoltaic performance.

In Chapter 4, a thin TiO_2 buffer layer has been introduced in between the (111)-Cu_2O layer and ZnO layer aimed to mitigate the voltage loss mechanism due to a low built-in voltage and leakage current at the interface. This layer serves as an electron-blocking layer and reducing the magnitude of the recombination current at the (111)-Cu_2O/ZnO interface. In order to achieve maximum benefit, this layer has been controlled to avoid significant optical absorption or resistive loss. However, the TiO_2 layer used in this study could not be full functionalized due to the low baking temperature. Higher baking temperature could not be applied due to the formation of undesired CuO with a sponge-like structure on the surface of Cu_2O annealed in air over 400 $^{\circ}$C. This is the reason why the TiO_2 layer prepared by sol gel method is not viable as a buffer layer in the AZO/ZnO/TiO_2/<111>-Cu_2O PV device.

5.2 Challenges in construction of <111>-oriented Cu_2O PV device

Since the ZnO layer prepared by the photo-assisted electrodeposition was not compact and homogenous due to pores in between the ZnO grains, the photovoltaic performance decrease because of the increase in the leakage current at the p-n heterojunction interface. And, the insertion of TiO_2 layer in between (111)-Cu_2O layer and ZnO layer has shown low photovoltaic performance especially the Voc, an AZO layer was directly deposited on the

(111)-Cu_2O layer to construct a PV device. The (111)-Cu_2O layer was prepared by conventional electrodeposition method and the AZO layer was prepared by sputtering method. The AZO layer needs to be very thin, compact and homogenous to avoid leakage current, and fabrication by sputtering method could fulfil this requirement.

5.3 Objective of this study

In this study, we demonstrate the preparation of <111>-Cu_2O/Al-doped ZnO (AZO) PV device by the electrodeposition of the Cu_2O layer followed by stacking the AZO layer by a sputtering, and reports the effects of Cu_2O layer thickness on the photovoltaic performance. The structural, optical, and electrical characterizations for the Cu_2O/AZO PV device were carried out by X-ray diffraction (XRD), scanning electron microscopy (FE-SEM) observations, optical absorption and electrical measurements.

5.4 Heteroepitaxial growth and characteristic of (111)-oriented Cu_2O layer prepared on (111)Au/Si substrate

5.4.1 Experimental procedures

The Cu_2O layer was deposited potentiostatically at −0.5 V referenced to Ag/AgCl electrode on the Au(111)/Si(100) substrate at various electric charge range from 1.0, 1.7 and 2.0 $C.cm^{-2}$ with a potentiostat (Hokuto Denko, HABF-501A) in an alkaline aqueous solution containing a 0.4 M copper(II) acetate monohydrate ($Cu(CH_3COO)_2.H_2O$, Nacalai Tesque, Inc.) and 3 M lactic acid (Kanto Chemical, Co., Inc.) at 328 K. The solution was prepared with deionized (DI) water purified by an Elix-UV system (Millipore), and KOH was added for the pH adjustment to 12.5. The Au(111)/Si(100) substrate (Kobelco Research Inst. Inc.)

was composed of 0.5μm-sputtered Au layer on a single-crystal Si(100) wafer, and prior to the electrodeposition, the Au(111)/Si(100) substrate was rinsed with acetone, polarized in 1 M NaOH and rinsed with distilled water. A Pt plate was used as the counter electrode. The AZO layer was sputtered on the Cu_2O layer by using radio frequency (rf) magnetron sputtering (ULVAC, RFS-200) with AZO target (99%). The substrate temperature was 25˚C, pressure chamber of 1.0 Pa, and the rf power of 100 W for 60 sec. The photovoltaic device was fabricated by stacking 100-nm-thick-Al electrode with a vacuum evaporation (ULVAC, VPC-260F) on the top of the AZO/Cu_2O heterostructures.

Structural characterization was carried out by X-ray Diffractometer (XRD, Rigaku RINT 2500) operated at 20 kV and 10 mA using Cu Kα radiation. The observation of surface and cross-sectional morphology of the layers was carried out with a field emission scanning electron microscope (FE-SEM, Hitachi High Technology SU8000) at an operating voltage of 3 kV. An X-ray photoelectron spectroscopy (XPS) analysis and valence band spectra measurements were performed using an ULVAC-PHI model 5700 MC with monochorometed Al Kα radiation at pressure of around 1.6 $x10^{-8}$ Pa. Optical absorption spectra were recorded using a UV-Vis-NIR spectrophotometer (Hitachi High-Technology UV-4100) with an integrating sphere. The photoluminescence spectrum was recorded with fluorescent spectroscopy (Hitachi, F-7000) at room temperature. The electrical characteristic of both AZO and Cu_2O layers were carried out by the van-der-Pauw method using a Hall effect measuring system(Toyo Technica, Resitest 8310) in air at ambient temperature and 0.3 T magnetic field. The AZO sample was prepared by mechanically splitting them off from the glass substrate followed by fastening in epoxy resin (Araldite 2091). The Cu_2O sample was prepared on Au/Si substrate in the same manner as that for AZO sample. The current density-voltage curve in the dark and under AM1.5 illumination with 100 $mWcm^{-2}$ in power was recorded using a solar simulator (Bunko Keiki, OTENTOSUN-III) with Keithley 2400 source

meter. The incident photon-to-electron conversion efficiency (IPCE) measurements were performed using an IPCE setup (Bunko Keiki, SM-250 KB).

5.4.2 Results and discussion

5.4.2.1 Structural characteristic of Cu_2O layer prepared on the (111)Au/Si substrate

The X-ray diffraction pattern of the Cu_2O layer with different electric charges varied from 1.0~2.0 $C.cm^{-2}$ prepared on the (111)-Au/Si substrate is shown in Figure 5.1. Only two peaks seen in X-ray diffraction pattern could be assigned to the (111) plane of Au with a face-

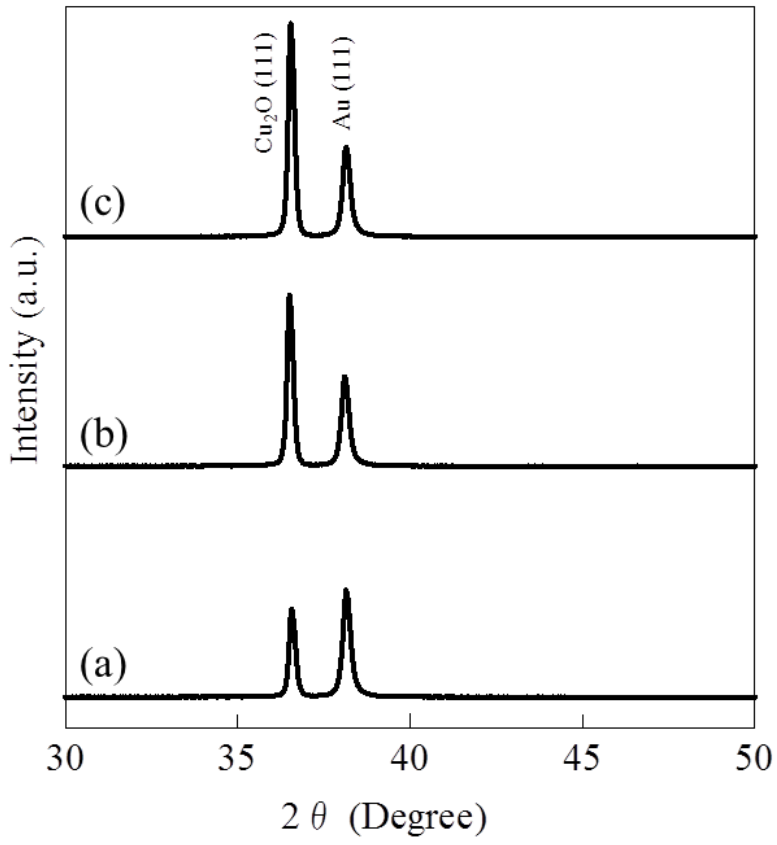

Figure 5.1 X-ray diffraction pattern of Cu_2O(111) and Au(111) for Cu_2O/Au/Si prepared with Cu_2O layers electric charges of (a) 1.0, (b) 1.7, and (c) 2.0 $C.cm^{-2}$.

centered cubic lattice and (111) plane of Cu_2O with the characteristic cubic cupric structure. The lattice parameter calculated from the Cu_2O (111) peak was 4.267 Å, which almost agreed with the standard value of 4.269 Å tabulated in the ICDD card.**[1]** The X-ray diffraction patterns for the (111)-Cu_2O layer and (111)-Au were almost the same in profile and peak angles, irrespective of the electric charges of the Cu_2O layers. The electrodeposition of Cu_2O layer had no effect on the intensity and angles of the (111)-Au peaks. And, the X-ray diffraction pattern for the Cu_2O layer increased in peak intensity as the electric charges increase.

5.4.2.2 Optical characteristic of Cu_2O layer prepared on the (111)Au/Si substrate

Figure 5.2 shows the correlation absorption coefficient and photon energy, and the room temperature photoluminescence spectra for the (111)-Cu_2O layer prepared on the (111)-Au/Si substrate. The absorption coefficient was calculated from the absorbance and thickness obtained with a SEM observation. The optical bandgap energy (E_g) was estimated by extrapolating the linear part with the assumption of a direct optical transition **[2]** for Cu_2O layer and was measured to be approximately 2.0 eV irrespective of the electric charges of Cu_2O layers.

The (111)Au/Si substrate showed no luminescence at room temperature. The (111)-Cu_2O layer emitted visible light at photon energies of 1.55, 1.61, 1.93 and 2.01 eV. The photoluminescence characteristics and the related energy level were widely investigated for single crystal and polycrystalline Cu_2O prepared by several techniques including electrodeposition.**[3,4]** The 2.0-eV-ultraviolet light originated from the near band emission due to the direct recombination of the phonon-assisted excitons.**[5]** The visible lights at the photon energies of 1.55, 1.61 and 1.93 eV were identified as deep level emissions due to

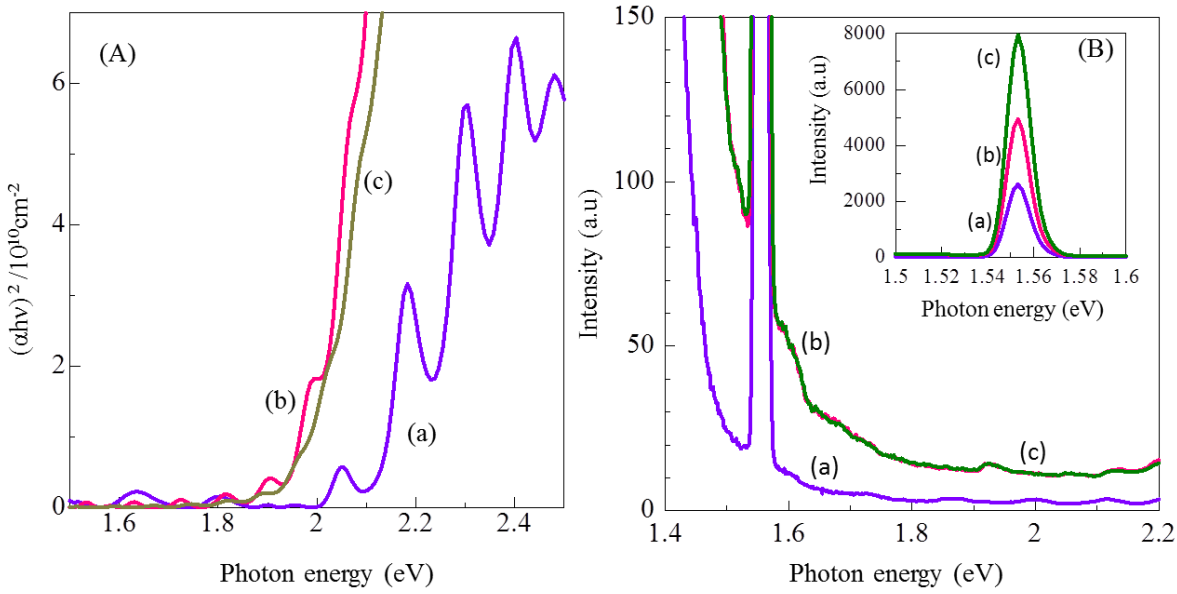

Figure 5.2 Correlation between absorption coefficient and photon energy (A), and photoluminescence spectra (B) for the <111>-Cu_2O layer prepared with electric charges 1.0 (a), 1.7 (b) and 2.0 $C.cm^{-2}$ (c) on (111)Au/Si substrate at room temperature. The inset shows the photoluminescence spectra for photon energy from 1.5~1.6 eV.

impurity and native defects, such as copper vacancies and oxygen vacancies.**[6]** The peaks intensity of the 1.55 eV visible light increased as the increase in the electric charges of Cu_2O layers which relates to the increase in amount of copper vacancies. The native defect of copper vacancies from the visible light at 1.55 eV could act as an acceptor and scattering center in the Cu_2O layer, which resulted in decrease of the carriers' mobility.

No emission due to the recombination of excitons could be observed for the randomly oriented Cu_2O layer prepared by electrodeposition on a transparent conductive glass substrate.**[7]** Since the lattice defects and impurities generate localized levels within the bandgap energy, the emission due to the impurities and native defects is dominant in low purity and low quality semiconductors and the emission due to the recombination of excitons can be observed for the high quality and high purity semiconductors. The 2.0-eV-visible light

emission is evident for the high quality and high purity of the (111)-oriented Cu_2O layers prepared by electrodeposition.

5.5.2.3 Morphological characteristic of AZO/Cu_2O PV device

Figure 3 show the schematic illustration of cell configuration of substrate type AZO/Cu_2O PV device and the FE-SEM images of the Cu_2O layers before and after stacking the AZO layer for 60 sec by using r.f. magnetron sputtering. The Cu_2O layers deposited on the Au(111) layer were composed of aggregates of the hexagonal columnar grains grown in direction perpendicular to the Au(111) substrate surface, and the thickness was estimated to

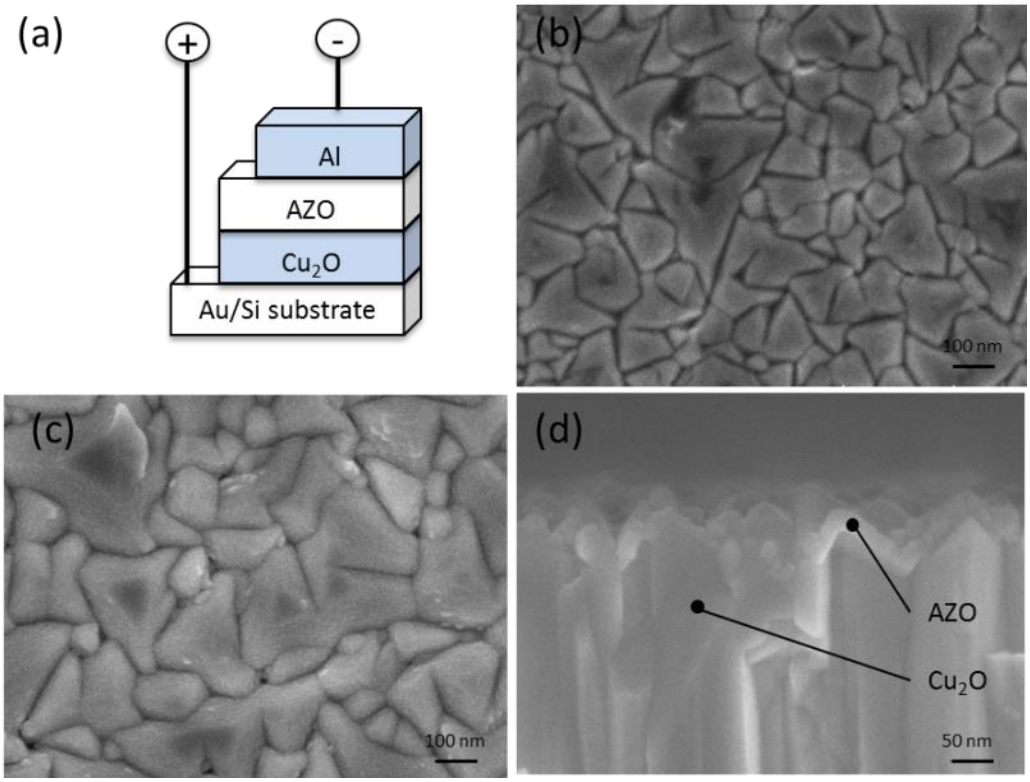

Figure 5.3 Schematic illustration of cell configuration of substrate type AZO/Cu_2O PV device (a) and surface and cross-sectional FESEM images of Cu_2O layer before (b) and after (c,d) depositing AZO layer.

be about 2.4, 2.0, 2.6 μm at the different of electric charge of 1.0, 1.7 and 2.0 $C.cm^{-2}$ respectively. The triangular facet corresponding to the (111)-plane of the Cu_2O crystal was obviously observed in the plan-view FE-SEM image even after stacking the AZO layer, and the surface morphology was similar to the typical pyramidal-shape-Cu_2O layer prepared on a conductive glass substrate as already reported.**[8]** The pyramidal-shape of Cu_2O grains increased from 0.3-0.4 μm to 0.4-0.5 μm as the electric charge increased from 1.7 to 2.0 $C.cm^{-2}$. The Cu_2O grains were reported to have an increase by the increase in electric charges.**[9]** No defects such as pores were observed throughout the layer thickness. The AZO

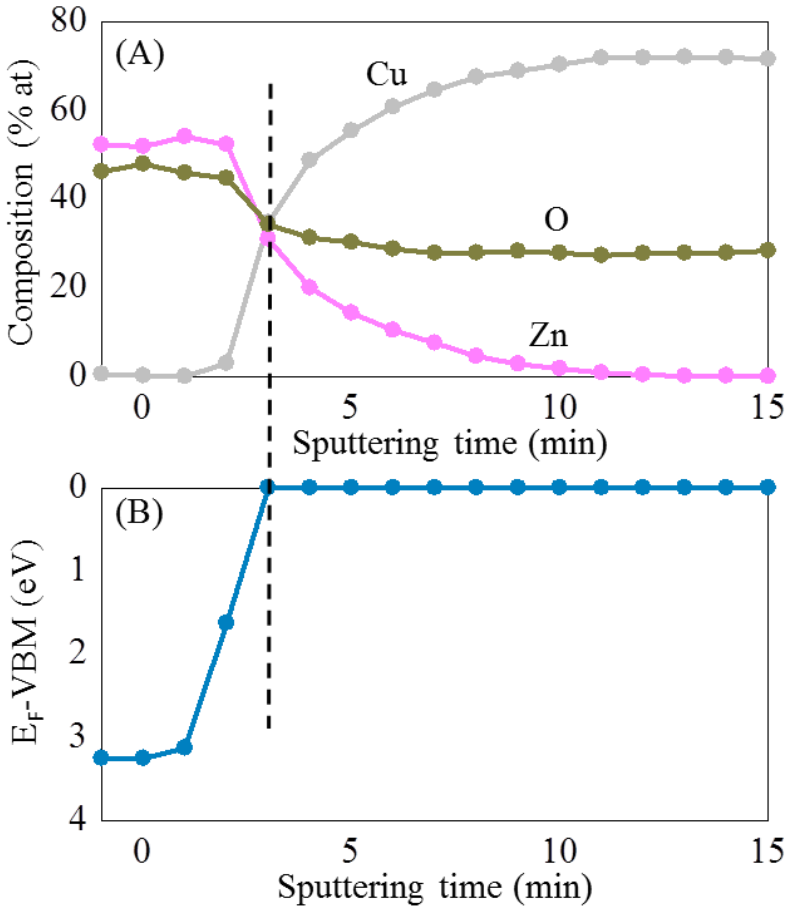

Figure 5.4 XPS depth profile (A) for AZO/Cu_2O PV device and valence band spectra (B) recorded for AZO layer.

layer could be observed both on the surface and cross-sectional images after sputtering for 60 sec. The AZO layer was found to be deposited on the entire surface of the Cu_2O layer. And, the thickness was estimated to be about 50 nm from the cross-sectional images, irrespective of the thickness of the Cu_2O layer. No voids could be observed between the Cu_2O layer and AZO layer.

Figure 5.4 show the XPS depth profile of the Cu, O, Zn elements for the AZO/Cu_2O PV device and valence band spectra recorded for the AZO layer. The XPS depth profile revealed the location of Zn was at the surface the Cu layer. This indicates the formation of AZO layer on the Cu_2O layer was consistent with the FE-SEM images in Figure 5.3. The formation of oxide could be observed relatively higher with the AZO layer compared to the Cu_2O layer, and the oxide was constant throughout the Cu_2O layer. The electron spectra for AZO layer were recorded before and after Ar sputtering for 15 min, and it was confirmed that the state of Zn^{2+} and O^{2-} agreed with those in the AZO semiconductor from the Zn2p3, and O1s electron spectra. The valence band maximum (VBM) was estimated by extrapolating the linear part of the spectra, and the AZO layer showed the value of approximately 3.25 eV. The value of 3.25 eV corresponded to the energy difference between the valence band maximum (VBM) and Fermi Level (E_F), since the 0 eV in the binding energy corresponded to the Fermi Level in the sample.

The location of the Fermi Level (E_F) is closely related to the carrier concentration. The energy difference (ΔE_c) between the conduction band minimum (CBM) and Fermi Level (E_F) is estimated for n-type semiconductor by the following equation:

$$\Delta E_C = CBM - E_F = \kappa T \log_e (N_c/n) \quad (1)$$

Where κ , T, and N_c are the Boltzman constant, temperature, and effective density of state in the conduction band. The energy difference between the conduction band minimum (CBM, E_c) and Fermi Level (E_F) was estimated to be 0.35 eV.

The energy difference (ΔE_v) between the valence band maximum (VBM) and Fermi Level (E_F) could be estimated for the p-Cu_2O layer by the following equation:

$$\Delta E_v = E_F - VBM = \kappa T \log_e (N_v/p) \quad (2)$$

The energy difference (Δ Ev) decreased with increasing the carrier concentration corresponding to the acceptor density until the acceptor density reached the effective density of state (N_v).

5.4.2.4 Optical characteristic of AZO/Cu_2O PV device

The optical absorption spectra for the AZO/Cu_2O PV device with different electric charges of Cu_2O layers are presented in Figure 5.5. The Cu_2O layers showed an absorption edge at 600 nm, and the interference fringe pattern was obviously observed at a wavelength less than 600 nm, indicating the formation of homogeneous Cu_2O layers. An absorption edge was also observed at a wavelength around 380 nm originated from the AZO layers in addition to that for the Cu_2O layers. Without stacking the AZO layer, the light absorption of the Cu_2O layer exhibited the lowest value compared to the AZO/Cu_2O PV devices. The maximum absorption was found to be with the 2.6 μ m-thick- Cu_2O layer due to the increased of photon absorption near the interface, arising from light scattering by the pyramidal-shape of Cu_2O layer. The light absorption increased with the increase in Cu_2O layer thickness, and trapped more light further within the active layer compared with the thinner Cu_2O layer. This will allow more generation of minority carriers far within the active layer for the thicker Cu_2O layer.

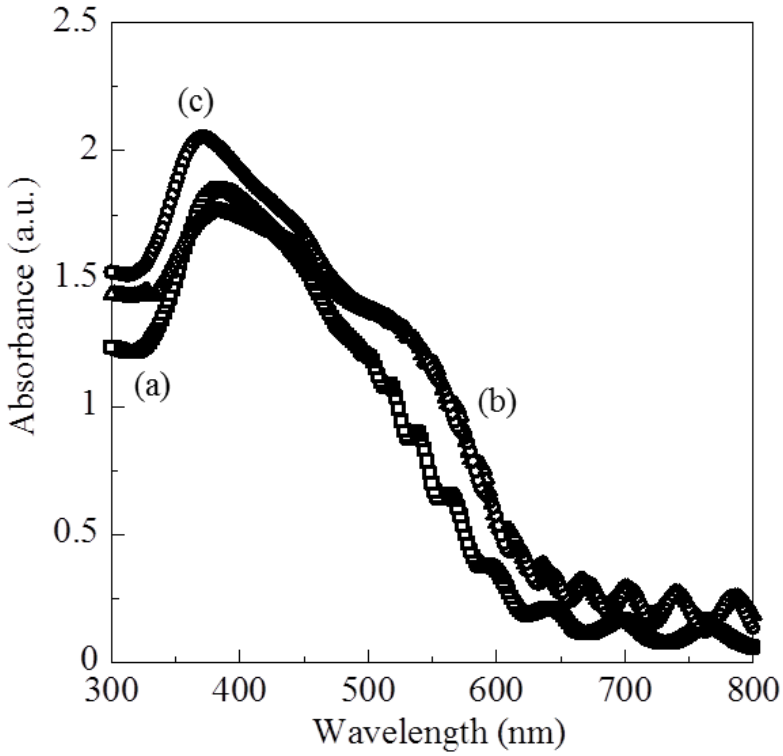

Figure 5.5 Absorption spectra for AZO/Cu_2O PV device prepared with Cu_2O layers electric charges of (a) 1.0, (b) 1.7, and (c) 2.0 $C.cm^{-2}$.

5.4.2.5 Electrical characteristic of AZO/Cu_2O PV device

Figure 5.6 shows current density-voltage curves of the AZO/Cu_2O PV devices with different electric charges of Cu_2O layer in the dark and under AM 1.5 illumination (100 $mWcm^{-2}$). And the correlation of conversion efficiency, Jsc, Voc and FF for AZO/Cu_2O PV devices as a function of the Cu_2O layer thickness are summarized in Figure 5.7. In the dark condition (A), the AZO/Cu_2O PV device with Cu_2O layer deposited for 1.0 $C.cm^{-2}$ showed a proportional increase in the current density to the applied voltage, indicating an ohmic behavior. The Cu_2O layer with thickness of 2.0 μm formed at 1.7 $C.cm^{-2}$ exhibited a slight rectification, while an obvious rectification could be observed for the Cu_2O layer with thickness 2.6 μm formed at2.0 $C.cm^{-2}$. The rectification feature is improved by increase in the thickness, as shown in

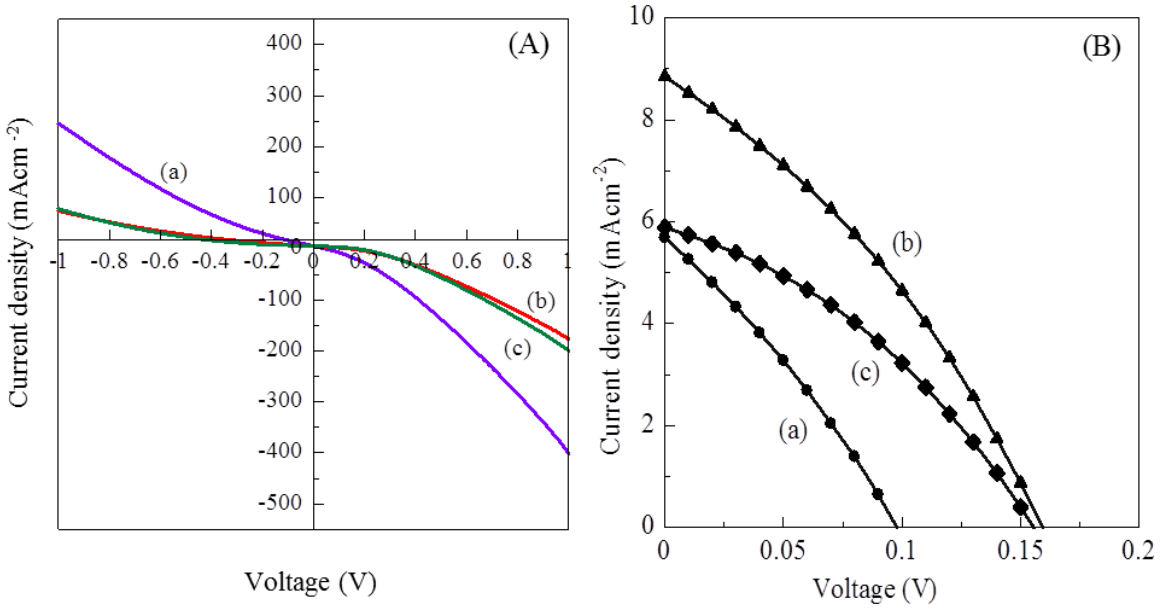

Figure 5.6 Current density-voltage curves evaluated for AZO/Cu_2O PV devices with different Cu_2O layers electric charges of (a) 1.0, (b) 1.7, and (c) 2.0 $C.cm^{-2}$ in the dark (A) and under illumination (AM 1.5G spectrum) (B).

rectification ratio. The rectification ratio strangler depended on the heterointerfacial state, but the feature changed by the thickness, especially 1.0 $C.cm^{-2}$. Figure 5.6(b) shows current density-voltage curves of the AZO/Cu_2O photovoltaic devices with different Cu_2O thickness under AM 1.5 illumination. All of the AZO/Cu_2O PV devices showed the photovoltaic performance. The AZO/Cu_2O photovoltaic device showed a strong dependence on the Cu_2O layers thickness. The AZO/Cu_2O PV device with Cu_2O layer thickness of 2.4 μm exhibited a short-circuit current density (Jsc) of 5.7 $mAcm^{-2}$ with a fill factor (FF) of 0.29, open-circuit voltage (Voc) of 0.10 V, and a power conversion efficiency (PCE) of 0.16%. By optimizing the Cu_2O layer thickness to 2.0 μm, the photovoltaic performance was found to produce the highest Voc, Jsc, FF and PCE of 0.16 V, 8.85 $mAcm^{-2}$, 0.33 and of 0.47% respectively. The

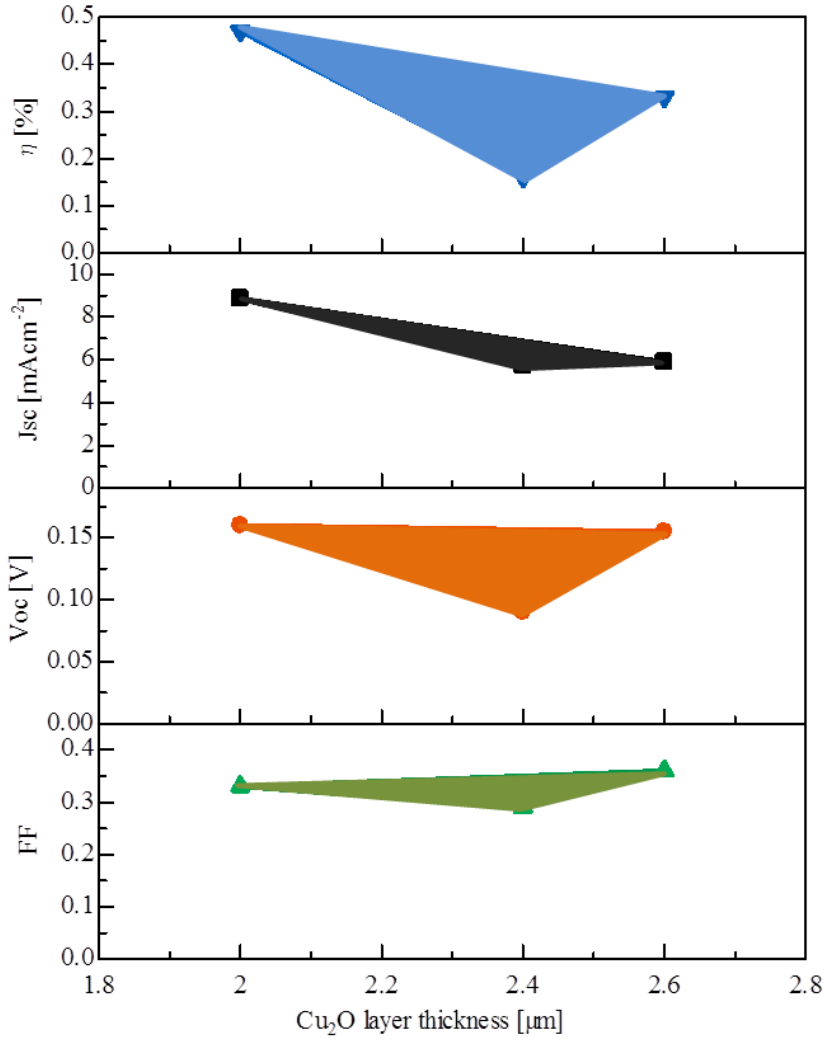

Figure 5.7 Correlation of η (a), Jsc (b), Voc (c) and FF (d) for AZO/Cu_2O PV devices as a function of the Cu_2O layer thickness.

photovoltaic performance for the AZO/Cu_2O PV device with 2.6 μ m Cu_2O layer showed a PCE of 0.33% with a Voc of 0.16 V, Jsc of 5.89 $mAcm^{-2}$ and FF of 0.36. The sputtered AZO layer completely covered over the entire Cu_2O layer and took the generated carrier out from the Cu_2O layer. The Jsc value of 8.85 $mAcm^{-2}$ obtained for the electrodeposited AZO/Cu_2O is slightly higher value than 8 mAcm-2 reported for the AZO/Cu_2O heterojunctions having thermally oxidized copper sheets over 1000˚C.**[10]**

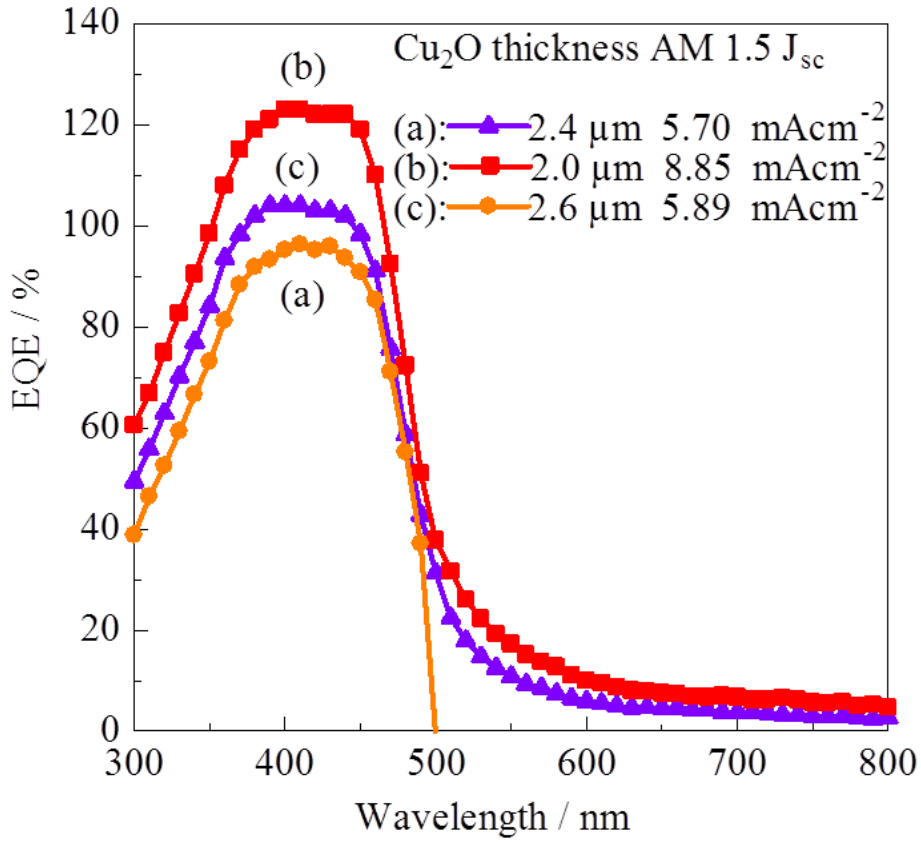

Figure 5.8 EQE spectra observed from AZO/Cu_2O PV devices fabricated with various Cu_2O layers electric charges of (a) 1.0, (b) 1.7, and (c) 2.0 $C.cm^{-2}$.

Figure 5.8 shows the external quantum energy (EQE) spectra observed from AZO/Cu_2O PV cells fabricated with various Cu_2O layer thicknesses. The beneficial effect of optimization of the Cu_2O layer is in the increasing of the Jsc could be also observed in the EQE measurement. This indicates that carriers were effectively generated in the Cu_2O layer upon illumination by light and hence, exhibits the increase in the diffusion length of the minority carriers. The onset of EQE at wavelength around 600 nm is corresponding to the absorption of Cu_2O layer, and is consistent with absorption spectra as in Figure 5.5. And, the drop-off of EQE for wavelength below 380 nm is mostly corresponds to the absorption in the AZO layer. The different of the EQE in the wavelengths of 380-460 nm, was mainly affected by the bulk properties of Cu_2O layer resulting from the increase of diffusion length of generated carriers

and light trapping effect. Thus, as expected, the EQE of the AZO/Cu_2O PV device with Cu_2O layer thickness of 2.0 μ m showing the maximum conversion efficiency of 123%, reveals the highest response especially in the medium wavelength region (380-460 nm) than the other PV devices. To the best of our knowledge, the obtained conversion efficiency of AZO/Cu_2O (2.0 μ m) PV device in the EQE spectra is the highest value ever reported for an AZO/Cu_2O heterojunction under AM 1.5 illumination. The reason for the increased EQE might be due to the light that travels through the Cu_2O layer reflected back at the mirror-like Au substrate, resulting in enhancement of the generated carriers further inside the Cu_2O layer. And the tuned Cu_2O layer thickness closed to the carrier diffusion length generated optimum minority carriers. While, the EQE for the AZO/Cu_2O PV devices with Cu_2O layer thickness of 2.4 and 2.6 μ m exhibit the conversion efficiency of approximately 98% and 105% respectively. These results indicate that the highly <111>-oriented Cu_2O layer could be carefully tuned to increase the diffusion length of the generated carriers.

The Jsc and Voc of 3.8 $mAcm^{-2}$ and 0.59 V were obtained for the randomly oriented Cu_2O/ZnO PV devices prepared by electrodeposition.**[8]** The change in the Cu_2O layer thickness has induced a remarkable increase in the Jsc from 5.7 to 8.85 $mAcm^{-2}$ due to the increase in the diffusion length of the generated carriers for the highly oriented (111)-Cu_2O layer. The Jsc reported here was 2.3 times higher than that for the Cu_2O/ZnO/FTO PV device, but the Voc was very low. The Voc value strongly depended on the heterointerface state including the band alignment, and the Voc ranging from 0.55 to 1.2 V**[11,12]** was reported depending on the oxide materials inserted between the AZO and Cu_2O layers.

The remarkable increase in conversion efficiency of 6.1% with 0.84 V in Voc, 10.95 $mAcm^{-2}$ in Jsc, and 0.66 in FF, has been reported for AZO/Al-Ga_2O_3/Na-Cu_2O PV device prepared by thermal oxidation of a metallic Cu sheet followed by a pulse laser deposition of

Ga_2O_3 and AZO layers.**[13]** Without any buffer layer and heat treatment, our AZO/2.0 μ m-Cu_2O PV device has shown the highest EQE of 123%, while the Jsc value obtained here was slightly lower than that for the AZO/Ga_2O_3/Cu_2O PV device and the Voc was very low compared with the AZO/Ga_2O_3/Cu_2O PV device. Further improvement of the quality including the homogeneity, thickness and energy state is indispensable to raise the photovoltaic performance.

5.6 Conclusion

In summary, a strong enhancement of short-circuit current density of the substrate-type ZnO/Cu_2O PV device is demonstrated. The substrate-type ZnO/Cu_2O PV device has been constructed by electrodeposition of the (111)-Cu_2O layer on an Au (111)/Si wafer substrate followed by stacking the AZO layer by sputtering. The (111)-Cu_2O layer was prepared by electrodeposition on (111)-Au/Si wafer substrate in an alkaline solution containing copper acetate and lactic acid. The PV device was fabricated by stacking the top Al electrode by evaporation. The thickness of Cu_2O layer was controlled by changing the electric charge during the electrodeposition process. All AZO/(111)-Cu_2O PV devices showed photovoltaic performance under AM1.5 illumination, and the performance changed depending on the Cu_2O layer thickness, resulting in the increase in diffusion length of the generated carriers. The photovoltaic performance of 0.015% with short-circuit current density of 5.87 $mAcm^{-2}$ and open-circuit voltage of 0.01 V was obtained for the substrate-type photo-assisted electrodeposited ZnO/<111>-Cu_2O PV device. And, the highest photovoltaic performance of 0.47% with short-circuit current density of 8.85 $mAcm^{-2}$ and open-circuit voltage of 0.16 V was obtained for the substrate-type sputtered AZO/<111>-Cu_2O PV device.

The Jsc value was larger than that for the super-straight type Cu_2O/ZnO-nanowire and Cu_2O/ZnO-layer PV devices with values of 3.8 and 7.1 $mAcm^{-2}$, respectively with an expanded active layer. The <111>-Cu_2O layer possessed an improved mobility of carrier, compared to that for the polycrystalline Cu_2O installed into the super-straight type Cu_2O/ZnO-nanowire and Cu_2O/ZnO-layer PV devices.

REFERENCES

[1] S. W. Lee,Y. S. Lee, J. Heo, S. C. Siah, D. Chua, R. E. Brandt, S. B. Kim, J. P. Mailoa, T. Buonassisi, R. G. Gordon, Adv. Energy Mater., 1301916 (2014).

[2] Kittel, C. Introduction to Solid State Physics, 6th edition, p.186, John Wiley & Sons, New York, 1986.

[3] D. W. Snoke, A. J. Shields, M. Cardona, Phys. Rev. B, 45, 11693 (1992).

[4] Y. Petroff, P. Y. Yu, Y. R. Shen, Phys. Rev. B, 12, 2488 (1975).

[5] T. Ito, T. Masumi, J. Phys. Soc. Jpn., 66, 2185 (1997).

[6] Y. Terui, M. Fujita, Y. Miyakita, N. Sogoshi, S. Nakabayashi, Trans. Mater. Res. Soc. Jpn., 30, 1049 (2005).

[7] S. Asbrink, A. Waskowska, J. Phys. D, Condens. Mater., 3, 8173 (1991).

[8] M. Izaki, T. Shinagawa, K. T. Mizuno, Y. Ida, M. Inaba, A. Tasaka, J. Phys. D: Appl. Phys., 40, 3326 (2007).

[9] M. Izaki, T. Ohta, M. Kondo, T. Takahashi, B. M. Fariza, M. Zamzuri, J. Sasano, T. Shinagawa, T. Pauporte, Appl. Mater. Interfaces, 6, 13461 (2014).

[10] Y. Nishi, T. Miyata, T. Minami, Thin Solid Films, 528, 72 (2013).

[11] Y. S. Lee, J. Heo, S. C. Siah, J. P. Mailoa, R. E. Brandt, S. B. Kim, R. G. Gordon, T. Buonassisi, Energy Environ. Sci., 6, 2112 (2013).

[12] Y. S. Lee, D. Chua, R. E. Brandt, S. C. Siah, J. V. Li, J. P. Mailoa, S. W. Lee, R. G. Gordon, T. Buonassisi, Adv. Mater., 26, 4704 (2014).

[13] T. Minami, Y. Nishi, T. Miyata, Appl. Phys. Express, 8, 022301 (2015).

CHAPTER 6

Summary and Future Directions

6.1 Research summary

This thesis has been devoted to the studies on the device structure of electrochemically prepared copper oxide photovoltaic devices. The main objectives were the use of the high quality of Cu_2O layer prepared by heteroepitaxy electrochemical growth and the construction of the electrodeposited-Cu_2O-based PV devices to improve the photovoltaic performance. The main results of this work can be summarized below.

In **Chapter 2**, I investigated the effect of insertion of the highly resistive ZnO (i-ZnO) intermediate layer in the super-straight-type electrodeposited ZnO-nanowire/Cu_2O photovoltaic device. The Cl:ZnO-nws layer was prepared on an FTO substrate, followed by electrodeposition of Cu_2O layer. The i-ZnO layer was sandwiched in the ZnO-nws/Cu_2O

layer by electrodeposition method. And, the thickness of i-ZnO layer was varied from 8.5 to 32 nm. The structural, morphological, optical, and electrical characterizations were carried out by X-ray diffraction, X-ray photoelectron spectroscopy, scanning electron microscopy, optical absorption spectra, and Hall measurements. The 32-nm-thick i-ZnO layer was found to be deposited on the entire side and top surfaces of the Cl:ZnO-nws, and the 3.3 μm-thick continuous Cu_2O layer with very smooth surface was deposited on the i-ZnO layer. The i-ZnO with precisely tuned the electrical and optical properties could reduce interfacial recombination by decreasing defect densities. The 32-nm-thick i-ZnO layer improved the heterojunction quality without scarifying carrier transport and optical transmission, resulting in an improvement in the photovoltaic performance. By insertion of the i-ZnO layer between Cl:ZnO and Cu_2O layers has induced an improvement in the photovoltaic performance from 0.40 to 1.26% with a 0.35 V open circuit voltage, 7.1 $mA.cm^{-2}$ short circuit current density, and 0.52 fill factor. The insertion of i-ZnO is a powerful tool to improve the heterojunction interface and so to increase the photovoltaic performance.

Chapter 3 discussed the growth mechanism of n-type semiconductor ZnO layer on a p-type (111)-oriented Cu_2O layer to construct the substrate-type Cu_2O PV device and the correlation between ZnO microstructure and the device performance. The ZnO layer has been prepared by photo-assisted electrodeposition technique on conventional electrodeposited Cu_2O layer. The structural, morphological, optical, and electrical characterizations were carried out by X-ray diffraction, scanning electron microscopy, and optical absorption spectra. To reduce the recombination problems at the interface, the ZnO layer is stacked on the highly oriented (111)-Cu_2O layer. The ZnO/Cu_2O PV device without the AZO layer showed the best photovoltaic performance of 0.06% in conversion efficiency with the short-circuit current density of 2.55 $mAcm^{-2}$ and open-circuit voltage of 0.08 V. While, the AZO/ZnO/(111)-Cu_2O PV device showed a relatively low photovoltaic performance of 0.015% with the short-circuit

current density of 5.87 $mAcm^{-2}$ and open-circuit voltage of 0.01 V compared to the ZnO/(111)-Cu_2O PV device. However, stacking the AZO layer induced the increase in Jsc from 2.55 to 5.87 $mAcm^{-2}$.

The incorporation of a TiO_2 intermediate layer was demonstrated to mitigate the interfacial defect-assisted recombination at the substrate-type Cu_2O/ZnO PV device. In **Chapter 4**, by introducing a thin TiO_2 in the ZnO/Cu_2O PV device, improved power conversion efficiency could be obtained. The TiO_2 intermediate layer was prepared by sol gel method. And, the TiO_2 layer thickness was controlled by sol concentration and spin coating speed. The structural, morphological, optical, and electrical characterizations were carried out by X-ray diffraction, scanning electron microscopy, and optical absorption spectra. The insertion of TiO_2 intermediate layer decreased the recombination at the Cu_2O/ZnO interface, and topping the PV device with AZO layer, showed an increase in short-circuit current density resulting from increased in carrier diffusion length. The substrate-type ZnO/TiO_2/(111)-Cu_2O PV device showed a photovoltaic performance of 0.08% with Voc of 0.1 V, Jsc of 2.17 $mAcm^{-2}$, and FF of 0.34. And the ZnO/TiO_2/(111)-Cu_2O PV device with AZO layer exhibited a photovoltaic performance of 0.03% with Voc of 0.02 V, Jsc of 4.86 $mAcm^{-2}$, and FF of 0.25. By stacking the AZO layer on the ZnO/TiO_2/(111)-Cu_2O PV device induced an increase in the Jsc from 2.17 to 4.86 $mAcm^{-2}$ due to the increased in carrier diffusion length.

To enhance photo-generated carrier collection efficiency, the photo-generated carrier mobility of Cu_2O layer needs to be increased. In **Chapter 5**, I developed Cu_2O-based photovoltaic devices comprising a substrate-type Aluminum-doped ZnO (AZO)/Cu_2O PV device and discuss the Cu_2O layer thickness on device performance. The AZO layer has been prepared on Cu_2O layer by radio frequency (rf) magnetron sputtering technique. The structural, morphological, optical, and electrical characterizations were carried out by X-ray diffraction, X-ray photoelectron spectroscopy, scanning electron microscopy, optical

absorption spectra, and Hall measurements. The AZO layer acts as a carrier transporter to take out the minority carrier from the Cu_2O layer. By controlling the Cu_2O layer thickness, the carrier diffusion length and optical depth are tuned to create an optimum minority carrier, resulted in increased in the device short circuit current density. And, the photovoltaic performance of 0.47% with short-circuit current density of 8.85 $mAcm^{-2}$ and open-circuit voltage of 0.16 V was obtained for the substrate-type AZO/<111>-Cu_2O PV device.

The approaches to improve photovoltaic performance in this research work can be extended to other photovoltaic material systems. Also, the materials developed in this study may be useful to other types of materials and photovoltaic devices. The i-ZnO intermediate layer can be used in various heterojunction PV devices to replace cadmium-containing buffer layers and increase open-circuit voltages. The (111)-Cu_2O may be useful in other photovoltaic materials systems, for improving carrier transport properties.

6.2 Acknowledgement

This thesis is the outcome of my research from April 2013 until March 2016 at Thin Film Laboratory, Department of Mechanical Engineering, Toyohashi University of Technology, Japan under supervision of Prof. Dr. Masanobu Izaki.

This thesis would not have been possible without the guidance and the help of several individuals who in direct or indirect way contributed and extended their valuable assistance in the preparation and completion of this study.

First and foremost, my utmost gratitude to my supervisor, Prof. Dr. Masanobu Izaki, who has supported me throughout my research work with his patience, ideas, discussions, comments, supports and knowledge whilst allowing me the room to work in my own way.

Special thanks to the examiners, Prof. Dr. Masahiro Fukumoto and Assc. Prof. Dr. Masakazu Kobayashi for provided me very valuable ideas, suggestions and comments that improved this thesis.

Next, I want to gratitude my special thanks to Assc. Prof. Dr. Seiji Yokoyama and Dr. Junji Sasano for their kind comments and ideas especially during the discussion in laboratory's seminars. Then, also many thanks to Mr. Kouichi Muramoto and Mr. Akihiko Kawanishi of Cooperative Research Facility Center, Toyohashi University of Technology for their uncountable assistance and cooperation in some of the analytical equipment. I also want to give my gratefulness to Prof. Dr. Tsutomu Shinagawa from Osaka Municipal Technical Research Institute, Osaka, Japan for their help in some of my measurement, ideas and discussions.

In my daily work I have been blessed with a friendly and cheerful group of lab members. They are very helpful and always assisted me to complete my works, as well as daily life; especially to the "Cu_2O electrodeposition" group members, Mr. Ohta, Ms. Kondo, Mr.

Takahashi, Mr. Kanayama, Mr. Khoo, Mr. Ogawa and other lab members. A lof of gratefulness to the lab secretary Mrs. Ito for her kind supports and assistance.

I would like to express many thanks to the Ministry of Higher Education Malaysia and Universiti Malaysia Perlis for their financial and spiritual supports.

My parents deserve special mention for their inseparable support and prayers. My late father, Mohammad Zain, in the first place is the person who put the fundament my learning character, showing me the joy of intellectual pursuit ever since I was a child. My Mother, Wan Munah, is the one who sincerely raised me with her caring and gently love. And also thanks to all my caring and supportive siblings.

I want to thank my family in Kemaman and Besut, Terengganu, Malaysia, especially to my parents-in-law; Mat Harun and Haminah, and all my relatives, for their patience, supports and understanding.

Words fail me to express my appreciation to my wife Hafizah whose dedication, love, care and persistent confidence in me, has taken the load off my shoulder. I owe her for being unselfishly let her intelligence, passions, and ambitions collide with mine. I cannot put into words how much your support means to me and only hope this happiness will never end.

To my lovely sons, Zharif and Zaqer, thanks a lot for your biggest understanding and patience. It was a great experience to carrying the whole tasks (being a husband, father and a Ph.D. student as well) that somehow I couldn't imagine. I only hope that someday you will benefit from this journey. I believe that both of you'll be a better person someday, and can't wait that precious time.

Finally, I would like to thank everybody who was important to the successful realization of thesis, as well as expressing my apology that l could not mention personally one by one.

Last but not lease….of course GOD that always keeps us moving

Toyohashi, Japan

March 2016

Mohd Zamzuri Bin Mohammad Zain

6.3 Research achievements

6.3.1 List of publications

[1] Photon-Assisted Electrochemical Construction of <0001>-n-ZnO/<111>-p-Cu_2O Photovoltaic Devices with Intermediate TiO_2 Layer, **Mohd Zamzuri**, Junji Sasano, Fariza Binti Mohamad, Masanobu Izaki, The Electrochemical Society (ECS) Transactions 64 (15), 21-26 (2014).

[2] Electrodeposited ZnO-nanowire/Cu_2O photovoltaic device with highly resistive ZnO intermediate layer, Masanobu Izaki, Takayuki Ohta, Misaki Kondo, Toshiaki Takahashi, Fariza Binti Mohamad, **Mohd Zamzuri**, Junji Sasano, Tsutomu Shinagawa, Thierry Pauporte, ACS Appl. Mater. Interface, 6, 13461 (2014).

[3] Photon-Assisted Electrodeposition of <0001>-n-ZnO/<111>-p-Cu_2O Photovoltaic Devices with TiO_2 Intermediate Layer, **Mohd Zamzuri**, Junji Sasano, Fariza Binti Mohamad, Masanobu Izaki, Applied Mechanics and Materials 773-774, 622-625 (2015).

[4] Electrodeposited <111>-oriented Cu_2O Photovoltaic Device with Al:ZnO, **Mohd Zamzuri**, Fariza Binti Mohamad, Masanobu Izaki, Journal of the Surface Finishing Society of Japan, 66, 544-545 (2015).

[5] Substrate type <111>-Cu_2O/<0001>-ZnO photovoltaic device prepared by photo-assisted electrodeposition, **Mohd Zamzuri**, Junji Sasano, Fariza Binti Mohamad, Masanobu Izaki, Thin Solid Films, 595, 136-141 (2015).

6.3.2 List of conferences

[1] Photon-Assisted Electrochemical Construction of <0001>-n-ZnO/<111>-p-Cu_2O Photovoltaic Devices with Intermediate TiO_2 Layer, Mohd Zamzuri, Junji Sasano, Fariza Binti Mohamad, Masanobu Izaki, The 226th ECS & SMEQ Joint International Meeting, October 5-9, 2014 (Oral) Moon Palace Resort, Cancun, Mexico

[2] Photon-Assisted Electrodeposition of <0001>-n-ZnO/<111>-p-Cu_2O Photovoltaic Devices with TiO_2 Intermediate Layer, Mohd Zamzuri, Junji Sasano, Fariza Binti Mohamad, Masanobu Izaki, International Integrated Engineering Summit (IIES), December 1-4, 2014 (Oral) UTHM, Malaysia